FIELD OBSERVATIONS OF RIP CURRENTS

By

JAMES H. MACMAHAN

A DISSERTATION PRESENTED TO THE GRADUATE SCHOOL
OF THE UNIVERSITY OF FLORIDA IN PARTIAL FULFILLMENT
OF THE REQUIREMENTS FOR THE DEGREE OF
DOCTOR OF PHILOSOPHY

UNIVERSITY OF FLORIDA

2003

This dissertation is dedicated to my family and friends, who supported me throughout this process.

ACKNOWLEDGMENTS

As my academic career comes to a conclusion, I have many people to thank who have assisted me either scientifically, socially, or both, all of which has contributed to making this a wonderful and rewarding experience. First, I would like to express my appreciation to Dr. Robert Dean, who believed in me in the beginning and gave me the necessary latitude to allow me to develop as a person and a scientist. The lessons I have learned from this will aid in my future and I am grateful for Dr. Dean's unselfishness and wisdom. Though I probably have frustrated him at times, he never indicated it and he always supported me in my times of need.

Before I started at the University of Florida, Dr. Dean planted an idea of investigating rip currents in my head. Since the day I stepped foot in the department, I wanted to study rip currents. Though I did end up studying rip currents, the pathway to this goal was not very direct. After spending the first spring semester writing a proposal to the Office of Naval Research with Dr. Dean, I worked at the United States Geological Survey with Dr. Guy Gelfenbaum and Dr. Doug Wilson investigating ripples off the coast of St. Petersburg, FL. While working at the USGS, Guy Gelfenbaum learned of my interest in building a hydrographic surveying system using a personal watercraft for investigating rip currents. After an unsuccessful first round in obtaining funding to study rip currents, Guy sponsored me to build the PWC system for the Southwest Washington

Coastal Erosion Study. This is when I met the "one and only" Peter Ruggerio, who is one cool dude. I had a blast that summer collecting bathymetric profiles off the Washington and Oregon shorelines and staying in some of the shadiest hotels in the Pacific Northwest. I would also like to thank Mark Hansen for suggesting that I go to UF and work with Dr. Dean. Mark also assisted me with my surveying questions during the design of the USGS PWC. Dave Wegener helped me out a lot with the construction of the USGS PWC.

At this point, we finally received funding to study rip currents in Florida. I began collaborating with Dr. Robert Thieke, who is one of the most articulate and captivating professors that I know. I have enjoyed many of our long conversations that originated over rather simple questions. Though our dream data set has yet to come to fruition for an intense collaboration, I have enjoyed our discussions and look forward to future ones.

I extend my appreciation to Lynda Charles and Tom Watters for funding the coastal department for developing a UF PWC, which has allowed me to collaborate in many additional projects, which eventually contributed to this body of work. James Joyner made the UF PWC top notch and has always supported and assisted me in my efforts.

It has been a pleasure to work with Sidney Schofield and Vik Adams in the field and out at the laboratory. Vik is one of the most relaxed field guys and I will never forget the time he was inverted in a 5 foot deep jetted sand pit on the shore-break of Daytona Beach during the recovery of the Aquadopp. Sidney was always available to answer my questions and I enjoyed our discussions of electronics, biking, and his extracurricular activities. Mr. Vernon Sparkman always greeted me with a friendly "hello" , but always followed it by some joking remark.

I extend my appreciation to Dona Moss and Lucy Hamm for treating me as individual and not as a student, thereby allowing me to understand the funding and proposal process. I learned a lot of valuable lessons from them, which will assist me in the future. Thanks to the rest of the office staff: Thelma, Donna, Carol, and Debra.

During the summer of 2000, Dr. Ed Thornton came to visit the department, as he was on the external visiting committee. The students had the opportunity to meet with the committee and I was anxiously interested in chatting with Ed. I spoke with Ed for about an hour and he mentioned the potential opportunity for me to come to Monterey in the future to assist in collecting bathymetric measurements. Several months later while sitting at my desk, I received a call from Distinguished Professor Thornton asking me if I was interested in heading to Monterey in the spring of 2001. I was excited about the opportunity, but I never realized how significant this opportunity would be. I am probably the only student to turn down a Fulbright Fellowship to study artificial surfing reefs in New Zealand to work in the United States.

During the Monterey experiment, known as RIPEX, I got the opportunity to participate in a large field experiment. This was a dream come true, as I missed all of the Duck experiments. The experiment was a blast. During this experiment, I met Ed and Tim Stanton's crew: Edith Gallagher, Rob Wyland, Mark Orzech, and Jim Stockel. Greg Miller and I stayed at the beach front Naval Postgraduate School bed and breakfast, where the showers did not work initially. A friendly guy, Ad Reniers, Ed's post-doctoral fellow, brought Greg and me into his house for a hot shower and good meal. I did not realize it at the time, but Ad would become a great friend, a mentor, and person for whom I inspire to be. Ad unselfishly allowed me to utilize the rip current data array, which he suggested for his own scientific pursuits, that has now become a significant portion of my dissertation. I must thank Stella and Femke for being my adopted Monterey family. I will treasurer the times at Che' Reniers. My collaborations with Ed and Ad have just begun and I look forward to the future interactions.

I would like to thank Dan Hanes, an original committee member, for assisting me on proposals, providing useful scientific discussion, and letting me teach in his classes. I would also like to extend my appreciation to the remaining committee members, Dr. Ochi and Dr. Mossa

Besides the scientific folks that I have met along the way, my comrades in Gainesville have always supported me. Susan "Powell" Devine and Kerry Ann Donahue introduced me to Gainesville allowing me to continue being myself without skipping a beat. Thanks goes to Al Browder, Hugo Rodquiez, and Eric Thosteson for teaching me the ways of the department and sharing their enthusiasm for coastal engineering. I have had rewarding experiences with assisting Jason Engle and Gregory Miller in their Masters. I extend my appreciation to Jon Miller, Oleg, Justin, Loraine Chiale, and Jack Puleo. Thanks for a two great years with my original class, though not one of them are still here; Cris Weber, Dave Altman, Lisa Heckman, Beth Cranston, Heather Summerell, and Sean Mulcahy. I extend my appreciation to the Stats group for providing some diversity and the football block (STA); Jeff Thompson, Wolfgang Yank, Brian Caffo, and Patches Johnson. The new group (Robert Weaver, Kristen Splinter, and Jodi Eshleman) of coastal students have been a lot of fun.

I would like to thank Paul Devine, Lee Gordon, and Paul Gayes for their support in various avenues. I will continue to interact with these folks.

I would like to thank my mom and my sister for supporting me and understanding my goals and dreams.

Finally, I would like to thank Heather for emotionally supporting me during my highs, lows, and my injuries. She truly understands my hardships and dreams and has helped me embrace them.

TABLE OF CONTENTS

Page

ACKNOWLEDGMENTS iii

ABSTRACT xi

CHAPTER

1 INTRODUCTION 1

Present Work 2

2 RIP CURRENTS-BACKGROUND 8

Rip Current Measurements and Observations 10
Field Setting 10
Laboratory Experiments 13
Rip Current Modeling 14
Mass Transport 17
Rip Current Morphodynamics 19

3 HYDROGRAPHIC SURVEYING FROM A PERSONAL WATERCRAFT 23

Introduction 23
Nearshore Bathymetric Surveying System 26
Instruments 26
Sampling Scheme & Error 34
Field Tests 38
Results 39
Conclusions 43

4 FEASIBILITY OF MEASURING CURRENTS IN THE NEARSHORE FROM A PERSONAL WATER CRAFT 45

Introduction 45

Rip Current Application 48
    Instrumentation 48
    Field Experiment: RIPEX 50
Sampling Errors 55
Discussion 56
Conclusion 57

5 RIP CURRENT STABILITY 58

Data set and Methodology 58
Concurrent Wave and Longshore Current Measurements 64
Chronological Stability of Rip Current Channels 66
    Rip Stability Period 1: (March 24, 1998 - August 21, 1998) 67
    Rip Stability Period 2: (September 10, 1998 - December 28, 1998) 68
    Rip Stability Period 3: (January 19, 1999 - March 3, 1999) 68
    Rip Stability Period 4: (April 10, 1999 - August 27, 1999) 68
    Rip Stability Period 5: (September 25, 1999 - January 12, 0000) 69
    Rip Stability Period 6: (March 25, 2000 - July 26, 2000) 70
Discussion 70
Conclusion 77

6 RIPEX AND MORPHODYNAMICS 79

Introduction 83
RIPEX-SBE Experiment 86
    Instrumentation 86
    Bathymetric and Beachface Surveys 89
Wave Climate 92
Complex Beach Morphology 96
    Spatial Sediment Distribution 97
    Beach Cusps 99
    Bathymetric Measurements 101
    Video Images 103
    Erosional-Accretions Trends 105
Rip Current Flow Kinematics 107
    Sea Breeze Influence 119
Summary 119

7 RIP CURRENT PULSATIONS 121

Introduction 121
The RIPEX-SBE Experiment 126

Observation of Infragravity Energy 132
    Cross-shore and Alongshore Spectral Statistics 132
Edge Waves and Leaky Waves 140
Cross-shore Structure of Wave Groups and Long Waves 143
Rip Current Pulsations 151
    Alongshore Structure of Current Velocities 151
    Cross-correlation of Infragravity Waves 153
    Cross-correlations of Infragravity Motions with Rip Current Pulsations 156
Discussion 158
Conclusion 160

8 VERY LOW FREQUENCY MOTIONS 163

Introduction 163
    Field Site 169
Very Low Frequency Motions 171
Rip Current Conceptual Modeling 191
Discussion 195
Conclusion 202

9 SUMMARY, CONCLUSIONS, AND RECOMMENDATIONS FOR FUTURE WORK 204

REFERENCE LIST 213

BIOGRAPHICAL SKETCH 222

Abstract of Dissertation Presented to the Graduate School
of the University of Florida in Partial Fulfillment of the
Requirements for the Degree of Doctor of Philosophy

FIELD OBSERVATIONS OF RIP CURRENT DYNAMICS

By

James H MacMahan

May 2003

Chair: Dr. Robert Dean
Cochair: Dr. Robert Thieke
Major Department: Civil and Coastal Engineering Department

Field observations of rip currents have been one of the most difficult measurements to obtain owing to their hazardous nature and the fact that the rip current channels tend to migrate. This dissertation examines 1) innovative methods of obtaining nearshore bathymetry and current profiles within rip current channels, 2) the analysis of long-term video monitoring of rip current morphology at Duck, NC, and 3) the hydrodynamics (steady, sea breeze, infragravity (0.004-0.04 Hz), and very low frequency (<0.004 Hz)) and morphodynamics of a rip current field experiment (RIPEX) in Sand City, Monterey Bay, CA.

In order to acquire proper measurements of nearshore morphology, traditional hydrographic surveying gear was placed in water-tight containers and mounted on a personal watercraft (PWC). The PWC system was tested and evaluated in Myrtle Beach, SC, and utilized on the beaches of California, Florida, Oregon, and Washington. An acoustic Doppler current profiler was added to the PWC for the acquisition of vertical velocity profiles within a rip current system, which was evaluated against fixed instruments.

Three years of time-averaged video images from an Argus Station at Duck, NC were analyzed to gain insight on rip current channel behavior. Long-term observations suggest that rip current morphology is quasi-stable and is only modified during extreme storms (H_{mo}>3 m) when there is a significant longshore current (V>1m/s).

During spring 2001, a rip current field experiment (RIPEX) was carried out in which an extensive array of wave current sensors were deployed on a complex beach where rip currents were relatively persistent and plentiful. The measurements obtained during RIPEX allowed for a complete evaluation of rip current behavior through current, pressure, video, and bathymetric measurements, currently missing in the existing literature. Particular attention was focused on rip current pulsations, steady flows, sea breeze conditions, morphodynamics, vertical flow structure, and newly observed very low frequency motions.

CHAPTER 1
INTRODUCTION

The surf zone is a very dynamic environment. Rip currents, in particular, are one of the most fascinating nearshore processes owing to their quasi-periodicity and complexity. The lack of field measurements presents a challenge to measure these very interesting features. In addition to the scientific interest, there is important societal significance associated with rip currents, as they claim the lives of many beach-goers each year. Furthermore rip currents have been stated to be a mechanism for transporting sediment offshore (Cooke, 1970, Komar,1998).

Rip currents account for 80 percent of beach rescues. In 1997, more than 36,000 beach-goers were rescued from rip currents (Farrell, 1998). In the State of Florida, there are thousands of rip-current related rescues reported annually, with approximately 30 related drownings per year, compared with approximately 150 nationwide (Lushine 1991). The Atlantic Ocean shoreline of Central-East Florida (four counties) has averaged 4-5 drownings per year since January 1989 (Figure 1.1) [Lascody, 1998]. The number of drownings increases during the summer months due to the increased numbers of beach goers and possibly other factors. One hundred and twenty people were rescued in the month of August in Volusia County alone between 1986-1995. Most rip current "events" occur in the three major vacation destinations in Florida; Panama City Beach (Bay County, West Coast), Daytona Beach (Volusia County, East Coast) and Miami Beach

(Dade County, East Coast). More important are the number of Florida drownings for 1989-1996 totaling 180 around the entire coastline of Florida (Figure 1.1). Lascody (1998) stated more deaths occur each year in Florida from rip currents than all other meteorological events (hurricanes, tornadoes, and lighting) combined.

For most beaches throughout the United States, local newspapers, weather reports, and some state Sea Grant newsletters post warnings about rip currents and provide information about appropriate response if caught in a rip current. Rip currents may be ephemeral and transient features on non-barred beaches. However the " triggering" of significant rip currents may still be sensitive to a number of forcing factors including wave height, direction, tide stage, and local wind conditions; the threshold conditions for these factors require considerably more study.

The effort described in this body of work will aid in understanding rip currents for science and hopefully assist in rip current rescue prevention and deaths.

Present Work

Chapter 2 discusses the background of rip currents and presents a literature review of previous studies of measurements, observations, and theoretical developments. It will be shown that measurements of rip currents have lacked detailed quantitative measurements and most of the current understanding is based on qualitative assessment of rip currents systems or theoretical approaches. In the last ten years, there have been more quantitative investigations of rip currents systems in the field and laboratory. Various observations and theory will be examined.

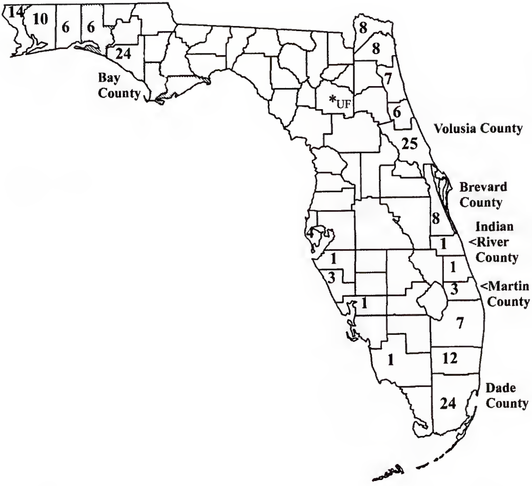

Figure 1.1 Number of deaths throughout Florida for 1989-1996 *totaling 180 rip current deaths.*

Chapter 3 describes the development of an instrument to aid in acquiring bathymetric measurements of rip current systems. A hydrographic surveying system has been designed and tested to acquire nearshore beach profile data. Traditional vessel-mounted echosounder surveying instrumentation was placed in watertight containers and configured for a personal water craft (PWC) for measurements of subaqueous nearshore beach profiles. The system can withstand the harsh environment of the nearshore and acquire beach profile information across the surf zone. This chapter describes the system and results of a comparison in Myrtle Beach, SC, between surveys collected over a three day period by the PWC system and by a similar system mounted aboard a traditional coastal survey vessel. The bathymetric measurements for the personal water craft mounted echosounder surveying system display mean repetitive differences of 6 cm.

In Chapter 4, the need is described for *spatial surveys* of combined nearshore bathymetry and associated velocity fields in many nearshore investigations. To complement the hydrographic surveying system, an acoustic doppler current profiler (ADCP) was configured onto a PWC to allow measurements of nearshore currents. The system was tested at Sand City, CA, during the RIPEX field experiment. The depth-averaged mean cross-shore velocities of the PWC were on the same order of magnitude as fixed instruments, but with a significant error (~20 cm/s). This chapter describes the system and results of current measurements in rip channels.

In Chapter 5, analysis of 3 years (1998-2000) of Argus Images and field observations from the Army Corps of Engineers Field Research Facility (FRF) in Duck, NC, was performed, which suggest that low areas or rip current channels in the longshore bar are quasi-relict features which persist in the same location for time periods as long as several months (~120±40 days). The rip current channels also persist with different spacings O(125-1000 m) suggesting considerable variability in the forcing and response. Wave measurements from the 8-meter FRF wave array suggest that these rip current channels in the bar may only be "erased" during storm events with a significant wave height, Hmo> 3 m, and with a longshore current, $V_l > 1.5$ m/s, while many smaller storm events were observed to modify only slightly the rip current channel configurations. During the summer months, the bar was observed to migrate onshore, and the rip current channels remained relatively in the same location and migrated with the bar. Rip currents are thus present nearly at all times in the rip current channels, however the typical velocity may not typically be of sufficient magnitude to create a public safety hazard except during the high wave events.

Chapter 6 discusses the rip current kinematics and beach morphodynamics, which are documented for 44 days at Sand City, Monterey Bay, CA, during the RIP current field EXperiment (RIPEX) in conjunction with the Steep Beach Experiment (SBE). Observations were obtained from approximately 26 instruments composed of co-located velocity and pressure sensors and acoustic Doppler current profilers. Hydrographic and land differential global positioning system (DGPS) surveys were conducted from and mounted on a personal watercraft, an all-terrain vehicle, and a walking person. Considerable temporal variation in the local wave climate occurred for the two month experiment allowing documentation of rip current hydrodynamics and morphological evolution under different forcing. The wave climate was dominated by shore-normal swell waves with the occurrence of local sea breeze conditions affecting the local nearshore processes. The morphology is classified as shore-connected shoals with longshore quasi-periodic incised rip channels with beach cusps on the upper-beach face. Though the rip channels within the study site were persistent, morphological evolution occurred inducing variations in the hydrodynamic setting. The mean velocity magnitudes within the rip channel increased with decreasing tidal elevations and increased with increasing sea-swell energy.

In Chapter 7, rip current pulsations within the infragravity frequency band (0.004-0.04 Hz) are investigated as to the origin of these motions by analyzing 20 days of nearly continuous measurements during RIPEX-SBE experiment from alongshore and cross-shore arrays of co-located pressure and velocity sensors. Analysis of field data from the alongshore array indicates that there is significant energy in the cross-shore infragravity velocities, and that there is little alongshore spatial variation even in the presence of rip channels. The infragravity velocities are smaller within the rip channel than on the shore-connected shoal owing to differences in water depth. The infragravity energy increases shoreward and with increasing sea-swell energy but does not vary tidally. The infragravity motions are dominated by standing infragravity waves and high mode edge waves with a small amount of energy in low mode edge waves. Unlike open coast observations of infragravity energy, the infragravity energy density is narrow-banded due to the lack of wave directional variability. Rip current pulsations at the infragravity band frequencies are linked to the infragravity motions of the bound and free long waves, as opposed to being forced by the dynamic hydraulic head (wave set-up) associated with incoming short-wave groups.

Chapter 8 describes energetic very-low-frequency motions (VLF) (frequencies less than 0.004 Hz) were observed on a complex beach in Sand City, Monterey Bay, CA. The beach system is comprised of shore-connected shoals with quasi-periodic (~125 m) incised rip channels. The wave climate consists of predominantly shore-normal, narrow-banded swell waves. Though the existence of longshore currents is minimal, rip currents are plentiful. The VLFs are concentrated within the very-low-frequency band within the non-gravity region in k_y space and do not appear to exist in higher frequency bands. The VLFs have significant amounts of energy (U ~0.25 m/s) and are correlated (r^2=0.49) with sea-swell wave energy. The VLFs are fairly constant within the surf zone and decrease in energy offshore (U ~0.05 m/s). There is little difference in magnitude between alongshore and cross-shore VLF variances. The VLFs are not forced by very low frequency surface elevations and are not well correlated (r^2=0.18) with rip current flow. There is an indication that the VLFs are related to wave forcing. F-k_y-spectra illustrate a strong relationship between rip channel spacing and cross-shore velocity, and a minimal alongshore variation in wave number for alongshore velocities. A simple conceptual model is developed to examine the spatial behavior of the VLFs, suggesting that entire rip current cells oscillate in the cross-shore and alongshore. Mechanisms are postulated for the origin of these motions based on observations.

Chapter 9 summarizes results outlined from chapters discussed above. Recommendations and future work are also be briefly described.

CHAPTER 2
RIP CURRENTS- BACKGROUND

For a two dimensional beach, the momentum balance associated with waves shoaling and breaking force variations in the local mean water level, known as wave set-up/down (Longuet-Higgins and Stewart, 1962; Bowen, 1969), and with the inclusion of continuity, a two-dimensional return flow is developed, known as undertow (Svendsen, 1984). There is shoreward mass transport between the trough to crest region and seaward transport between the bed and trough region. When alongshore variations of wave breaking are present, alongshore variations of wave set-up develop, which drive alongshore and seaward flows, creating a three-dimensional flow field. Generally the return flow is focused in a relatively narrow region, referred to as a rip current (Figure 2.1). The occurrence of rip currents generally occur on complex beaches or due to non-linear wave interactions, making it a difficult process to investigate.

Rip currents are approximately shore-normal seaward directed flows that typically reach speeds up to 1 m/s and some have been reported as high as 2 m/s in mega-rips such as at Palm Beach, Australia, a relatively short (≈ 2 km) pocket beach (Short, 1985) [Figure 2.2]. Some of the earliest research (Shepard, 1936; Shepard *et al.*, 1941) provided excellent qualitative insight into the characteristics of rip currents and their associated components. The classical definition of a rip current includes a narrow neck where the seaward flow is concentrated extending past the breakers into an expanding seaward terminus referred to as the head (Figure 2.1). Sometimes, the rip current jets out at a slight angle, due to obliquity of the incoming waves (McKenzie, 1958). The precise mechanisms behind the formation of rip currents have so far eluded clear understanding. This chapter will discuss briefly rip current field measurements and observations, laboratory studies, conceptual models, and rip current morphodynamics presented in the literature. Note that due to the relative differences in individual chapter contents, each chapter has its own more detailed literature background.

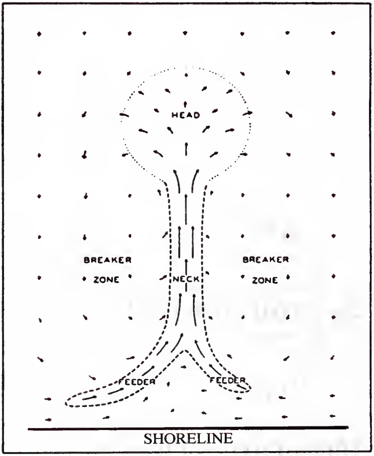

Figure 2.1 Classical definition of a rip current system (Shepard *et al.*, 1941).

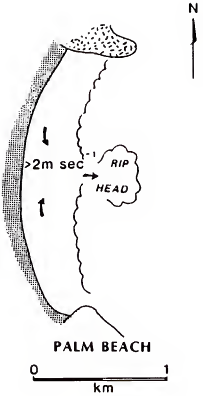

Figure 2.2 Mega-rip on Palm Beach, Australia

Rip Current Measurements and Observations

Field Setting

Shepard and colleagues were some of the original pioneers, who studied rip currents (Shepard, 1936; Shepard *et al.*, 1941; Shepard and Inman, 1950), for the most part these observations were qualitative. Shepard *et al.* (1941) provide a detailed account of rip current characteristics and behavior through observations on beaches within the vicinity of Scripps pier. Shepard and Inman (1950) California used dye, drifters, and wave measurements, and a tsunami recorder (Munk *et al.*, 1949) to study rip current behavior on La Jolla Beach. They found that the intensity and the distance that rip currents extended seaward increased with increasing wave height, and that the rip currents pulsed on the same time scale as the approaching wave groups. Munk (1949) characterized observations of surf beat and suggested that the cumulative nearshore wave mass transport should have significant "surf beat" return flows, which would increase the steady flows within rip currents.

McKenzie (1958) determined through visual observations in Australia that rip current spacings were related to the volumetric flow characteristics of the approaching waves. For large wave conditions, the rip currents were characterized by greater spacing resulting in relatively strong rip current flows, whereas rip currents are narrowly spaced on small wave energetic beaches with smaller rip current return flows.

Sonu (1972) obtained detailed physical measurements in a rip current and on the shore-connected shoals. This beach system was represented by shore-connected shoals with an incised rip channel on the West Coast of Florida. His results showed the rip current velocity fluctuated in time and was correlated with wave groups. He suggested that the rip current pulsations were a result of the standing infragravity waves, explained by the 90° phase lag associated with the high coherence between sea surface elevation and cross-shore velocity. He also determined that there was significant vertical variation of the flow within the rip current channel. However, his measurements were relatively short in duration, which were deployed for approximately one day.

During the Nearshore Sediment Transport Study at Torrey Pines, CA, Tang and Dalrymple (1989), observed migrating rip currents and related these observations to wave group forcing through various statistical techniques. This observation was later conceptualized and verified in the laboratory by Fowler and Dalrymple (1991). They measured energetic, very low frequency motions composed of slowly migrating rip currents formed by intersecting wave groups. This mechanism is a modified version of Dalrymple's (1975) generation of stationary rip currents formed by two intersecting monochromatic wave trains at equal and opposing angles. The conceptual model by Fowler and Dalrymple(1991) confirmed previous observations by Kim and Huntley (1986), who utilizing cross-correlation functions, determined temporal lags of ~26 seconds between cross-shore and alongshore velocity measurements at a co-located instrument. They suggested that these delays were a result of intersecting wave groups caused by reflection or diffraction from a local headland.

Smith and Lagrier (1995) examined rip current behavior outside the surf zone at Scripps pier and found the rip current aperiodically fluctuated and appeared unstable. Aagaard *et al.*, (1997) fortutiously obtained measurements within a rip current channel and observed a strong tidal modulation of the cross-shore rip current flow intensity. Brander (1999) and Brander and Short (2000) investigated rip current dynamics for both a low and high energy beach. Both systems had a rip current channel located between two adjacent shore-connected shoals. Brander and Short (2000) results also observed that the rip current velocity was modulated by tidal elevation, increasing at low tidal stages, and there was significant very low frequency (<0.004 Hz) energy.

Laboratory Experiments

In 1969, Bowen and Inman generated rip currents in the laboratory at anti-nodal location associated with the intersection of incoming waves and alongshore propagating edge waves. They illustrated that the variation of the surf zone wave set-up was responsible for the formation of rip currents based on Bowen (1969). Dalrymple (1978) showed that steady rip currents could be developed by intersecting monochromatic wave trains at equal and opposing wave angles. This mechanism was further modified with the inclusion of wave groups with varying wave angles used to develop migrating rip currents (Fowler and Dalrymple, 1991).

Oh and Dean (1996) utilizing a fixed longshore-bar beach with a gap between the end longshore bar and tank wall, illustrated through drifters and a torque meter the nearshore flow field associated with the complex bathymetry. Furthermore, they initiated a rip current on a planar beach with a water jet to evaluate whether the rip current was self-maintaining as proposed by Dalrymple and Lozano(1978). Oh and Dean (1996) were not able to generate a self-maintaining rip current and determined that wave-current interaction produces a counter torque, which works against the pressure gradient. Dronen *et al.*, 2002 with a set-up similar to that of Oh and Dean (1996) documented the nearshore flow field using drifters and particle image velocimetry. Haller and Dalrymple (2001) and Haller *et al.*, (2002) obtained detailed measurements of rip current flow dynamics for longshore-bar trough beach with gaps between the bars. The variation of wave breaking along the bar and channel induced an alongshore variation in wave set-up at the shoreline, driving "feeder currents" toward the channels as suggested by Bowen (1969) and

Dalrymple (1978). Therefore, low lying areas present in nature in an alongshore bar will tend to encourage a rip current formation. Haller *et al.*, (2002) documented that the wave set-up was lower within the vicinity of the rip channel than the on the neighboring shoals, wave heights were generally larger within the rip channel, and confirmed some of the observations by Oh and Dean (1996) of the wave-induced counter torque that reduced the feeder current and rip current flow. Dronen *et al.* (2002) and Haller *et al.* (2002) demonstrated that there is a linear relationship between non-dimensional rip current flow ($U/\sqrt{(gh)}$ and gamma (H/h_{shoal}). Haller and Dalrymple (2001) observed from the same experiment that rip currents were unstable and fluctuated aperiodically. Haas and Svendsen (2002) utilizing the experimental set-up by Haller *et al.* (1997) evaluated the vertical structure of the rip current, which was uniform within the surf zone and a surface current outside the surf zone.

Rip Current Modeling

In 1962, Arthur developed a simple conceptual model to evaluate rip current characteristics through stream function theory described by potential vorticity. He assumed steady forcing, velocity independent of depth, the incompressible flow, constant density, neglected Coriolis terms, and did not consider non-linear terms, such as wave-current interaction. Arthur's conceptual model resulted in a strong, narrow rip current for a seaward flow entering deeper water associated with conservation of potential vorticity. Bowen (1969) ammended Arthur's stream function theory (1962) by including linearized bottom friction and non-linear terms, and assumed alongshore periodic bathymetry (cuspate features) that induced alongshore varying radiation stress gradients. Bowen's model (1969) qualitatively explained rip current behavior. Bowen and Inman (1969) suggested that edge waves may provide the necessary alongshore variation for the development of rip currents for beaches without alongshore bathymetric variations.

Tam (1974) applied a stream function approach in a non-dimensional coordinate frame and established a solution for the Bickley jet (Bickley, 1939) assuming the rip current is a jet-like flow. This solution evaluated the flow and offshore extent of the rip current. Tang and Leblond (1974) evaluated the importance of wave-current interaction by including it in the stream function. Their results were similar to Bowen's (1969) with little additional benefits for the required extra computations. Noda (1974) numerically solved the stream function formulation including wave refraction for various wave directions. Computations indicated that the rip current velocities were on the order 4 m/s, which are much larger than found in the field. In addition, Noda (1974) realized the importance of the unsteadiness of the flow, in particular rip current pulsations found by Sonu (1972). Dalrymple and Lozano (1978) determined through theoretical derivations that the wave-current interaction of the waves and rip current were self-maintaining, after the initiation of the rip current. Zyserman *et al.* (1990) evaluated the Bernoulli solution for rip current discharge for steady state forcing and determined the flows were alongshore on the shoreward side of the bar. Recently, Haller and Dalrymple (2001) developed an analytical stability solution for steady state forcing to describe the fastest growing modes of a jet instability to explain the unsteadiness of the rip current flow observed in laboratory measurements.

Owing to the complexity of rip currents, detailed numerical models using sophisticated numerical techniques have been developed, for example, DELFT3D and SHORECIRC. The models are continuously being adapted to improve the physics of the forcings to better describe the flow mechanics.

Several hypotheses have been proposed for the generation and behavior of rip currents; however, there is no consensus regarding which mechanism(s) is primarily responsible under specific conditions. Some of the proposed mechanisms include incident/edge wave interaction (Bowen, 1969; Bowen and Inman, 1969), wave/current interaction (Tam, 1974; Dalrymple and Lozano, 1978), instability mechanisms (Bowen and Holman, 1989), bar morphology effects (Zyserman *et al.*,1990), intersecting wave trains (Dalrymple, 1975), shear wave instabilities (Falques personal conversation), and structural interaction (Wind and Vreugdenhil, 1986). Dalrymple (1978) complied a list of the general mechanisms for the formation of rip currents into two categories. This list has been augmented for completeness and is presented as Table 2.1 in which rip currents are grouped into two sub-categories: structural related, or (as Dalrymple defined) wave-wave interaction related (which exist along predominantly straight beaches).

Mass Transport

A simple relationship can be established by considering continuity over the bar, i.e. $Q_{in} = Q_{out}$, with the volume transport by Stokes drift over the bar equal to the rip current velocity times the cross-sectional area of the channel (Aagaard *et al.*, 1997; Brander and Short, 2000; Svendsen *et al.*, 2000)

$$Q_{in} = \frac{E}{\rho C}\lambda \tag{2.1}$$

$$Q_{out} = Vwd \tag{2.2}$$

where E is wave energy, ρ is density, C is wave celerity, and λ is rip current spacing. Assuming $V \sim 1$ m s^{-1}, $d \sim 2.21$ H (Kuelegan, 1945), and $w = \alpha$ H, then

$$\lambda = 6.51\alpha H^{0.5} = \beta H^{0.5} \tag{2.3}$$

showing that the rip current spacing increases with wave height, which is in agreement with Huntley and Short (1992).

Table 2.1 Rip Current Mechanisms (Modified After Dalrymple, 1978).

Wave-Wave Interaction	Reference
Incident Wave - Edge Wave	
Synchronous	Bowen and Inman (1969)
Infragravity	Sasaki (1975)
Intersecting Wave Trains	Dalrymple (1975), Fowler & Dalrymple (1990), Hammack (1991)
Wave-Current Interaction	Dalrymple & Lozano (1978), Falques *et al.* (1999), Murray & Reydellet (2001)
Wave Set-up Instability	Hino (1974), Falques *et al.* (1999)
Shear Waves	(Falques, personal communication), Smith (1995)
Wave Structure Interaction	
Bottom Topography	Arthur(1962), Bowen (1969), Tam (1973), Noda (1974), Zyserman *et al.* (1990), Haller & Dalrymple (2001), Falques *et al.* (1999)
Coastal Boundaries	
Breakwaters	Liu & Mei (1976)
Islands	Mei & Angelides (1977)
Barred Coastlines	Dalrymple (1978), Haller & Dalrymple (2001), Yu & Slinn (manuscript)

The assumption is that the rip current spacing is a result of all of the volume flux over the bar returning through the rip channel. Applying this simple relationship to both the Brander and Short (2000) and Brander (1999) data sets shows the relationship holds well for Palm Beach, Australia, but not for Muriwai, New Zealand (Table 2). Therefore this relationship is either too simplistic, the concurrent conditions were not responsible for the observed rip spacing, or a portion of mass transport is being returned as a seaward flow over the bar. Svendsen and Haas (2000) demonstrated that the total shoreward volume flux over the bar does not all return through the rip channel and a portion of the return flow is over the bar in the typical two-dimensional sense.

Rip Current Morphodynamics

In general, field observations of rip currents have been coupled to morphological controls, such as feeder channels, that are fed into shore-normal rip current channels. Rip currents can form on low-tide terraced (shore-connected shoals) beaches within incised channels or at low lying areas separating longshore bar-trough beaches. Wright and Short [1984] conceptualized the nearshore morphodynamics by a series of beach states forced by the local hydrodynamics ranging from reflective to dissipative beaches. The beach state is defined by the dimesionless fall velocity parameter (Ω=H/ωT) [Gourlay, 1968; Dean, 1973] where H is wave height, ω is mean sediment settling velocity, and T is the wave period. The intermediate beach states are generally representative of rip current systems; longshore bar-trough, rhythmic bar-beach, transverse bar-rip, and low tide terrace, which we define as shore-connected shoals. Most field observations of rip current systems have been related to low-tide terraced beaches with incised rip channels (Shepard *et al.*, 1941, Sonu 1972; Wright and Short, 1984; Brander, 1999; Brander and Short, 2000; Ranasinghe *et al.*, 2000; RIPEX-Chapter 6). Aagraad *et al.* (1997) documented an episodic rip current event on a longshore bar-trough beach. Interestingly, recent laboratory studies (Oh and Dean, 1996; Dronen et al, 2002; Haas and Svendsen, 2002, Haller *et al.*, 2002) have investigated rip current dynamics on longshore trough-barred beaches. Though the differences between these systems is still unknown, the morphodynamics induce relatively similar alongshore variability in wave breaking and forcing, which drives a flow from the shore-connected shoal (longshore bar) towards the rip channels (Bowen, 1969, Dalrymple, 1978).

There have been only a few field measurements of detailed morphological setting and evolution and concurrent measurements of the rip current dynamics. This is due to the difficulty in measuring bathymetry within the surf zone and deploying instruments in the rip channels, because of the tendency for the channel to migrate in the alongshore directions. More recent field studies investigating rip currents (Aagaard *et al.*, 1997; Brander 1999; Brander and Short, 2000; Brander and Short, 2001) all noticed that the mean rip current velocities increased with decreasing tidal elevation, as previously observed by (Sonu, 1972). However, these latter experiments were generally short in duration (with the exception of Brander [1999]) and only focused on rip current measurements (within the rip channel); velocity measurements on the neighboring bars (shore-connected shoals) were not available to determine relationships about rip current behavior or morphodynamic feedback. In addition, the surveying techniques did not provide a high resolution of the nearshore bathymetry for a complete understanding of the morphodynamic evolution and lacked offshore directional wave measurements. These experiments provide an initial understanding upon which to build future experiments.

Wright and Short (1985) evaluated the long-term (6.5 years) morphodynamic evolution on Narrabeen Beach, Australia through visual observations and determined that rip current morphodynamic systems are a stable beach stage. Brander (1999) documented rip current morphodynamic behavior, at Palm Beach, Australia, which evolved considerably over the eleven day experiment. Little information has been obtained on the long-term (> few days) temporal variations of rip current dynamics, the relationship to sea-swell variations, tidal elevation, and morphodynamic response. The diurnal effects of sea breezes on nearshore processes can have significant influence on nearshore circulations and local erosional/accretional events (Pattiaratchi *et al.*, 1997). Yet the sea breeze effects on rip currents have only been qualitatively studied for lifeguard awareness (Lushine, 1991 ; Lascody, 1999)

McKenzie (1958) found that rip currents spacings were large for high-energy wave conditions, while under mild wave conditions, rip current flows were weaker but more numerous leading to smaller rip spacing. These observations are supported by qualitative regional analysis by Short and Brander (2000). Short (1985) and Huntley and Short (1992) analyzed and correlated rip spacings with wave length, wave height, surf zone width, wave steepness, surf zone width, fall velocity parameter, and surf similarity parameter. These correlations were poor with surf zone width having the best fit line with a $R^2 = 0.60$. However, Ranasinghe *et al.* (1999) found no correlation of rip current spacing and surf zone width. Short (1985) and Huntley and Short (1992) illustrated that there was considerable scatter amongst their observation of rip current spacings. These results support the argument that, in general, the concurrent wave conditions are not responsible for the formation of the observed rip current configurations.

A significant advancement in visual observations of rip current morphodynamics is provided by the application of time-lapse video images (Lippmann and Holman, 1990) allowing for long-term evaluations of beach systems. Ranasinghe *et al.* (2000) analyzed two years of time-averaged video exposures for various conditions at a pocket beach in

Palm Beach, Australia, and determined that the formation of rip channels occurred in the same locale. Once a rip current formed, it would either remain relatively fixed in location or migrate alongshore, dependent upon the angle of wave incidence. The results indicated that once formed, rip current spacing did not adjust to variation in offshore wave height, suggesting that rip currents may be topographically controlled. MacMahan [Chapter 3] documented that rip spacing can vary on one beach (Duck, NC) and is not predisposed to a particular length scale. His results also indicated the persistence of rip channels and noted that only large storms with significant longshore currents were responsible for the destruction of rip channels. The video studies indicate that the concurrent wave and meteorological conditions are not responsible for the formation of active rip current configuration, but the antecedent (previous) conditions are the mechanism for the formation of rip currents; see potential mechanisms (Dalrymple, 1978).

CHAPTER 3
HYDROGRAPHIC SURVEYING FROM A PERSONAL WATERCRAFT

Introduction

Surveying the beach is a common procedure employed by coastal engineers and scientists to determine the natural and altered beach systems, the results of which are used for evaluating the performance of a beach (Aubrey *et al.*, 1980) [Figure 3.1]. Nearshore bathymetric surveys have been used systematically to assess shoreline changes, volumetric changes along the beach, performance of beach renourishment projects, inlet migration, and navigability of entrances. Surveys are generally repeated on either an intra-annual or annual time frame.

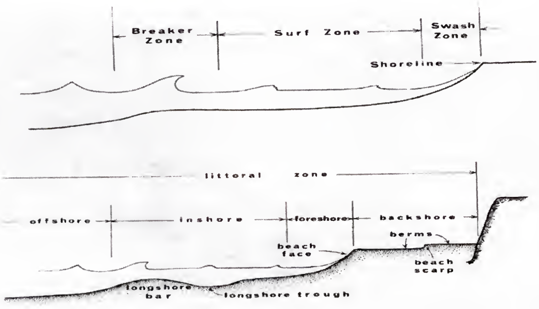

Figure 3.1 Nearshore coastal profile.

In order to employ nearshore bathymetric data, *e.g.* volumetric changes, a substantial amount of high quality data must be collected. The International Hydrographic Office (IHO) maintains standards for shallow water surveys (<30 m water depth) that specify errors in depth measurements should not exceed 30 cm (Gibeaut *et al.*, 1998, IHO, 1987). In addition, the IHO standards require a 90% and 95% probability for repeatability in the vertical and in the horizontal, respectively. The Army Corps of Engineers suggests a vertical accuracy of approximately 5 cm (Headquarters, USACE, 1994). Clausner *et al.* (1986), Dally (1993), and Gibeaut *et al.* (1998) point out that small systematic horizontal and vertical errors in measurements of bathymetry can result in gross errors in estimates of sand volumes along a beach or within an inlet. With the recent advances in surveying techniques, due in part to GPS (Global Positioning System) technology, accuracies and speed of data collection have improved substantially. Nevertheless, the acquisition of nearshore bathymetric data is a difficult and challenging task; and surveying errors will obviously exist and must be rectified to the degree possible.

There have been many different nearshore surveying systems: US Army amphibious landing craft with lead line (Bascom and McAdam, 1947); hydrostatic pressure transducer system (Seymour and Bothman, 1984); surveying sled (Sallenger *et al.,* 1983); Coastal Research Amphibious Buggy [CRAB] (Birkemeier and Mason, 1984); remote-controlled amphibious vehicle (Dally *et al.*, 1994); Scanning Hydrographic Operational Airborne LIDAR Survey (SHOALS) helicopter (Lillycrop *et al.*, 1996;

Gibeaut *et al.*, 1998); and vessel-mounted echosounder and GPS systems (Gibeaut *et al.*, 1997; Work *et al.*, 1998). Vessel-mounted echosounder and GPS systems provide relatively fast and accurate bathymetric measurements at reasonable cost, however, these systems are unable to provide measurements across the surf zone.

In 1994, Beach *et al.* configured a conventional vessel-mounted echosounder surveying system on a personal water craft (PWC) to complete bathymetry measurements across the surf zone (Figure 3.2). This system, the Coastal Profiling System (CPS), was later tested at Duck, NC in 1997 and in 1998 along the Washington State Coastline (Cote, 1999).

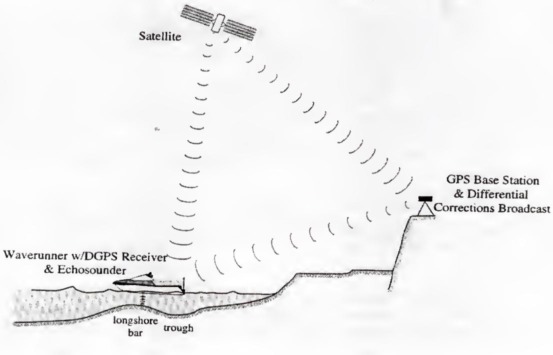

Figure 3.2 Schematic of surveying (Cote, 1999)

The comparison of the CPS and the CRAB from the 1997 Duck experiment indicated a mean bias of 4.6 cm and 5.5 cm for the horizontal and vertical measurements, respectively (Cote, 1999). Modifications to the CPS have been made and will be discussed in this paper, such as: 1) a monitor for visual aids, 2) an echosounder with higher sampling frequency, 3) a keypad for operator control, and 4) surveying software for navigation, data collection, and data analysis. Since the development of the CPS, a similar system was created by Arete Associates to measure bathymetry and currents. Arete's system, the Surf and Coastal Area Measurement Platform (SCAMP), produced bathymetric measurements with vertical errors of less than 5 cm when compared to the CRAB (Dugan *et al.,* 1999).

Motivation for configuring a conventional vessel-mounted echosounder surveying system onto a PWC arose out of a need to assess nearshore morphology. Many nearshore dynamic coastal phenomena vary both temporally and spatially along the beach. Configuring the instrumentation on a PWC creates a platform that can be deployed: 1) on most beaches that are far from boat ramp access; 2) in energetic seas; and 3) in shallow water regions of the coast and back bays, while providing stability and maneuverability.

Nearshore Bathymetric Surveying System

Instruments

The major components of the system used in this study are: (1) a 1998 3-man Yamaha Venture 700 Wave Runner; (2) a Trimble 4600 GPS which samples at 5 Hz; (3) an Oceandata Bathy 500 single- frequency echosounder with a 208 kHz transducer; (4) a 25.4 cm (10 inch) Computer Dynamics VAMP 1000 day light readable screen with 900

NIT reading; (5) a 17-button programmable Logic Controls keypad; (6) a Pentium Toshiba Libretto 100 CT laptop computer; and (7) Hypack surveying software from Coastal Oceanographic, Inc. Figure 3.3 illustrates the system with component configurations. The complete system costs approximately $90,000, not including labor costs.

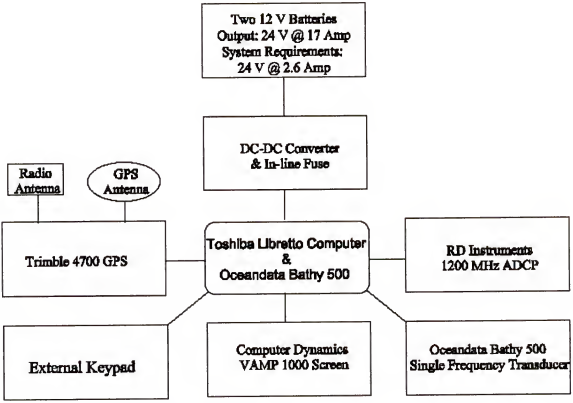

Figure 3.3 System component configuration.

The wave runner model was chosen because of its stability, compartment space, and low price. The three-man PWC is the most stable of all PWCs and measures 3.15 m in length, 1.25 m in width, and 1.05 m in height. The wave runner during normal surveying operation, traveling at approximately 5 m/s (8 knots), can operate for about 5-6 hours on one 50- L fuel tank. The instruments are placed in the compartment space located under the back seat, the stern on the vessel, and forward upper part of the vessel in front of the handlebars (Figure 3.4).

The Oceandata Bathy 500 single frequency echosounder has adjustable gains, offset, serial outputs, and speed of sound control. The sampling rate is a function of water depth with the highest sampling rate of 8 Hz applied in shallow water (0-10 m). The depth resolution of the echosounder is approximately 3 cm. The transducer has a 10 degree conical beam width and generates a pulse at 208 kHz. The echosounder transducer is mounted just below the engine jet on a removable plate on the underside of the vessel at the stern. It is located 29.2 cm below the waterline of the unmanned wave runner (Figure 3.5). The electronics of the echosounder were reconfigured and along with the laptop computer, placed in a watertight case (Pelican Case 1400), which is watertight to 2.08×10^5 Pa (30 psi).

Echosounder transducers can have different beam configurations. A wide beam generates a large spatial coverage and a narrow beam has a small spatial coverage. The spatial coverage can be estimated by

$$Area = \pi(h_{water} \tan\frac{\theta}{2})^2 \qquad (3.1)$$

where h_{water} is the water depth and θ is the transducer beam width. Figure 3.6 illustrates the spatial coverage of an echosounder transducer of various beam widths as a function of water depth. Surveying with high precision requires a narrow beam and typical surveying echosounder transducer have beam widths as narrow as 3 degrees. When surveying in an area with waves, a narrow beam may result in a loss of data. Therefore, a typical beam configuration used in wave environments is approximately 10 degrees. In general, the PWC system collects data at 5 Hz while traveling at approximately 4 m/s thus generating a spatial resolution of approximately 0.8 meters.

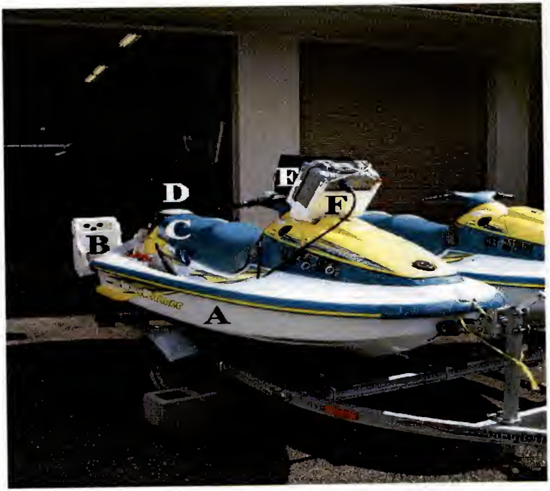

Figure 3.4 Front view of the PWC system: (A) three-man wave runner; (B) ADCP mount; (C) stern wave runner compartment where the GPS, echosounder, and laptop computer are stored; (D) GPS antenna; (E) external screen bellows; and (F) external screen mounted in a watertight case.

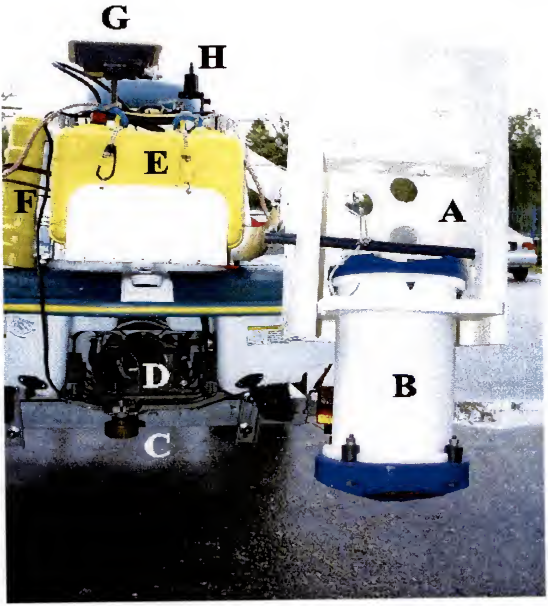

Figure 3.5 Back view of the PWC system: (A) ADCP mount; (B) ADCP; (C) echosounder transducer; (D) wave runner jet; (E) battery case; (F) fire extinguisher; (G) GPS antenna; and (H) radio antenna.

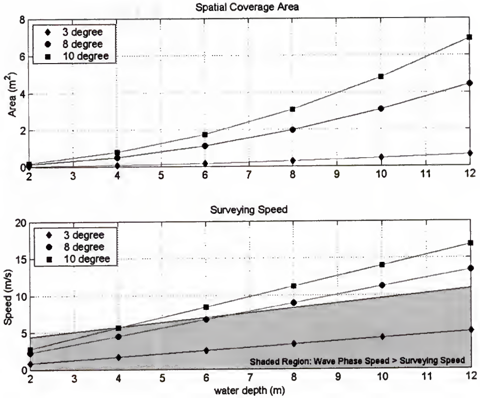

Figure 3.6 (top) Spatial area covered by the echosounder with various transducer beam configurations at various depths; (bottom) the maximum speed the survey vessel may traverse before drop-outs occur for various transducer beam configurations at various depths; shaded region represents when the wave phase speed is greater than the maximum allowable surveying speed.

The beam width also affects the speed at which the vessel can survey. The speed of the surveying vessel, for quality echosounder measurements, depends on the water depth, the beam width, and the sampling time of the echosounder. Simply stated, the larger the spatial coverage is, the faster the surveying vessel can travel within the nearshore region and successfully collect data.

The surveying speed before dropouts occur can be estimated by

$$Speed = \frac{2h_{water}(\tan\frac{\theta}{2})}{t} \tag{3.2}$$

where *t* is the sampling period of the echosounder (in seconds). Figure 3.6 illustrates the surveying speeds for a 3, 8, and 10-degree beam with 0.125 s sampling time in various depths.

A small A-frame was attached to the topside stern of the vessel for mounting the GPS antenna and the radio antenna. The GPS antenna is mounted 91.4 cm directly above the echosounder transducer. Toward the vessel bow, forward of the handlebars, a bracket holds the view screen (Figure 3.7). The screen is mounted in a watertight case and the lid has been modified to permit viewing. A retractable bellows was mounted onto the screen case, sheltering the screen from direct sunlight to allow better viewing of the external monitor which shows the real-time surveying data. The small keypad (24 cm, 8.9 cm, 3.2 cm) is placed in a waterproof radio bag mounted on the handlebars for easy driver accessability.

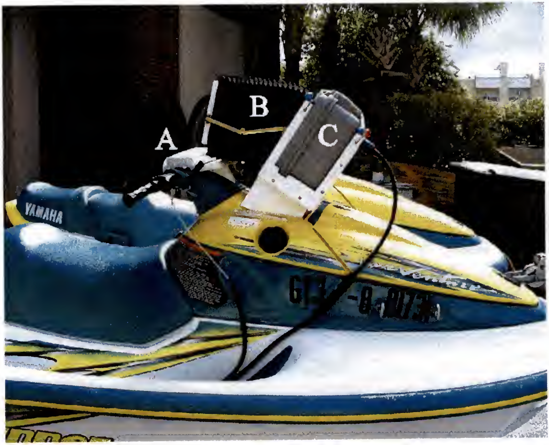

Figure 3.7 Side view of the system: (A) external keypad; (B) external screen bellows; and (C) external screen mounted in a watertight case.

In storage space under the rear seat of the PWC, a small platform has been mounted with a small watertight case located on the underside. This case holds a DC-DC converter and an in-line fuse. On the topside of the platform are two larger watertight cases, which house the GPS, computer, and echosounder. Within the GPS case resides the GPS receiver and the GPS radio which is used to communicate with the shore base station. In the computer case, the echosounder and the laptop computer are mounted. This case has six external watertight Seaconn connectors: two are for serial communication between the GPS and a Acoustic Doppler Current Profiler (ADCP), one for the echosounder transducer, one for the external screen, one for the external 17 button keypad, and one for power. The system is also configured to carry an ADCP to concurrently measure currents, however ADCP measurements will not be discussed in this chapter, see Chapter 4. The Toshiba Libretto laptop computer was chosen for this system for its power and size. This laptop has a Pentium processor with 32 megabytes of RAM and a 2 Gigabyte hard drive, and measures 21 cm in length, 16 cm in width, and 4 cm in depth. The Libretto has only one serial port, so a four serial port Quadtech PCMCIA card is used to communicate with the echosounder, GPS, and ADCP. The computer is used as the platform to run Hypack and for data storage. Attached to the A-frame on the stern of the vessel, is a small shelf where a battery case is located. The battery case has two gel cell 12 volt marine batteries configured in series. The system draws approximately 24 volts at approximately 2.8 amperes.

Hypack is used as the data synchronization software and navigation system. Hypack allows visual observation of trackline, distance offline, depth, latitude, longitude, easting, northing, corrected depth, filename, line number, satellite quality, number of satellites, collection mode, and recording mode. All of this information is useful to the operator when collecting hydrographic data.

Sampling Scheme & Error

The PWC echosounder-mounted surveying system does not have a pitch and roll sensor. Therefore, data are only collected while traversing from offshore to onshore in order to limit the number of waves encountered by the vessel, thus reducing the error induced by pitching. The system can stay within the trough of the wave when collecting data outside the surf zone.

For different echosounder beam configurations, Figure 3.6 illustrates the range in which the wave phase speed exceeds the maximum allowable surveying speed, while traversing from offshore to onshore. Assuming linear shallow-water wave theory, wave phase speed is estimated by

$$C = \sqrt{g h_{water}} \tag{3.3}$$

where C is the wave phase speed (m/s) and g is acceleration due to gravity (9.81 m/s^2). Hence for a 10-degree beam, wave phase speeds will become a concern at a water depth of approximately 4 meters. This is typically immediately outside of the surf zone. Within the surf zone, it is prudent to have the breaking waves behind the vessel when collecting data, allowing the vessel to travel quickly away from rather than into the face of the breaking waves. Furthermore, the operator is able to collect data some distance behind the breaking waves/broken waves to reduce the amount of data loss in the echosounder from sound attenuation by bubbles generated from the breaking waves. The system will experience drop-outs by bubbles within the wave-breaker region, due to the fact that the waves will be traveling faster than the maximum allowable surveying speed (Figure 3.3). Once the water depths become too shallow (approximately less than 60 cm), data collection is ceased and the PWC moves quickly out of the surf zone onto the next survey line. The maneuverability, stability, and safety of the personal water craft is of most value within the surf zone.

The error in vertical position generated by the pitch motion of the waves can be approximated by

$$V_{GPS} = M_{ARM} - \frac{M_{ARM}}{\cos(p)} \tag{3.4}$$

$$V_{echosounder} = \frac{h_{water}}{\cos(P)} - h_{water} \tag{3.5}$$

$$E_{vertical} = V_{echosounder} + V_{GPS} \tag{3.6}$$

where M_{arm} = 91.4 cm which is the vertical distance between the echosounder transducer and the GPS, V_{GPS} is the vertical error associated with the moment arm, P is the pitch of the vessel in degrees, $V_{echosounder}$ is the vertical error associated with the pitch in the echosounder and $E_{vertical}$ is the total error in the vertical (Gibeaut *et al.*, 1998). The moment arm describes the variation associated with the GPS elevation. Note depth measurements are positive. Therefore, when the vessel tilts, the distance between the echosounder transducer and the bottom increases but the elevation associated with GPS decreases. A small moment arm produces a smaller vertical error associated with the GPS elevation. To reduce errors in offsets, the GPS was mounted directly above the echosounder.

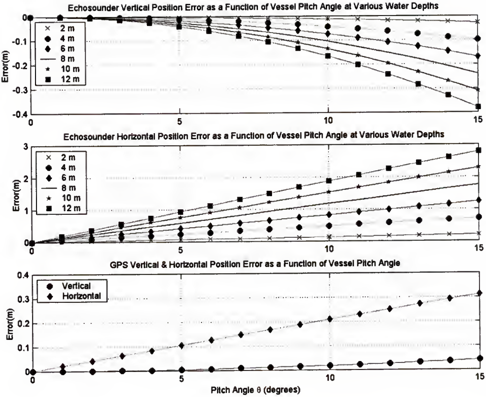

Figure 3.8 (top) Vertical position error associated with the echosounder produced by the vessel pitch in various water depths; (middle) the horizontal position error associated with the echosounder produced by the vessel pitch in various water depths; (bottom) the horizontal and vertical position errors associated with the GPS moment arm produced by vessel pitch, regardless of water depth.

Figure 3.8 illustrates both the vertical and the horizontal errors associated with varying depths in the nearshore at different degrees of pitch. The horizontal error associated with the pitch of the vessel can be approximated by

$$H_{GPS} = M_{ARM} \sin(P) \tag{3.7}$$

$$H_{echosunder} = h_{water} \sin(P) \tag{3.8}$$

$$E_{horizontal} = H_{echosounder} - H_{GPS} \tag{3.9}$$

where $E_{horizontal}$ is the horizontal error associated with pitch in the moment arm of the GPS and the echosounder. On average, the surveying pitch angle is less than five degrees which corresponds to a less than 5 cm error in the vertical and 100 cm error in the horizontal.

Field Tests

The system was field tested June 7-June 9 in Myrtle Beach, SC, and compared with the bathymetry obtained by a traditional coastal survey vessel (TCSV) from the United Stated Geological Survey (USGS). The TCSV system from the USGS includes: (1) a 23 ft Boston Whaler; (2) a Marimatech Echosounder with a single frequency 208 kHz transducer sampling at 10 Hz; (3) an Ashtech Z-Survey GPS sampling at 1 Hz; (4) a TSS Ltd. Model 333 Heave, Pitch, and Roll Sensor sampling at 10 Hz; and (5) Hypack. Other than the heave, pitch, and roll compensator, the Whaler and PWC systems are comparable. In 1998, Work *et al.*, tested the bathymetric surveying techniques utilizing a heave, pitch and roll compensator onboard the TCSV from the USGS. Their results indicated that a heave, pitch, and roll compensator increases the accuracy of bathymetric measurements acquired with a conventional echosounder system. As the PWC system does not include a pitch and roll compensator, two important issues present themselves: 1) evaluation of the pitch and roll sensor and 2) its necessity for surveying beach profiles.

On June 7, 1999, three shore-normal lines (beach profiles) were surveyed with each system directly off South Carolina Coastal Council monuments (5875, 5880, and

5885). The first day, the seas were calm with swell-waves normal to the shoreline. June 8, the wave period decreased and the seas were considerably more energetic. During the second day, the PWC system was able to navigate out of Hogs Inlet, a shallow, unstabilized tidal entrance to the north of Myrtle Beach, and survey several beach profiles as well as Hogs Inlet itself. The TCSV system was not able to navigate through the extreme and dangerous conditions associated with the ebb-tidal delta. On June 9, the seas remained energetic and became even rougher in the afternoon. On this last day, three lines (5830, 5835, 5885) were surveyed and some repetitive spot measurements were taken in the morning by both vessels.

Results

The TCSV system acquired GPS data independently at two locations; the base station and the rover station onboard the surveying vessel. Post-processing merges the two data sets together, calculates the geoid height at each point, and determines the beach profile. The PWC collected GPS data in real-time kinematic mode, which is phase-resolving, and no smoothing algorithms were applied. However, outliers greater than 3 m from the mean profile depth were removed visually. Outliers were numerous within the surf zone due to bubbles affecting the echosounder return. However outside the surf zone, there were only a few outliers (on average about 3-5 outliers). The PWC was the only vessel able to traverse and collect data through the surf zone safely.

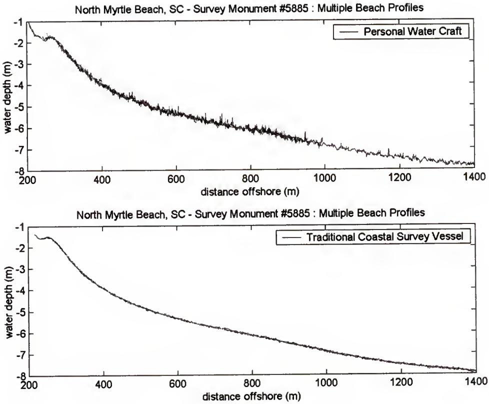

Figure 3.9 (top) Repetitive beach profiles collected by both the PWC; (bottom) and the TCSV for two days under different sea conditions.

Since most coastal engineers are interested in the repeatability of beach profile data, the following procedures were employed. Assuming the alongshore variation in bathymetry is minimal, surveys were juxtaposed to a shore-normal transect to determine the beach profile (Figure 3.9). The data were then interpolated every meter to determine statistics at each point and to determine if there were any statistical trends as a function of depth (Figure 3.10). Interpolation was performed by a spline fitting algorithm. Figure 3.10 depicts the standard deviation at one meter intervals for both systems between 300-950 meters in the cross-shore section of the beach profile. This region was selected because it had the most extensive overlapping coverage within the beach profile. Bathymetric data from South Carolina coastal monument number 5885 which was surveyed on day 1 and day 3 by both systems was used to evaluate the echosounder surveying system.

The two surveying systems compare well. The addition of the pitch and roll compensator used onboard the TCSV reduced the amount of noise along the beach profile and increased the repeatability of the profile lines. The mean standard deviation for repeatability was 3 cm and 6 cm for the TCSV and the PWC, respectively. Average profiles were computed from the multiple beach profiles for both systems and a mean difference between average beach profile of the two systems was 0 ± 6 cm (Figure 3.10). Assuming the TCSV system produced the more accurate beach profile, a root-mean-squared (RMS) error of 5.7 cm was computed against the TCSV beach profile. There was a slight variation between the two systems from onshore to offshore which is hypothesized to be related to small differences in the echosounder speed of sound setting. This was not verified. Detrending this slight systematic error between the two systems, yields an RMS error 4.7 cm. It is hypothesized that the addition of a heave, pitch, and roll compensator on the PWC would reduce measurement errors by approximately 3 cm. The estimated cost for a heave, pitch, and roll compensator is $30,000. Presently, the cost and relative accuracies do not warrant the addition of this device.

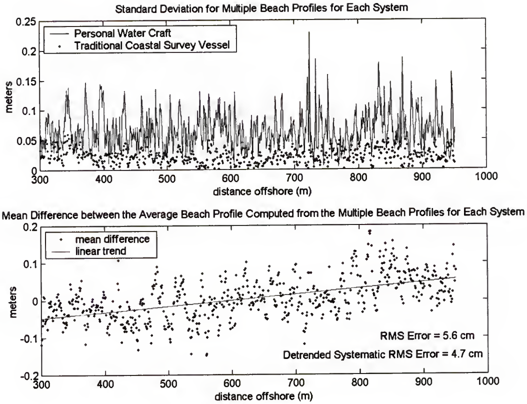

Figure 3.10 (top) The standard deviation for repetitive surveys for both systems; (bottom) the mean difference between the two systems and the linear trend for the mean difference.

which is hypothesized to be associated with slight variations in the speed of sound setting.

The PWC's ability to stay on a trackline was remarkable, with a standard deviation from the trackline of 1.5 m. Therefore, the horizontal repeatability of the beach profile trackline is high compared to the TCSV. The average surveying speed of the PWC was approximately 4 m/s while the TCSV was 2.5 m/s.

Conclusions

The configuration of a conventional vessel-mounted echosounder surveying system onto a PWC provides a useful platform for measuring nearshore beach profiles. This system yielded a large amount of nearshore bathymetric data with a relatively high repeatability in both the horizontal and vertical. The standard deviation of the repeatability of the system was 6 cm with a RMS error from the TCSV beach profile of 5.7 cm. The detrended systematic RMS error was 4.6 cm, hypothesized to be associated with differences in speed of sound settings for the two different echosounding systems. Collecting data while traversing from offshore to onshore reduces the number of waves encountered by the PWC increasing the accuracy and repeatability of the bathymetric measurements. The system set up and sampling scheme allow beach profile data to be measured without the necessity of a pitch and roll sensor. The system is also able to collect data across the entire surf-zone, including the region inside the breakers, and can be deployed from many beaches along the coast in energetic seas; these operations are beyond the capabilities of conventional surveying systems.

Following the design and fabrication of the system described above for the United States Geological Survey, a new and improved system has been developed for the University of Florida, Civil and Coastal Engineering Department (Figure 3.11). This system is discussed in more detail in Chapter 4 with the inclusion of the ADCP.

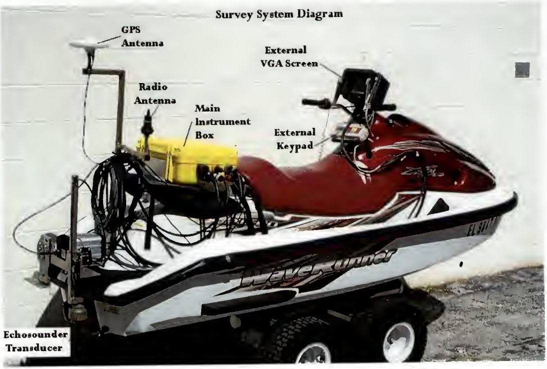

Figure 3.11 The University of Florida PWC hydrographic surveying system.

CHAPTER 4
FEASIBILITY OF MEASURING CURRENTS IN THE NEARSHORE FROM A PERSONAL WATER CRAFT

Introduction

Spatial surveys of nearshore bathymetry and associated velocity fields are essential for many nearshore investigations. The deployment of fixed instrument arrays is generally very costly and requires a large field operation for installation and maintenance. Nearshore, especially in the surf-zone, complete data sets with measurements of the horizontal and vertical distributions of currents are scarce (*e.g.* FRF Duck experiments, SCRIPPS, and Torrey Pines). Distributions of current velocity in the nearshore have been obtained, but only in one horizontal plane (Smith and Largier, 1995). Arrays of anchored tripods provide both temporal and (to a lesser degree) spatial resolution, but are not readily portable. While technological developments in acoustics have increased tremendously within the last few years, the problem of flexibility in the location of the site of the actual measurements and the spatial coverage of the measurements still exists. Therefore, a system has been developed which provides flexibility in measurement location and portability to other sites.

Beach *et al.* (1994) configured a conventional vessel-mounted echosounder surveying system on a personal water craft (PWC) to conduct bathymetric measurements across the surf zone. This system, the Coastal Profiling System (CPS), was later tested at

Duck, NC in 1997 and in 1998 along the Washington State Coastline (Cote, 1999). The comparison of the CPS and the CRAB from the 1997 Duck experiment indicated a mean bias of 4.6 cm and 5.5 cm for the horizontal and vertical measurements, respectively (Cote, 1999). Since the development of the CPS, similar systems were developed by University of Florida (UF) and Arete Associates to measure bathymetry and currents. UF's system obtained results of a comparison test in Myrtle Beach, SC between surveys collected over a three day period by the PWC system and by a similar system mounted aboard a traditional coastal survey vessel (Chapter 3). The bathymetric measurements for the PWC mounted echosounder surveying system display mean repetitive differences of 6 cm bias. Arete's system, the Surf and Coastal Area Measurement Platform (SCAMP), produced bathymetric measurements with similar vertical errors of less than 5 cm when compared to the Coastal Research Amphibious Buggy (CRAB) (Birkemeier and Mason, 1984; Dugan *et al.,* 1999).

Since the PWC platforms are becoming a common tool for measuring nearshore beach profiles, the incorporating the ADCP onto the PWC would allow nearshore current measurements to also be obtained. At the time when the UF's system was being modified with the ADCP (Figure 4.1), Arete Associates were also reconfiguring their system for the addition of an ADCP. Arete Associates carried out a comparison test within a shipping channel in Oregon Inlet, NC and computed a difference between a fixed bed ADCP and the SCAMP of 5 cm/s in each direction (Dugan *et al.*, 2001). This test was undertaken during ebb tide with a maximum water speed of 0.75 m/s. The operation of this system in an inlet is similar to the proposed design of the UF's system, which is for measuring active rip current velocities that on order of magnitude are between 0.5-2 m/s, but with large wave heights. The results from Arete Associates were not available at the time UF's system was designed or field tested, but the measurements are relevant to the evaluation of this platform.

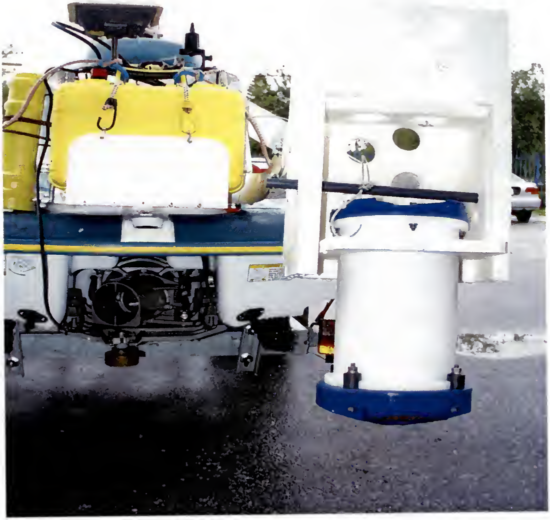

Figure 4.1 Personal watercraft with Acoustic Doppler Current Profiler

Rip Current Application

Motivation for configuring instrumentation onto a PWC arose out of a need to assess nearshore currents and morphology. Many nearshore features are ephemeral dynamic coastal phenomena which vary both temporally and spatially along the beach (for example, rip current channels). There are ***very few*** field measurements of rip currents because they are extremely hazardous and occur at varied locations for relatively short times. Due to the limited quantification of rip currents in the field, much of the existing knowledge is based on classical observations, theoretical approaches, and laboratory studies. Collection of simultaneous bathymetry and current data in an active rip current system seems a sensible prerequisite to enable nearshore processes research to make significant strides in this area.

Rip current morphology and hydrodynamics are an ideal objective for the utilzation of this PWC platform to be utilized. First the currents are relatively fast obtaining speeds up 1-2 m/s (large signal to noise ratio). The rip current velocities and the greater depths associated with the rip channels generally inhibit wave breaking. Wave breaking aerates the water column causing acoustical instruments to malfunction. Thus rip channels provide less aerated water.

Instrumentation

The major components of the system are: (1) a 2000 3-man Yamaha Venture 700 Wave Runner; (2) an Ashtech Z-Surveyor which samples 5 Hz; (3) a Ceeducer single-frequency echosounder with a 200 kHz transducer which samples at 6 Hz; (4) daylight-readable screen; (5) a 17-button programmable keypad; (6) a Pentium Toshiba Libretto 100 CT laptop computer; (7) Hypack surveying software from Coastal Oceanographic, Inc; (8) KVH Gyro which samples at 10 Hz, and (9) RD Instruments ADCP which samples at ~4 Hz. The system with component configurations is illustrated in Figure 4.2. The complete system costs approximately $100,000. For more infomation about the PWC platform for measuring bathymetry please refer to Chapter 3.

These instruments have been integrated together and mounted on a personal water craft (PWC) (Chapter 3) [Figure 4.2]. The ADCP has the advantage of measuring the three components of velocity at several depths, while simultaneously providing bathymetry and bottom

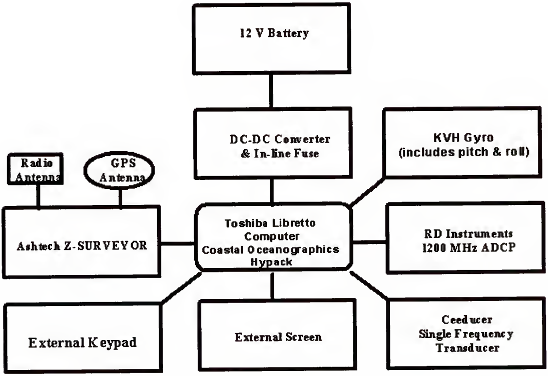
12 V Battery
DC-DC Converter & In-line Fuse
KVH Gyro (includes pitch & roll)
Radio Antenna
GPS Antenna
Ashtech Z-SURVEYOR
Toshiba Libretto Computer Coastal Oceanographics Hypack
RD Instruments 1200 MHz ADCP
External Keypad
External Screen
Ceeducer Single Frequency Transducer

Figure 4.2 Schematic of PWC Instrumentation.

tracking. The ADCP and bathymetric information are then tagged by a KGPS time-stamp and position. The system has been developed to measure accurately the horizontal and vertical distributions of currents and the accompanying bathymetry in the nearshore and surf-zone regions.

The ADCP transducer is located approximately 20 cm below the hull of the PWC. The ADCP was programmed with a 25 cm blanking distance with a 25 cm cell size. The estimated error for this set-up is 18.5 cm/s (horizontal) and 9.2 cm/s (vertical) for a 1 second average. The first velocity measurement is 95 cm below the water surface.

Resolving the underlying current structure in a random wave field from a moving platform is difficult, but the complexity increases due to nearshore bathymetric variations. The instrumentation provides water depth, sea surface fluctuations, x, y, and z components of the wave-current velocity field, and the PWC speed and direction, which are all time-tagged. Potentially three techniques can be applied to resolve the underlying nearshore currents: 1) Spatial and temporal averaging over one wave length (in the moving frame of reference) and assume changes in bottom slope are small, 2) Average spatial repeated runs by the PWC over the same line, 3) Implicitly determine wave period (in the moving frame of reference) and remove orbital velocities using shallow water wave theory.

Field Test: RIPEX

A group of researchers from the Naval Postgraduate School, Ohio State University, and University of Florida participated in a collaborative research effort to investigate rip currents at Sand City, CA (Chapter 6). These experiments provided a unique field data set documenting rip current behavior which was comprised of instruments (pressure and velocity) in two cross-shore arrays in which one array was deployed in the low lying rip channel and the second array across the neighboring shoal (Figure 4.3). The beach morphology at Sand City, CA is representative of low-tide terraces with incised rip channels. The wave direction is predominantly shore normal. The wave height ranged from 0.2-3 meters and wave periods ranged from 5-20 seconds. This experiment was an ideal setting for an evaluation of the performance of the ADCP on the PWC.

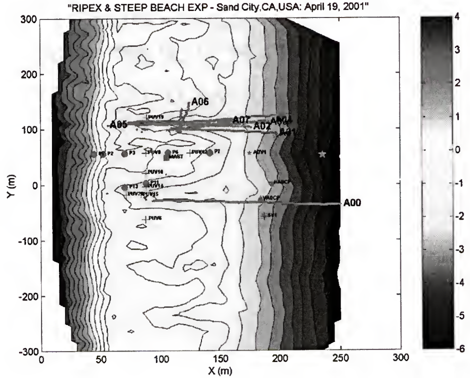

Figure 4.3 Bathymetry of Rip Current Channels at RIPEX, lines depict PWC track lines for ADCP measurements.

The PWC had two functions during the RIPEX experiment. The primary function was to acquire bathymetric measurements of the rip cells (Figure 4.3). After the bathymetric surveys were obtained, the PWC traversed through the rip channels to evaluate the performance of the ADCP in the surf zone. The most appropriate time to obtain bathymetric survey data is at high tide during low energy conditions. The morning high tide was favorable because of calm seas as through the day the afternoon sea breeze caused a harsher environment. However, the most suitable times for bathymetric surveying are not the periods of time associated with the most intense rip currents. Therefore most of the measurements that were obtained during the RIPEX are during low energetic rip conditions, which was not the initial intent of the system. Note that future experiments are planned to obtain measurements in larger velocity flows in higher wave environments.

The cross-shore variation of u,v,w velocities as a function of water depth below the PWC are illustrated in Figure 4.4. Note that x-axis represents both time and space. When the wave crest passes, the vessel moves upward, thus increasing the local water depth. Notice that the wave signal is very apparent in Figure 4.4. However, there is a significant amount of scatter associated with these plots.

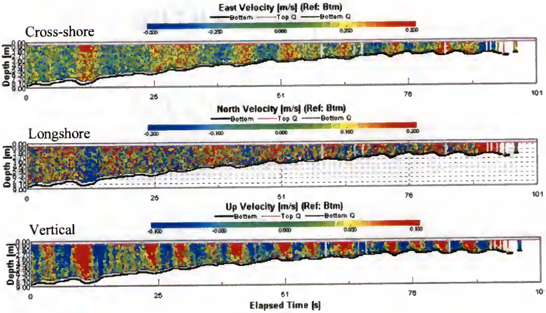

Figure 4.4 Velocity contour plots as a function of depth (meters) and time (seconds), positive velocities are onshore, North, and up. The vessel traversed from offshore to onshore (left to right). (top) Cross-shore velocity contour between -0.5 to 0.5 m/s (middle) Alongshore velocity contour between -0.2 to 0.2 m/s (bottom) Vertical velocity contour between -0.1 to 0.1 m/s.

Examining one vertical profile of the ADCP which represents one ping for one particular location in time and space illustrates a significant amount of vertical variation. Due to this variation, depth averaging was applied to reduce the noise level and to estimate the depth-averaged nearshore current. Figure 4.5 illustrates the depth-averaged cross-shore profile. This figure documents waves shoaling as they approach shallow water and within the shallow water region, the wave velocity depicts the saw-tooth profile. The error velocity was depth averaged and the standard deviation was computed for the velocity profile. These two measurements were of the same order of magnitude. The error measurements were within the specifications of the instrument.

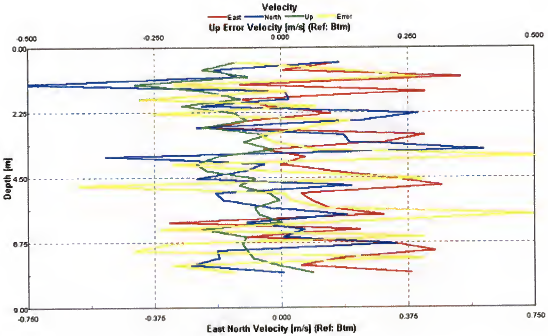

Figure 4.5 One ADCP ping for one particular location in space and time

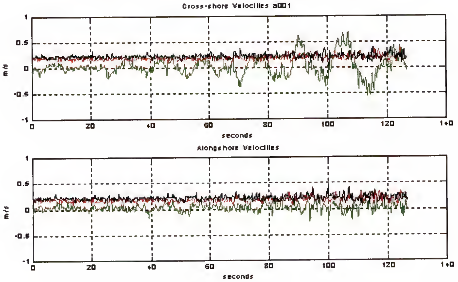

Figure 4.6 The depth-averaged velocity profile traversing from offshore to onshore. The lines about the positive 20 cm/s mark represent the std of the velocity profile and the depth-averaged error velocity.

Sampling Errors

In addition to the errors associated with the instrumentation, sampling errors were introduced by the vessel's speed. The PWC vessel speed would vary in the cross-shore due to the influence of the wave motion and is well correlated with the cross-shore wave velocity (Figure 4.7). This sampling over-estimates the onshore velocity and under estimates the offshore velocity. This is related to the PWC occupying more time within the crest and less time within the trough inducing a phenomenon that is similar to the well known Stokes drift. This error is on the order of 10 cm/s.

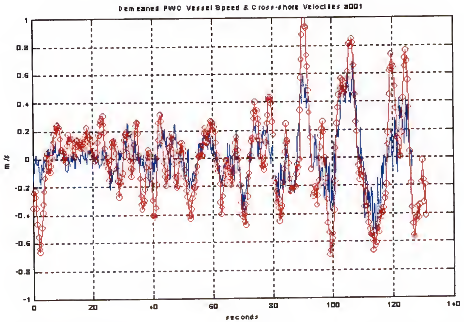

Figure 4.7 Demeaned PWC vessel speed (circles) which generally fluctuates about 1.5 m/s and the depth-averaged cross-shore velocity (solid line).

Discussion

Hourly depth-averaged measurements from a *fixed* ADCP (VADCP on Figure 4.3) within the rip channel were compared to cross-shore depth-averaged velocities obtained by the PWC (Table 4.1). The VADCP measured very low rip current velocities. Therefore the comparison between the two systems indicates that the system is operating reasonably well. However, there is still a significant amount of error associated with the system which is primarily associated with the fact that longer averages cannot be computed since the vessel is moving in a random wave field.

Table 4.1 Wave and Current Statistics during PWC ADCP Surveys

	4/19/01	**4/23/01**	**5/15/01**	**5/16/01**
Hmo (m)	0.41	0.6	0.31	0.55
Tp (s)	10.24	6.92	9.85	7.31
U (Fixed ADCP) [m/s]	-0.01±0.08	0.02±0.16	0.04±0.09	
V (Fixed ADCP)	-0.04±0.08	0.06±0.017	0.01±0.11	
U (PWC ADCP)	~0.0±0.20	~0.0±0.20	~0.0±0.20	~0.00±0.20

Due to the fact that the system was only operated in low energy wave conditions during high tides, which produced lower velocity rip currents, the measurements display a low signal to noise ratio. By temporal averaging over 1 second (or 1.5 meters spatially), which is approximately 4 pings, the error velocity is reduced from ~20 cm/s to ~10 cm/s. However, RD Instruments has released information that new RDI ADCPs will have a faster sampling rate (between 20-25 Hz) which reduce the error to ~ 5 cm/s for a 1 second average with 25 cm cells. In addition to the faster sampling rate, there will be zero blanking distance. Therefore by increasing the cell size from 25 cm to 35 cm, the error will be reduced to ~3 cm/s over a 1 second average. Therefore, the system can be adequately tested in low energy environments.

Conclusions

The PWC platform is becoming a common and effective tool for coastal scientists and engineers for measuring beach profiles. With the addition of an ADCP, nearshore currents can also be obtained. The field test of a PWC with an ADCP demonstrated that there was a significant amount of vertical variation in the velocity profile, requiring depth averaging. Since the PWC is collecting data in a random wave field, temporal and spatial averaging are limited to avoid biasing. Without averaging, the error was approximately 20 cm/s and 10 cm/s for a 1 second average. These errors are all within the specification of the instrument. New ADCP models will have a faster sampling rate and zero-blanking which will dramatically reduce the error velocity. The vessel speed varied with the wave motion such that a sampling error was introduced which is on the order of 10 cm/s. Arete Associates have shown success with their field tests. However, additional field tests are required within the surf zone to determine the limitations of the ADCP on the PWC. In addition to the ADCP limitation, the sampling associated with measuring cross-shore velocity profiles still needs to be addressed.

CHAPTER 5
RIP CHANNEL STABILITY

Data Set and Methodology

The US Army Corps Field Research Facility site at Duck, NC is located on a barrier island within the Outer Banks. The average significant wave height is 0.9 m, set in a microtidal environment with average annual tidal range of 0.97 m (Birkemeier *et al.*, 1985). It is classified as an intermediate energy beach with an inner and outer longshore bar-trough system. The inner bar is located approximately 125 m offshore in 1 m water depth and is the primary focus of this chapter (Konicki and Holman, 2000).

Three years (1998-2000) of time exposure video images were utilized to analyze the stability and persistence of rip channels located approximately 2000-5000 m south of the FRF pier. Camera Number 6 of the Duck, NC Argus cameras was chosen, because of its significant viewing distance from the FRF pier, under the assumption that the rip currents observed are unaffected by the presence of the FRF pier. The camera is mounted on the FRF tower approximately 44 m above the ground. Figure 5.1 represents the time averaged video field utilized to determine rip channel locations and spacings. The white pixel areas are the locations were the waves preferentially break in shallow water displaying the shape of the submerged longshore bar and the shoreline (Holman and Lippman, 1987) [Figure 5.1].

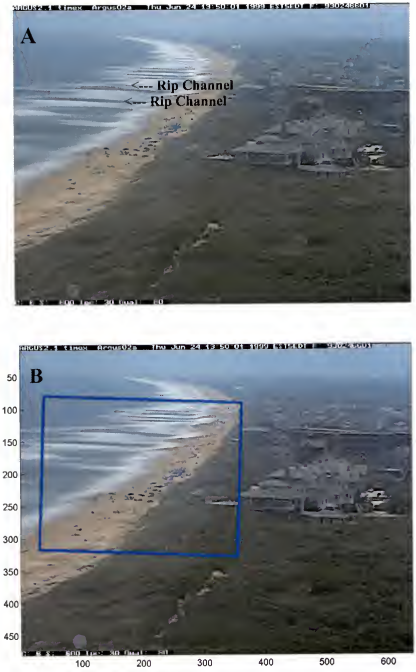

Figure 5.1 A) Sample video time average exposure image taken from camera 6 located at the FRF tower in Duck, NC, oriented southward, which is part of the Argus Stations. The dark swaths represent low lying areas, rip channels, where rip currents will occur. B) Outlines the region of rectification.

The variation in light and dark pixel intensities in the alongshore submerged bar corresponds to variations in the alongshore bathymetry (Holman and Lippman, 1987). Holman and Lippman (1987) verified with the Coastal Research Amphibious Buggy (CRAB) that the alongshore variation in pixel intensity is correlated to variations in alongshore bathymetry, with the dark intensity pixels located between light intensity pixels being associated with low lying areas, rip channels.

The video imagining technique provides a useful methodology for accurately investigating details of the alongshore bar and temporal variations. Video images are notably limited during adverse weather conditions obscuring the view, under low energy conditions resulting in a lack of wave breaking on the bar, or when large waves break across the bar and rip channels alike. These problems create difficulty in the pictorial representation of rip channel stability and reconfiguration. The benefits far outweigh any of these problems by providing a long-term data set of longshore bar signatures and their movements, which can be utilized for morphodynamic investigations.

A midday image, acquired at approximately 1 PM Eastern Standard Time, was utilized to represent the bar signature for that day, independent of tidal elevation, meteorological events, and wave climate. The afternoon image had the most year round consistency resulting in the highest contrast in pixel intensity, since the sun is at its relative diurnal apex. Images were rectified so that features could be scaled accurately (Figure 5.2). After the images were rectified, a line was visually drawn that best traversed along the middle of the longshore bar representing the bar signature (Figure 5.2). To eliminate potential bias, two pixels on both sides of the line and the pixel line were spatially averaged in the cross-shore, thus reducing sensitivity to line selection.

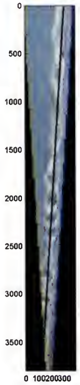

Figure 5.2 Sample rectified image and pixel line

The pixel intensity line represents the alongshore variation in the subaqueous longshore bar for a particular day. Multiple pixel intensity lines were then plotted in time (Figure 5.3), hereafter referred to as a "time stack", which visually represents the alongshore variations of the submerged bar in time. Pixel lines "quasi" represent the three dimensionality of the bar in a two dimensional line. White pixel lines represent storm events, when subsequent wave breaking occurs along both the bar and rip current channel (Figure 5.2). Blue pixel lines represent times during calm wave conditions with minimal depth-limited wave breaking (Figure 5.2). Pixel lines with both white and dark areas represent a three dimensional bar with wave breaking and non-wave breaking sections, indicating the presence of rip current channels.

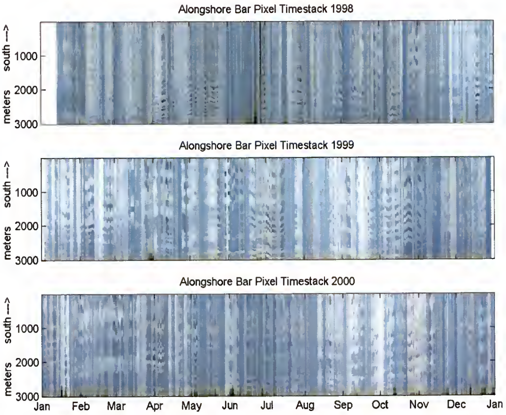

Figure 5.3 Daily time stack for 1998, 1999, and 2000 of alongshore pixel lines located slightly inward of the bar which describe the three dimensionality of the bar in a two dimensional line.

The three dimensional nature of the bar was observed to evolve spatially and temporally, which is attributed to depth-limited wave breaking, tidal elevation, daylight intensity, bar movements in the alongshore and the cross-shore, and rip current channel merging. Therefore selected rectified images were plotted in a chronological time history so that the reader can assess the persistence of the three dimensional bar patterns in a more physically appealing representation, opposed to the time stacks in Figure 5.3. Figure 5.4 demonstrates the rectified chronological time history for the year 1998 and 1999.

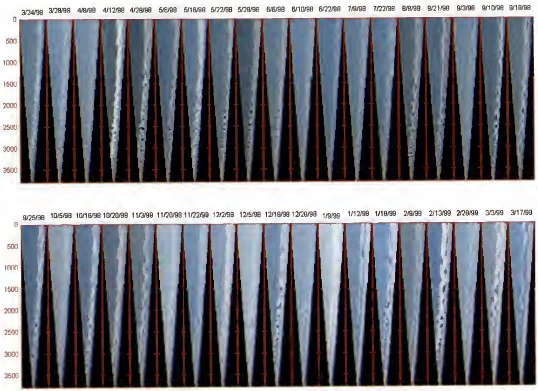

Figure 5.4 Chronological time history of rectified time average exposures displaying bar three-dimensionality for 3/24/98 to 3/17/99.

The selection of images without bias for the days that best represent rip channel patterns presented a difficult task. Observed intensity signatures that best represent the rip channel configurations did not occur during low wave heights nor when the wave heights were too large, causing breaking entirely across the bar and rip channel. Therefore, the selection of rectified images for the chronological time history was not performed rigorously, but simply the image that best represented the three dimensionality of the bar in my opinion. For scenarios with the same bar signature existing for several days, only one image was selected to represent this period for the sake of brevity. Storm events were not plotted in the rectified chronological time history. While this image selection process cannot preclude unintentional bias, patterns can be observed to persist for long periods of time, yielding significant information about the morphodynamic evolution of rip channels.

Concurrent Wave and Longshore Current Measurements

Instrumentation at the FRF site includes a directional wave array located in 8 m water depth. Significant wave height, wave period, and wave direction were recorded every three hours. Linear wave theory was employed to calculate deep water wave heights (H_o) from the wave array data and to calculate deep water wave lengths (L_o). Breaking wave heights (H_b) and water depths (h_b) were calculated from the 8 m array data using

$$\frac{H_b}{H_o} = 0.46\left(\frac{H_o}{L_o}\right)^{-0.28} \tag{5.1}$$

$$h_b = 0.109\log\left(\frac{1+XX}{1-XX}\right) \tag{5.2}$$

$$XX = 2.69\left(\frac{H_o}{L_o}\right)^{0.72} \tag{5.3}$$

Average longshore currents, V_l, from the breaking wave heights and water depths were computed following Komar (1979):

$$V = 1.17\sqrt{gH_b}\,\sin\alpha_b\cos\alpha_b \tag{5.4}$$

where g is the gravitational acceleration, and α_b is the breaking angle.

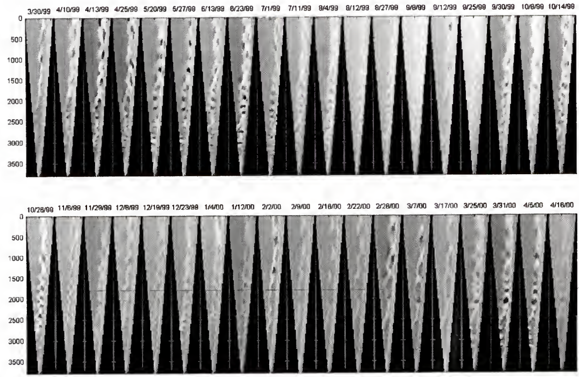

Figure 5.5 Chronological time history of rectified time average exposures displaying bar three-dimensionality for 3/30/99 to 4/16/00.

Chronological Stability of Rip Current Channels

A total of six periods of relatively stable rip current channel patterns existed over the three year time frame. Figures 5.4-5.6 of the rectified chronological time history for 1998-2000, Table 3.1, and Figures 5.7-5.9 for the significant wave height (H_{mo}) and the computed longshore currents (V_l) for 1998-2000 serve to describe the stability of the bar-rip current channel configuration. Below is a chronological history of the bar-rip current channel system and the concurrent wave characteristics from March 24, 1998 to November 11, 2000. The selected rectified images are plotted in Figures 5.4-5.6 that best represent the bar-rip current channel signature generally occurring during intermediate wave energy events. There are occasionally periods when the storms events are so frequent no image was selected and identification of the specific storm responsible for morphodynamic evolution is undetermined. Only storm events resulting in $H_{mo} > 2$ meters are discussed. During the three year period of observation, only 6 storm events

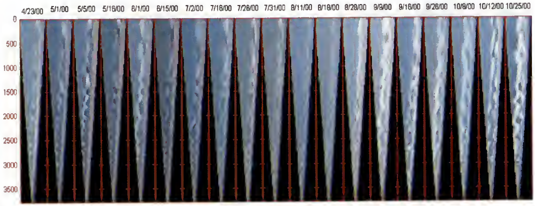

Figure 5.6 Chronological time history of rectified time average exposures displaying bar three-dimensionality for 4/23/00 to 10/25/00.

completely erased the previous rip current channel configuration (Figure 5.7-5.9). These storms were extreme and caused the three dimensional bar to evolve into a linear two dimensional bar-trough system.

Rip Stability Period 1: (March 24, 1998 - August 21, 1998)

March 24, 1998 is the first day of this study, which had an average rip spacing of O(125 m). Figure 5.4 illustrates the rip current channel configuration for March 24, 1998 to March 17, 1999. On March 24, 1998 a bar-rip current channel imprint evolves clearly on April 12, 1998. This rip channel configuration persists until August 8, 1998, and is then modified slightly producing an average rip spacing of O(143 m). From March to July 1998, there were several major storms (Figure 5.7), which appear to have minimal influence on the rip channel configuration. Only the August 2-3, 1998 (Figure 5.7) storm had a slight effect on modifying the bar-rip channel configuration, which had a maximum H_{mo} of 2.3 meters that was actually smaller than the other three storm events in April 1998 (H_{mo} of 3.2, 2.5 , 2.5 meters) [Figure 5.7] and a large storm in May 1998 with a maximum H_{mo} of 3.3 meters. Note the H_{mo} and V_l represent the maximum significant wave height and average longshore current at wave breaking for that particular storm event. The storm event in August 1998 persisted for several days and had a V_l of -1.25 m/s larger than the previous storm events (Figure 5.7). Following the August 2-3, 1998 storm event, the rip channel configuration remained stable until Hurricane Danielle occurred on August 25-29, 1998 with a maximum of H_{mo} of 3.5 meters and a V_l of 1.5 m/s. Hurricane Danielle erased the rip channel signature and produced a relatively linear bar (September 3, 1998). Note that subsequent rip channel patterns observed in

September 1998 are quite different from those in August 1998 (Figure 5.4).

Rip Stability Period 2 (September 10, 1998 -December 28, 1998)

On September 10, 1998 a new bar-rip channel configuration is observed with an average rip spacing of O(250 m) and persisted until December 28, 1998 (Figure 5.4). There were 6 storms with an H_{mo} greater than 2 meters during this period (Figure 5.7). The rip channel configuration was modified slightly by some major storm events that occurred in November and December, 1998. For the most part the rip channels retained thier original configuration. An extreme storm event occurring on January 2-4, 1999 with a H_{mo} of 3 meters and V_l of 1.6 m/s erasing the bar-rip channel configuration.

Rip Stability Period 3: (January 19, 1999 - March 3, 1999)

A new bar configuration O(166 m) was observed on January 19, 1999 and seem to persist until February 13, 1999 (Figure 5.4). In the latter part of February 1999, a storm event occurred for several days, which again modified slightly the rip channel configuration (Figure 5.8).

Rip Stability Period 4: (April 10, 1999 - August 27, 1999)

Following the February storms, a new rip channel configuration developed, however, this configuration only lasted a few days, because another long storm duration event occurred in March 1999 (Figure 5.5). After the March 1999 storms, a large scale O(1000 m spacing) continuous rhythmic rip channel pattern developed on March 17 and March 30, 1999 (Figure 5.5,5.8). On April 10, 1999, a smaller rhythmic bar pattern O(200 m spacing) is observed to be superimposed on top of the previous larger scale rhythmic pattern of March 1999 and these patterns persist until August 27, 1999 (Figure

5.5). Between April 10, 1999 and August 27, 1999, two large storm events occurred with H_{mo} values of 3.5 and 3.5 meters and V_l values of 1 and 1 m/s, respectively, but the rip channel configuration was largely unaltered. The rectified images shown throughout this period (Figure 5.5) provide perhaps the strongest evidence of long-term stability and persistence of rip channel morphology. During this period, the bar also migrated shoreward, yet the rip channel configuration remained stable during the onshore bar migration. Hurricane Dennis and Floyd occurred between August 30- September 6, 1999 erased the rip channel configuration. The maximum for each of these hurricanes was a H_{mo} of 5 meters and V_l of 1.7 m/s (Figure 5.8). Hurricanes Dennis and Floyd caused the bar to return to a largely linear configuration illustrated on September 8 and 12, 1999.

Rip Stability Period 5: (September 25, 1999 - January 12, 2000)

On September 25, 1999, a new rip channel configuration with a different rip current spacing of O(200 m) formed and persisted until January 12, 2000 (Figure 5.6). Between November 6, 1999 and December 3, 1999, many storm events occurred with maximum H_{mo} of 2.5 meters and V_l of up to 1.4 m/s (Figure 5.8). However, the rip channel system appeared reasonably stable during these events with minor changes (compare 10/26/99 to 12/23/99 in Figure 5.6). A significant storm occurred in January 24-26, 2000 erasing the rip channel configuration (Figure 5.9). While this storm may have been the primary storm modifying the rip channel system, a few smaller storms with a smaller H_{mo} occurred with relatively larger longshore currents. The storm responsible for erasing the rip channel configuration could not be determined definitively.

Rip Stability Period 6: (March 25, 2000 - July 26, 2000)

A new large bar configuration O(833 m spacing) was observed around February 22, 2000 and on March 25, 2000 a new smaller pattern O(200 m spacing) formed as a superposition on the previous large scale bar configuration (Figure 5.6). The smaller pattern O(200 m) followed a storm event that occurred on March 17-25, 2000. This new pattern was observed on March 25, 2000 appearing to persist throughout the summer until July 26, 2000. The rip channel configuration also slowly migrated onshore, illustrated in the images of August 11, 18, 28 2000 (Figure 5.6). Between April and July 2000, two large storm events occurred, which had a minimal effect on the rip channel configuration (Figure 5.6). Tropical Storm Ernesto erased the bar configuration.

Discussion

Initially a time stack of pixel images was used to examine the stability of rip channels, however this process did not provide an accurate physical description of the rip channel stability or modifications to the rip channel imprint. Therefore, rectified images for days that best illustrated the rip channel patterns were selected with intervals of several days. Note that no storm events were selected for Figure 5.4-5.6, because storm events visually confused the imprint of the bar pattern.

TABLE 5.1 Table describes video image analysis of rip current persistence, storm events which had a significant wave height greater than 2 meters, storm event which modified the bar-rip current configuration, and the order of magnitude of the rip current spacings (See *Results*).

Bar Channel Stability Event	Storm Events	Storm Hmo	Storm V*l*	Bar Channel Description
March 24, 1998 - August 21, 1998 (151 days)	March 24, 1998 April 4-6, 1998 April 13-15, 1998 April 25, 1998 May 12-15, 1998 August 2-3, 1998 August 25-29, 1998	3.2 2.5 2.5 3.3 2.3 3.5	-0.50 -0.50 0.80 -0.75 -1.25 1.60	RIPS O (125 m) no change no change no change no change slight change ERASED
September 3, 1998				linear bar
September 10, 1998 - December 28, 1998 (110 days)	September 10, 1998 September 25, 1998 October 2, 1998 October 24-26, 1998 December 9, 1998 December 14-17, 1998 December 25, 1998 January 2-4, 1999	2.5 2.3 2.2 2.5 3.5 2.4 3.0	1.20 -1.20 -1.30 -1.10 -0.70 -1.30 1.60	RIPS O (200 m) no change no change no change no change no change no change ERASED
January 9-12, 1999				linear bar
January 19, 1999 - March 3, 1999 (110 days)	January 19, 1999 January 31, 1999 - February 1, 1999 February 19-27, 1999	2.7 2.5	0.80 -1.20	RIPS O(200 m) no change ERASED
March 17-30, 1999				large sinuous bar O(1000 m)

April 10, 1999 - August 27, 1999 (157 days)	April 10, 1999			RIPS O(200 m)
	April 28, 1999- May 4, 1999	3.5	-0.35	no change
	May 14-18, 1999	3.5	1.40	no change
	June 12, 1999	.1 X2	-0.40	no change
	August 30, 1999 - September 6, 1999	5.1	1.70	ERASED
September 9-12, 1999				linear bar
September 25, 1999- January 12, 2000 (44 days)	September 25, 1999			RIPS O (250 m)
	October 17, 1999	2.7	-1.40	no change
	November 10-12, 1999	2.6	-1.20	no change
	November 15, 1999	2.3	-1.30	no change
	November 30, 1999 - December 3, 1999	2.8	-.075	no change
	December 19-21, 1999	2.4	1.20	no change
	January 14, 2000	2.5	-1.40	no change
	January 17, 2000	2.2	-1.45	no change
	January 24-26, 2000	4.5	-0.90	ERASED
February 2, 2000 - March 17, 2000				large sinuous bar O (1000 m)
STORM - March 17-25, 2000		3.2	-1.20	
March 25, 2000- July 26, 2000 (110 days)	March 25, 2000			RIPS O (250 m)
	April 13-15, 2000	2.2	-1.80	no change
	April 18-20, 2000	2.8	-0.70	no change
	April 25-30, 2000	3.3	NAN	no change
	September 5-8, 2000	3.2	-0.80	ERASED

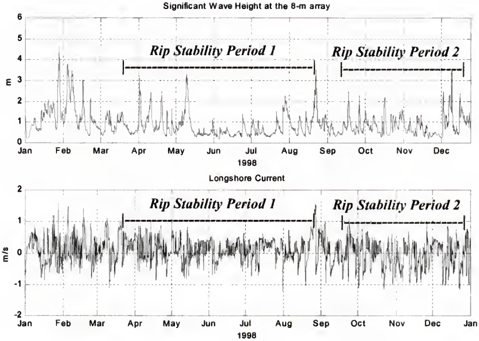

Figure 5.7 Significant wave heights (m) at the 8-m array and calculated mean longshore currents (m/s) at the break-point for the year 1998.

Based on the preceding results, the persistence of rip current patterns over many months is evident. Patterns of different sizes O(125-1000 m) were observed, indicating that the beach is not restricted to a specific set of rip current spacings (Short and Brander, 1999). The persistence of the rip channel configuration can also be determined from Figures 5.4-5.6, Table 5.1. The rip channel signatures persisted on average for approximately (120±40) days during the three year time period. In general, the patterns persisted longer in the Spring and Summer and less in the Fall and Winter, a result of the relative storminess of the season. Upon further analysis, it can be ascertained that only extreme storm events (H_{mo} >3 m) with a significant longshore current (V_l > 1.5 m/s) appear responsible for completely erasing the rip channel configuration.

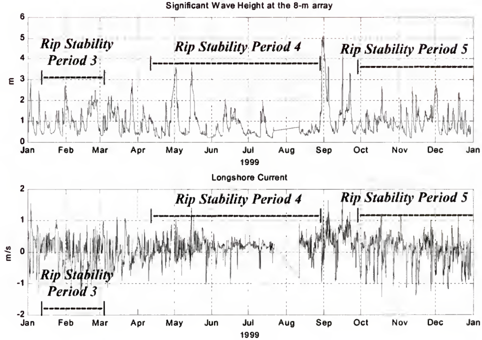

Figure 5.8 Significant wave heights (m) at the 8-m array and calculated mean longshore currents (m/s) at the break-point for the year 1999.

Once formed, the rip channel configuration appears self-maintaining. Mass transport over the longshore bar complemented by the alongshore pressure gradients aids in the maintenance of the rip channel by scouring it free of sediments. These hydrodynamic assumptions are based upon Chapter 2 and Chapter 6.

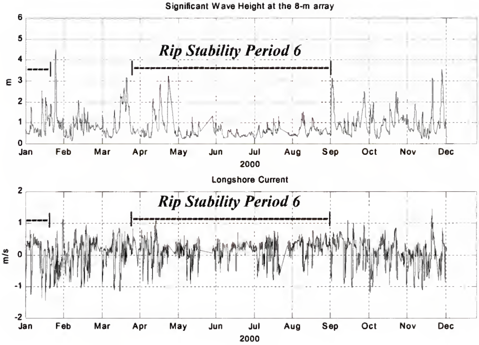

Figure 5.9 Significant wave heights (m) at the 8-m array and calculated mean longshore currents (m/s) at the break-point for the year 2000.

During storm events with H_{mo}> 3 m, the rip channel system is erased and the succeeding storm rip current channels appear to develop in differing arrangements. The events are often associated with strong longshore currents (V_l > 1 m/s). Longshore currents may be the significant mechanism for altering the rip channel positions either by: 1) causing the rip current channels to migrate alongshore, or 2) "filling in" the lower spots with sediment. The modification of the longshore bar-trough beach and possible generation of new rip current channels under large wave heights (H_{mo} > 3 m) and strong longshore currents may be related to shear wave instabilities, edge wave interactions, and/or simply the strength of the return flow (Chapter 2 and Chapter 6). The genesis of rip channels is still not completely understood and undoubtedly requires more field rip channels is still not completely understood and undoubtedly requires more field experiments focused around large storm events when the bar is modified into a linear system and a new rip channel configuration develops. Hence the wave conditions following the large events have a strong influence in the development of the new rip channels.

Twice during the study period, large storm events erased the previous bar configuration causing it to become linear and later resulted in large sinuous forms O(1000 m). Subsequent small storms created smaller rip-channel patterns O(200 m) superimposed on the larger scale sinuous bar form and would then persist for a long duration. Occurrence 1 (March 30, 1999 and April 10, 1999) and occurrence 2 (March 17, 2000 and March 25, 2000) are examples (Figures 5.5 and 5.6). This progression from large sinuous oscillations in the bar to smaller rip-channel patterns may offer some suggestions regarding the genesis of rip currents and the alteration of two-dimensional circulation patterns to become three-dimensional. However it is clear that a many more observations are required to clarify this process

Previous studies have correlated rip current spacing and generation to the incident wave characteristics (i.e. concurrent in time), and in many cases (particularly for rip spacing) the correlations have been weak or nearly nonexistent. This is consistent with the present results, i.e. the observed persistence of rip channel geometry over long periods of time and through large variations in wave forcing. The determination of the precise conditions causing formation and/or modification of the rip current channels in the bar has proved difficult, due to breaking along the entire length of the bar and rip current channels during large storm events. The video images suggest a completely linear bar morphology during the actual storm event, which may or may not be the case.

The quasi-relict nature of the observed rip current channels in the bar at Duck, NC is of fundamental importance to rip current morphology and the understanding of rip current generation, particularly if such behavior is more universal and occurs at other sites with differing wave and sediment characteristics. The stability of rip channels and their persistence provides an aid to the lifeguard community where rip currents are their primary cause of rescues and drownings. The notion that rip currents are an ephemeral and transient feature may still be appropriate on non-barred beaches. However, on barred beaches the observations suggest that rip channels may be far more common and persistent than originally proposed. Seaward directed currents are likely to be present nearly continuously; however the " triggering" of significant rip currents may still be sensitive to a number of forcing factors including wave height, direction, tide stage, and local wind conditions, the threshold conditions for these factors require considerably more study.

Conclusion

The video images have provided an means for examining the formation, spacing, and persistence of rip channels. The concurrent wave conditions and surf zone width have largely been shown not to be responsible for the formation of the active rip currents. The bar-rip channel configuration is a persistent feature that often remains in place for months, and has been observed to migrate in the alongshore and cross-shore directions. Only extremely large storms with substantial longshore currents have a major impact on the reconfiguration of the bar morphology.

Periodic bathymetric measurements and video images are required to assess accurately the bar morphology during times when the video imagery techniques fails and to further establish relationships between the two methodologies. Our future rip current research is focused on these types of measurements.

CHAPTER 6
RIPEX AND MORPHODYNAMICS

Introduction

Rip currents are strong shore-normal (jet-like) flows that originate within the surf zone and are directed seaward through the breakers, and have been known to reach velocities of up to 2 m/s (Short, 1985). The classical definition of a rip current includes a narrow neck where the seaward flow is concentrated extending past the breakers into an expanding seaward terminus referred to as the rip head (Shepard *et al.*, 1941). In general, field observations of rip currents have been coupled to morphological controls, such as feeder channels, that are fed into shore-normal rip current channels. Rip currents can form on low-tide terraced (shore-connected shoals) beaches within incised channels or at low lying areas separating longshore bar-trough beaches. Wright and Short [1984] conceptualized the nearshore morphodynamics by a series of beach states forced by the local hydrodynamics ranging from reflective to dissipative beaches. The beach state is defined by the dimesionless fall velocity parameter ($\Omega = H/\omega T$) [Gourlay, 1968; Dean, 1973] where H is wave height, ω is mean sediment settling velocity, and T is the wave period. The intermediate beach states are generally representative of rip current systems; longshore bar-trough, rhythmic bar-beach, transverse bar-rip, and low tide terrace, which we define as shore-connected shoals.

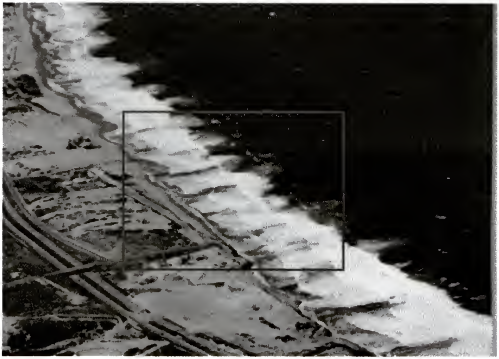

Figure 6.1 Overflight image of field site, Sand City, Southern Monterey Bay, CA.

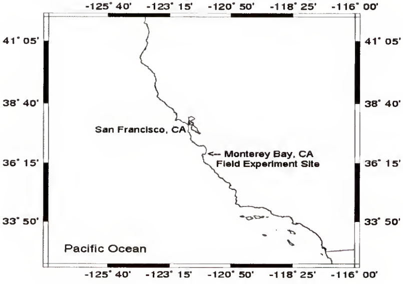

Figure 6.2 Map of west coast of the United States.

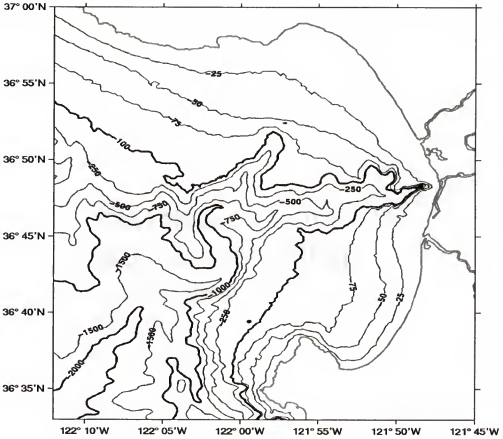

Figure 6.3 Bathymetry map of Monterey Bay, illustrating the Monterey Canyon, contours in meters.

Most field observations of rip current systems have been related to low-tide terraced beaches with incised rip channels (Shepard *et al.*, 1941, Sonu 1972; Wright and Short, 1984; Brander, 1999; Brander and Short, 2000). Aagraad *et al.*, 1997 documented an episodic rip current event on longshore bar-trough beach. Most recent laboratory studies

(Oh and Dean, 1996; Dronen et al, 2002; Haas and Svendsen, 2002, Haller *et al.*, 2002) have investigated rip current dynamics on longshore trough-barred beaches. Though the differences between these two types of systems is unknown, the morphodynamics induce relatively similar alongshore variability in wave breaking and forcing, which drives a flow from the shore-connected shoal (longshore bar) towards the rip channels (Bowen, 1969, Dalrymple, 1978).

There have been only a few field measurements of detailed morphological setting and evolution and concurrent measurements of the rip current dynamics. This is due to the difficulty in measuring bathymetry within the surf zone and deploying instruments in the rip channels, in part because of the tendency for the channel to migrate in the alongshore. More recent field studies investigating rip currents (Aagaard *et al.*, 1997; Brander 1999; Brander and Short, 2000; Brander and Short, 2001) all noticed that the mean rip current velocities increased with decreasing tidal elevation, as previously observed by (Sonu, 1972). However, these latter experiments were generally short in duration (with the exception of Brander [1999]) and only focused on rip current measurements (within the rip channel); velocity measurements on the neighboring bars (shore-connected shoals) were not available to determine relationships regarding rip current behavior or morphodynamic feedback. In addition, the surveying techniques did not provide a high resolution of the nearshore bathymetry for a complete understanding of the morphodynamic evolution and lacked offshore directional wave measurements. These experiments do provide an initial understanding upon which to design future experiments. Laboratory studies have also indicated that rip current velocities increase with increasing wave heights and decreasing water elevation (Haller *et al.*, 2002; Dronen *et al.*, 2002; Haas and Svedsen; 2002).

Wright and Short (1985) evaluated the long-term (6.5 years) morphodynamic evolution on Narrabeen Beach, Australia and determined that rip current morphodynamic systems are a stable beach state. Brander [1999] documented rip current morphodynamic behavior at Palm Beach, Australia, which evolved considerably over the eleven day experiment. Little information has been obtained on the long-term (> few days) temporal variations of rip current dynamics, their relationship to sea-swell variations, tidal elevation, and morphodynamic response. The diurnal effects of sea breezes on nearshore processes can have significant influence on nearshore circulations and local erosional/accretional events (Pattiaratchi *et al.*, 1997). Yet the sea breeze effects on rip currents have been studied only qualitatively to assist in lifeguard awareness (Lushine, 1991 ; Lascody, 1999)

McKenzie (1958) found that rip currents spacings were large for high-energy wave conditions, while under mild wave conditions, rip current flows were weaker and more numerous leading to smaller rip spacing. McKenzie observations are supported by qualitative regional analysis by Short and Brander (2000). For Narrabeen Beach, Australia., Short (1985) and Huntley and Short (1992) developed relationships between rip spacing and persistence based on breaking wave height, direction, and period . An improvement to visual observations of rip current morphodynamics is the application of time-lapse video images (Lippmann and Holman, 1990) allowing for long-term evaluations of beach systems. Ranasinghe *et al.* (2000) analyzed two years of time-averaged video exposures for various conditions at Palm Beach, Australia, and determined that the formation of rip channels occurred in the same locale for this large pocket beach. Once a rip current formed, it would either remain relatively fixed in location or migrate alongshore, dependent upon the angle of wave incidence. The results indicated that rip current spacing once formed did not adjust to variation in offshore wave height, suggesting that rip currents may be topographically controlled. MacMahan [2002-video] documented that rip spacing can varied on an open, relatively straigh beach (Duck, NC) and is not predisposed to a particular length scale. His results also indicated the persistence of rip channels and noted that only large storms with significant longshore currents were responsible for the destruction of rip channels. The video studies indicate that the concurrent wave and meteorological conditions are not responsible for the formation of the active rip current configuration, but the antecedent morphologic conditions are the mechanism for the formation of rip currents; see potential mechanisms (Dalrymple, 1978).

The aim of this chapter is to describe the morphodynamics for rip current system in the field on a complex beach, which evolves over the course of the experiment at Sand City, Monterey Bay, CA (Figure 6.1-6.3). The rip currents on this beach are topographically controlled by shore-connected shoals with quasi-periodic incised rip channels. Section RIPEX-SBE Experiment outlines the instruments and the surveying techniques performed during the RIPEX-SBE. A description of the morphodynamic evolution and rip current kinematics will follow.

RIPEX-SBE Experiment

Instrumentation

A RIP current field EXperiment (RIPEX) was perfomed in conjunction with a Steep Beach Experiment (SBE) during the months of April and May 2001 at Sand City, Monterey Bay, CA. The field site is located in the Southern corner of Monterey Bay (Figure 6.1-6.3). The foreshore of the beach was relatively steep with a slope of 1:10, flattening out to a low-tide terrace (1:100) with quasi-periodic, O(150 m), incised channels (rip channels) and beach cusps O(35m). Nearshore measurements obtained on the complex beach system provide an adequate evaluation of the primary mechanisms for both varying spatial and temporal scales of incident waves, wave reflections, infragravity motions, rip current behavior, morphological evolution, by using a combination of *in situ* current and pressure sensors (PUV), long-term video observations, and rapid deployment bathymetric and current profile surveys (Figure 6.4).

The measurements obtained with the cross-shore array (y=55 m) are utilized to examine the sea-swell waves, reflected waves, and infragravity structure across the shoal. These instruments consisted of a combination of stand-alone pressure sensors (denoted by a circle) and co-located pressure sensor and current meters (denoted by a cross)[Figure 6.4]. To examine the effects of variations in waves and currents associated with the alongshore variability in the bathymetry, an alongshore array (x=88) of six co-located pressure sensors and current meters are utilized. The alongshore array was located approximately 50 meters offshore from the mean water level. Additional instruments were deployed to extend the spatial coverage of the two primary arrays.

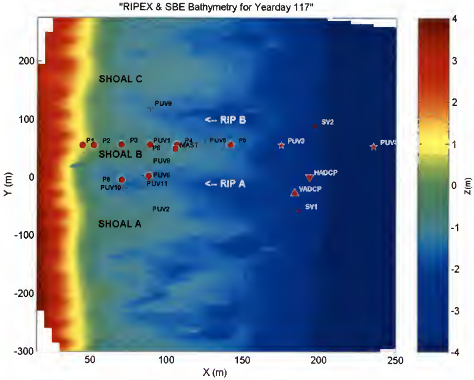

Figure 6.4 Bathymetric contour plots obtained from two methodologies 1) hydrographic survey system mounted aboard a personal watercraft (high-tide) and 2) water-tight back-pack mounted on a person (low-tide). The dots indicate pressure sensors, crosses represent co-located pressure and bi-directional electromagnetic current meters, triangles represent ADCPs, and stars indicate acoustic doppler velocimeters.

Two Acoustic Doppler Current Profilers, ADCP, were deployed at the offshore extent of the rip channel; one was oriented upward to examine the current profile, and the second was oriented in horizontally directed facing across the rip channel so that alongshore variations in the rip current could be explored. Additional vertical profile measurements were obtained by placing a smaller portable ADCP (PADCP) within the rip channel, which had a 5 cm blanking distance and 20 cm bins. After yearday 117, the current meters within the rip channels were oriented downward in order to obtain measurements during lower tidal elevations. Current meters on the shoal were oriented upward, resulting in their exposure at low tides. All instruments were sampled nearly continuously at 8 Hz throughout the duration of the experiment, except for the vertical ADCP which sampled at 0.1 Hz. All instruments were recorded in UTC (Universal time), which is 8 hours ahead of Pacific Coast Time during daylight savings. One of the most exciting experiences of the RIPEX-SBE experiment was in the deployment (Figure 7.1) of a 12 ft vertical tower consisting of 8 electromagnetic current sensors and 12 conductivity cells, an x-y scanning altimeter, a co-located surface piercing wave staff and pressure sensor, along with the new high resolution velocity, sediment and morphology instruments.

The tidal elevation data were obtained from the NOAA/NOS-wave gauge (#9413450) deployed near the Monterey Harbor, Monterey, CA approximately 7 km south of the experiment site. The station measures tidal elevation at 1 Hz and computes a six minute mean water level referenced to mean sea level (MSL).

Though the field experiment was carefully planned out, minor mishaps did occur and modifications were required. Some of the filters on the pressure sensors became clogged and acted as a low-pass filter so that only the tidal signal was measured. An autonomous ADCP was set within a rip channel at a location where the rip currents were hypothesized to be the fastest, but was covered by sand and lost during a large storm on yearday 122, which had a maximum significant wave height of ~3 meters. Professional divers hired to install the offshore instruments accidently broke one of the arms off the acoustic doppler current meter. Due to the significant storm which occurred on yearday 122, large amounts of kelp were torn from the sea floor and became entangled on the

PUV sensors. Thus, swimmers performed daily removal of the kelp from the current meters. Even after periodic maintenance of the sensors, a massive amount of kelp became entangled on PUV8 and ultimately bent the em current meter, which was located directly in the center of the rip channel. The difficulties associated with the experiment were largely related to the hazardous nature of the rip currents and the energetic nearshore conditions.

Bathymetric and Beachface Surveys

Traditional vessel-mounted echosounder surveying instrumentation was placed in watertight containers and configured for a personal watercraft (PWC) for subaqueous measurements of nearshore beach profiles (Chapter 3). The system is able to withstand the harsh environment of the nearshore and acquire beach profile information across the surf zone. The system has been used routinely (without the ADCP, Chapter 4) to obtain nearshore bathymetry for several years. A base station (GPS with a transmitting radio) set-up on top of a known benchmark transmits real-time differential corrections of x, y, and z measurements to a roving unit (GPS and a receiving radio). This set-up is generally referred to as kinematic surveying or kinematic GPS (KGPS).

The incoming positions are in the WGS84 (World Geodetic System established in 1984) ellipsoid, which are transformed to local state coordinates NAD83 (North American Datum established in 1983) and to a local vertical datum NAVD88 (North American Vertical Datum established in 1988). The local state plane coordinates were rotated in local experiment grid with (0,0) being the location of the benchmark set on top of the dune at location 36 37’00.3710 N, 121 51’09.2225 W. The difference between the

NAVD88 and actual water levels was -0.4m.

Plunging breakers broke on top of the relatively steep profile leading up to the flat shore-connected shoal injecting significant amounts of air bubbles into the water column making it acoustically opague for the echosounder over the shore-connected shoals. Due to the difficult surf conditions of the complex beach, an alternative surveying methodology was adapted. At high tides, the PWC traversed the offshore region (~7 m water depth) to the outer edge of the shore connected shoals and within the rip channels. The wave breaking was generally less dramatic within the rip channel systems allowing for safe PWC operation. Though wave breaking was reduced within the rip channel, the echosounder still experienced a considerable amount of drop-outs, which occurred periodically. We determined that bubbles induced by plunging breakers on the shore-connect shoals were being advected by the rip current cell circulation through the rip channels, similar to observations by Smith and Largrier [1995] and Vagle *et al.* [2001]. Due to the groupiness of wave breaking and the associated rip current pulsations (Chapter 7), the PWC operator would traverse within the rip channels during the minima of the short-wave groups, which reduced the amount of injected bubbles and the occurrence of echosounder drop-outs within the rip channel.

During average surf conditions, the minimum PWC operational water depth was approximately one meter. At low tides, the shore connected shoals and feeder channels (and the shallow water regions of the rip channel) were surveyed by a walking person carrying the KGPS housed in a water-tight back-pack. In addition, the beachface was surveyed with the KPGPS mounted on an all-terrain vehicle, ATV.

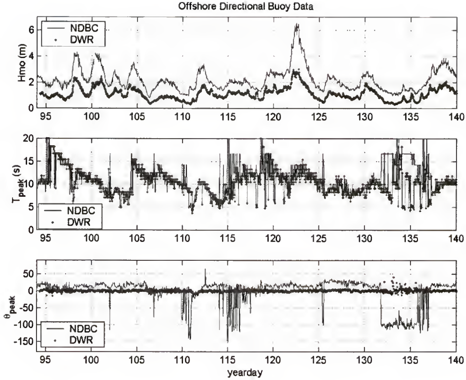

Figure 6.5 Directional wave buoy (DWR) located in 17 m water depth, approximately 650 m offshore, and the NDBC buoy #46042 (bold line) located approximately 40 km offshore outside of Monterey Bay, CA. (Top) significant wave height, (middle) peak wave period, and (bottom) peak wave direction for the two buoys relative to shore-normal.

Beachface surveys were conducted in hopes of quantifying the alongshore variation of beach cusps and their potential forcing. The beach surveys were performed by alongshore transects with the ATV from the swash zone to the upper beach face during times of low tides. Each survey consisted of approximately 11 alongshore transects covering approximately 45 m of beach width. The beachface surveys were conducted periodically on yeardays 95, 104, 108, 113, 117, 119, 125, 128, 133, 136 at the experiment site. In addition six beach surveys were conducted on yearday 114-

117,119,120 along the entire shoreline of Sand City (experiment site) and Del Monte Beach (area ~ 1 km downcoast of Sand City). The beach slope was steepest at Sand City with an average of approximately 7 degrees decreasing to the south.

Wave Climate

The local offshore wave climate was recorded by a directional wave rider buoy (DWR) located approximately 650 m offshore in a depth of 17 m and by the National Oceanographic and Atmospheric Association National Data Buoy Center Buoy (NDBC) #46042 located approximately 40 km offshore, outside of Monterey Bay, CA. DWR showed considerable variation in both significant wave heights and peak wave periods during the duration of the experiment corresponding well to the wave climate at the NDBC (Figure 6.5). During the experiment at DWR, the waves height and periods ranged from 0.20 m – 4 m and 5 –20 s. In view of the large temporal variability in wave height and period, the nearshore mean wave incidence angle shows surprisingly little variation with a predominant direction normal to shore. The peak wave direction ranged from 280-335 degrees with mean direction and standard deviation of 295° and 3°. For the most part, the waves approach at a shore normal direction (295°), even though the variation in wave directions outside the bay are significantly larger at the NDBC. This lack of directional variation is associated with sheltering by headlands and strong refraction over Monterey Canyon, which filters out most wave directions (Figure 6.3, 6.5). Due to the lack of directional variability, there are essentially no longshore currents.

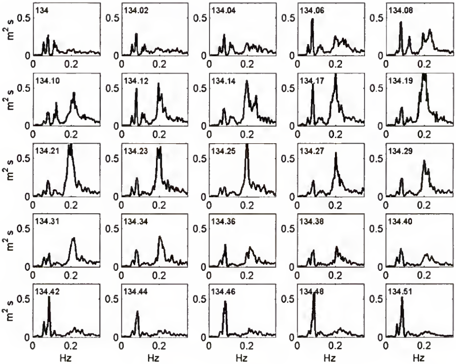

Figure 6.6 The temporal evolution of sea breeze conditions shown as 30 minute sea-surface elevation spectra during year day 134 recorded at PUV4 starting at noon.

During the occurrences of local wind generated sea waves, usually associated with diurnal sea breeze, the wave direction shows an increase in its variability as well as a local increase in wave height (Figure 6.5, see yearday 134-136). A signature of these events is a decrease in the average wave period decreasing from a predominantly swell period to a sea wave period. The sea breeze generally started around 1300 hrs (local time), early in the afternoon. The sea breeze on rare occasions occurs offshore at the NDBC buoy, suggesting that sea breeze conditions are generally locally induced within Monterey Bay, CA. The sea breeze develops in the afternoon lasting approximately six

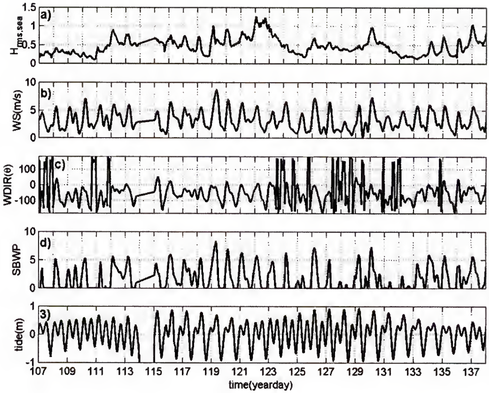

Figure 6.7 Time series of $H_{rms,sea}$ (a) measured at PUV4, wind speed (b) and wind direction (c) measured at Del Monte Beach, CA, weighted directional sea breeze wind parameter (d), and tidal elevation (e) for yeardays 107-138.

hours, resulting in an relatively rapid increase in wave energy within the 0.15-0.35 Hz frequency band (Figure 6.6). The onset of the sea breeze condition is related to broad seas, as the sea breeze duration persists, the energy within the high frequency builds quickly and becomes more narrow-banded, focused around 0.2 Hz. As the winds diminish, the energy broadens while decreasing in sea breeze energy (Figure 6.6).

Wind speed (U_{wind}) and directional (θ_{wind}) measurements, relative to shore normal, obtained by an ultrasonic anemometer were mounted on a 10 m tower at an elevation located on the dune, 5 m above MSL at Del Monte Beach with a 2 minute sampling rate.

Diurnal variation of wind speed and direction is evident (Figure 6.7). During the land breeze (directed offshore) conditions, the wind speed is approximately 2 m/s. During the sea breeze, which occur in the afternoon, the wind speed increases to a maximum of ~ 8 m/s and the direction is shoreward. Sea breeze occurred daily throughout the experiment varying only slightly in maximum speed, duration, and direction. Sea breeze wave height variance ($H_{rms,sea}$) was computed by integrating the wave energy density spectrum from 0.15-0.35 Hz frequency range. A time series of $H_{rms,sea}$ for the experiment is shown in Figure 6.7a. A directional weighting function (*wf*) was applied to the wind speed (U_{wind}),

$$wf = \begin{matrix} \cos\theta_{wind} & |\pm 90^0| \le \theta_{wind} \\ 0 & \theta_{wind} < |\pm 90^0| \end{matrix} \qquad (6.1)$$

$$SBWP = U_{wind} * wf$$

so that SBWP, sea breeze wind parameter, is maximum for onshore directed winds (Figure 6.7d) and decreases with deviation from shore normal. Cross-correlating the $H_{rms,sea}$ and SBWP results in a correlation value of 0.49 with a 1-2 hour temporal lag from the onset of sea breeze conditions.

Complex Beach Morphology

As noted, the beach-face was relatively steep with a slope of 1:10, which then flattened out to shore-connect shoals (low-tide terraces) with a slope 1:100 with quasi-periodic, O(150 m), incised channels (rip channels) and beach cusps O(35m) [Figure 6.4]. Qualitative long-term visual observations by Dr. Ed Thornton (personal communication) indicate that the rip current systems are relatively persistent throughout much of the year. Throughout the experiment, the rip current system was relatively much of the year. Throughout the experiment, the rip current system was relatively persistent (Figure 6.8). The system as described by Wright and Short [1984] is an intermediate state beach with transverse bars (shore-connected shoals) and rip channels; though the system differs from their definition because the shore-connected shoals are completely separated by the rip channels. Feeder channels were present close to the shoreline connecting to the incised rip channels. The rip channels begin at the low-tide line and increase in width in a quasi-exponential fashion seawards to a depth of approximately 4 meters (Figure 6.4).

Beach cusps and rip channels co-existed on this complex beach system, but the governing processes controlling these features differ. Beach cusps occur at smaller spatial scales than the rip channel system and vary on different temporal scales. This is related to the large contrast in the slopes of the beachface and the shore-connected shoals. In addition to the large scale morphologic features, smaller bed-forms existed, in particular mega-ripples. Mega-ripples within rip channels were observed throughout the experiment similar to observations of rip channel systems by Cooke [1970], Sherman *et al.*[1993] and Thornton *et al.* [1997], but no quantitative measurements were obtained. On the shore-connect shoals, the scanning-altimeter record a plethora of ripple dimensions (Stanton and Weltmer personal communication).

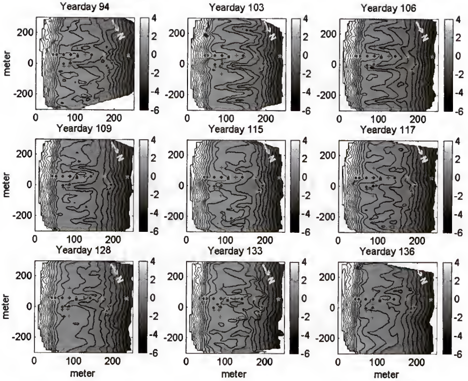

Figure 6.8 Bathymetric surveys for the RIPEX-SBE experiment.

Spatial Sediment Distribution

Surface (<8 cm deep) sediment samples were obtained on the beachface, rip channels, feeder channels, and shore-connected shoals. Cumulative size distributions of the sediment samples were determined using sieve analysis. D_{50} was linear interpolated from the cumulative distribution. The spatial sediment distribution (Figure 6.9) of D_{50} indicates that the beachface is composed of a course sediment (D_{50} 0.66-0.72 mm), which is reflected in the steep profile. The top of the beachface, located at the toe of the beach dune, has finer sediments (D_{50}:0.47-0.54 mm) associated with wind-driven processes and erosion of the beach dune. The sediment sizes are also much finer (D_{50}:0.34-0.37 mm) at the base of the beachface where the profile becomes milder. The sediment sizes (D_{50}:0.32-0.43 mm) are reasonably uniform across the shore-connected shoal to its outer edge, at which point the profile begins to steepen and D_{50} increases to 0.47 mm. At the low tide swash break, there is narrow region occupied by larger sediments (D_{50}: 0.61 mm) created by the swash back-rush, located at the shoreward extent of the rip channel. Sediment is generally coarser within the rip channels (D_{50}:0.40-0.48 mm), decreasing in size closer to the shore connected shoals (D_{50}:0.34-0.38 mm).

The cross-shore distribution of sediment characteristics is explained by the dimensionless fall velocity parameter, Ω, (Gourlay, 1968; Dean, 1973), also known as the Dean Number (Dalrymple, 1992), which implies that large grains are transported shoreward while finer grains are transported seaward. The fall velocity parameter explains the overall sediment distribution associated with waves only, not including currents (Figure 6.9). For this complex bathymetry, rip current cells were relatively persistent in the background flow. The influence of the rip current cell transports sediments through the rip channel with coarser sediments being deposited at the onset of the rip channel and finer sediments being transported offshore. Due to the celluar nature of the rip currents, the fine sediments are actually re-deposited on the seaward side of the shore-connected shoals. The spatial distribution of surface sediment sizes reflects the complex morphology as well as the associated wave and current behavior.

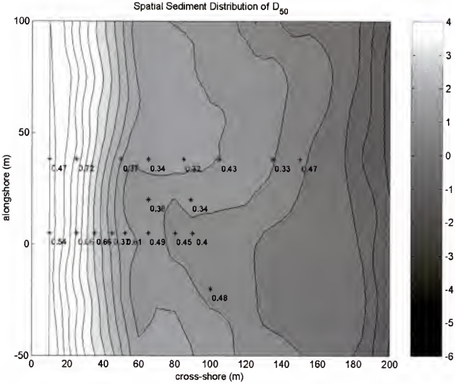

Figure 6.9 Spatial distribution of D_{50} related to the complex bathymetry.

Beach Cusps

From the five weeks of survey data collected from yearday 94-136 on Sand City, and Del Monte Beach, CA, the observed swash zone cusp spacing remained remarkably stable at relatively fixed longshore wavelengths until a storm event (yearday 122) occurred, which destroyed the cusp pattern. Hence, once cusp spacing was established, it did not adjust to the existing wave conditions (Miller, 2001). This behavior supports previous observations of Wright *et al.* (1982) that once the cusp spacing has been cut into a beach, it will dominate until a wave event occurs that establishes a different cusp spacing. Unfortunately, during the observational period, there was only one storm event (yearday 122) significant enough to modify the beach cusp spacing. The cusp spacing remained essentially constant along the entire length of the beach, despite the fact that the beach slope decreased from 7.5 to approximately 4.5 from Sand City to Del Monte Beach. Due to the curvilinear shape of the bay, wave heights are largest in the center by Marina, CA and decrease laterally to the North and South. Qualitatively, a 50% reduction of wave height was measured at the Naval Postgraduate School beach laboratory, which is approximately 1 km south of the field experiment site.

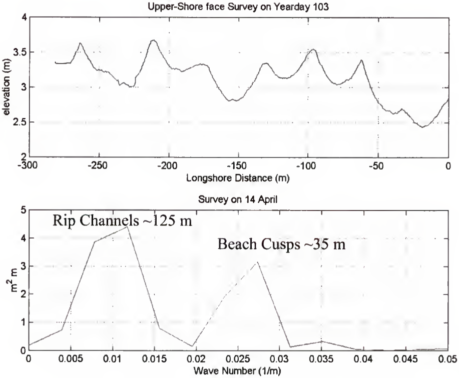

Figure 6.10 Beachface survey along the 25 m cross-shore location (top panel). Spectral estimate of the alongshore profile, indicating significant variance occurring at the rip channels and beach cusp scales (bottom panel).

Two beachface features are prominent: 1) the smaller scale beach cusp features and 2) the background larger scale features associated with the rip channel geometry (Figure 6.10). It is difficult to identify any conclusions on the causative mechanisms of beach cusps, since the beach cusps were always present during the experiment.

Bathymetric Measurements

Considerable bathymetric variation occurred throughout the experiment, even though the wave angle was predominantly shore normal. The rip channel and shore-connected shoal geometry persisted throughout the experiment, and the features slowly migrated alongshore causing the beach profile to vary in the cross-shore (Figure 6.11). There was a slow downcoast migration of the rip channels, with one channel north of the array almost migrating into the cross-shore array. There were a total of 10 storms ($H_{mo} > 1$ m) causing the nearshore morphology to evolve continuously. The largest storms occurred on yearday 98 and 100 (maximum H_{mo} of 2.5 m) and yearday 122 (maximum H_{mo} of 2.9 m), creating significant bathymetric variations. The storms of yearday 98 and yearday 100 were responsible for rip channel migration downcoast approximately 50 meters (unfortunately, no nearshore measurements were obtained until yearday 100). At the onset of the experiment, the bathymetry was well organized and rip channels and shore-connected shoals were clearly defined. After the storms of yearday 98 and 100, the rip channels shifted orientation and began accreting until the storm of yearday 122. The storm of 122 caused significant amounts of erosion moving the system offshore with relatively random deposition. This storm reduced the bathymetric relief, reducing the alongshore variability associated with the rip channels and shore-connected shoals. The rip channels were still present but their amplitudes decreased (in the alongshore), as opposed to the deep channels at the onset of the experiment. The rip channels near the cross-shore instrument array were relatively stable throughout the experiment, but the morphology associated with rip channels located north of the instrument array experienced significant bathymetric variations and at times no rip channels were present. Note that the shoreline around y= -350 m is characterized as a sea-wall with significant wave reflections potentially influencing the rip current in the local vicinity, which was not surveyed.

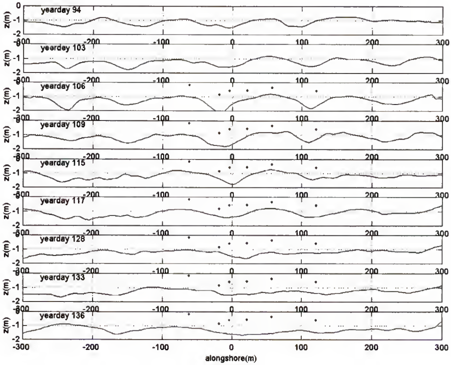

Figure 6.11 Alongshore profiles at cross-distance 100 m for the various days of bathymetric surveys and PUV instruments (dots) for cross-shore distance 88 m.

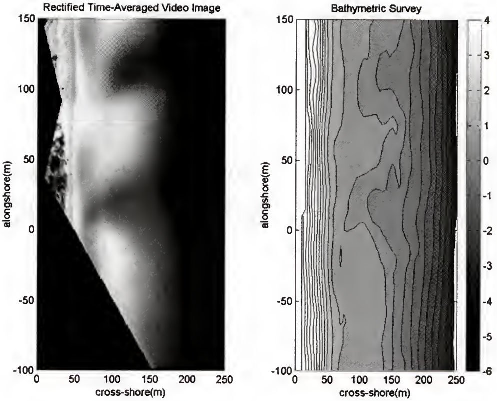

Figure 6.12 Rectified time-averaged video exposure (left) and underlying bathymetry (right) on yearday 128.

Video Images

Two video cameras were mounted on 10 m tower with its base 8.2 meters above the mean water line, overlooking the experiment site. The rectified images from the cameras began on yearday 118. Snap shots and 5 minute time-average images were obtained every 20 minutes to document the intermediate morphodynamics between bathymetric surveys. The rectified time-averaged intensity images compare well with the bathymetric surveys (Figure 6.12) for yearday 128. An alongshore pixel intensity line was selected at the 100m cross-shore distance and plotted as a function of time (Figure 6.13), referred to as a timestack (Holman reference). The timestack indicates that the rip channels were ~30 meters in width and the shore-connected shoals were ~70 m in alongshore width before the storm of yearday 122. After the storm event of yearday 122, the rip channels became slightly wider ~40 m and the shore-connected shoals became narrower ~60 m. However, the smaller storm event of yearday 130 had the most influence of modifying the underlying morphology, the rip channels became ~60-70 meters wide and the shore-connected shoals became relatively narrow ~30-40 meters in alongshore width. The video images correspond with the alongshore profile evolution (Figure 6.11).

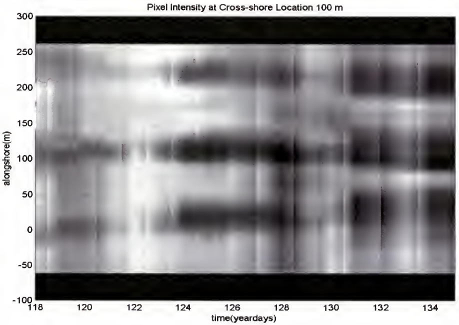

Figure 6.13 Alongshore pixel timestack at the 100 m cross-shore location.

The relatively abrupt change in morphology for yearday 130 is puzzling, though the wave heights increased, the wave period and direction are relatively consistent throughout the experiment. The sea breeze energy for this day is relatively large, 1 m (Figure 6.7).

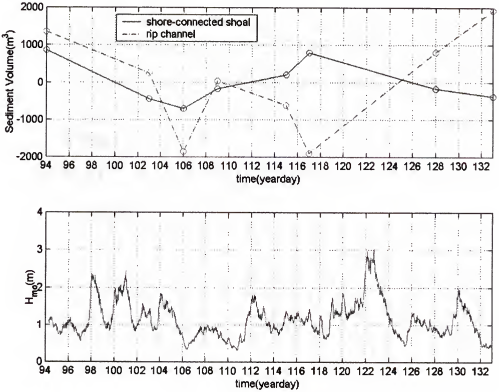

Figure 6.14 (top panel) Calculated volumes within the shore-connected shoals and rip current channels (bottom panel) H_{mo} measured at the offshore buoy during the periods of bathymetric surveys shown as reference.

Erosional-Accrectional Trends

The erosional and accretional patterns associated with complex beach systems has yet to be fully investigated. Wright and Short (1984) suggested that beaches change morphodynamic states redistributing the sediment within the surf zone, and inferred minimal loss of sediment offshore. However, the beach system off Sand City, CA remains within the same morphodynamic state (shore-connected shoals with incised rip channels), though the rip channels and shore-connected shoals experience cross-shore and alongshore movements of sediment under various wave conditions.

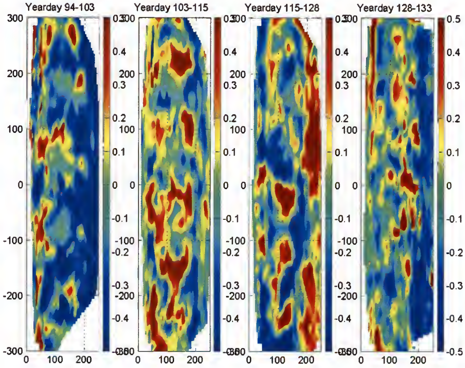

Figure 6.15 Bathymetric differences between periods of significant morphologic change.

The volume of sediment was calculated for the shore-connected shoals between depths -1.2 m (offshore minimum tidal elvation) and MWL (onshore). The volume of sediment within the rip channels was computed between -2.4 m to -1.2 m. The first survey was conducted on yearday 94. After yearday 94, four relatively short storms induced a significant amount of erosion (Figure 6.14,6.15) on both the shore-connected shoals and rip channels. Following the survey of yearday 106, the system began accreting and became stable around yearday 109. Once the system stabilized, an inverse relationship developed between erosion and accretion for the shore-connected shoals and the rip channels. While sediments accrete on the shoals, they are erode within the rip channels (and vice-a-versa) [Figure 6.14, 6.15]. A large storm occurred on yearday 122 (H_{mo}>2.6 m) eroding the beachface and redistributing the sediment within the sub-areal profile, smoothing out the alongshore variability (Figure 6.11). At the offshore extent, there is evidence that sediment is deposited offshore of the rip channel, evidenced by the ~3.5 m isobath bends slightly offshore (Figure 6.8). This is the location where the strength of the rip current is hypothesized to begin diminishing.

For two-dimensional beaches, the cross-shore movement of longshore sandbars tend to migrate seaward during intense storms due to significant wave breaking inducing strong offshore two dimensional return flows (undertow) [Thornton *et al.*, 1996; Gallagher *et al.*, 1998]. For two-dimensional shallow water wave conditions, a non-dimensional return flow is defined as

$$\frac{U_b}{\sqrt{gh}} = \frac{1}{8}\left(\frac{H_o}{h}\right)^2 \qquad (6.2)$$

where U_b is the mean return flow at breaking, H_o is the deep water wave height, and h is the local water depth. Shoreward bar migration (accretional beach states) has been associated with wave steepness (Johnson, 1949; Dean, 1973; Dalrymple, 1975), velocity skewness (Bowen, 1980; Bailard, 1981) and more recently by acceleration skewness (Elgar *et al.*, 2001). Dean (1973) used heuristic arguments, which included sediment suspension and settling, and determined that erosional and accretional trends could be determined by wave steepness and fall velocity parameter. Dalrymple (1975) modified equations by Dean (1973) and Kriebel *et al.* (1986) determined differences erosional and accretional states could be inferred by

$$\frac{H_o}{L_o} = 0.0007\Omega_o^3 \tag{6.3}$$

where H_o is deep-water wave height, L_o is deep water wave length, and Ω_o is the Dean number. This parameter is generally larger than 0.0007 $\Omega_o{}^3$ indicating that the beach is always eroding, and is therefore not a good proxy for determining accretional/erosional states for this complex beach system.

Rip Current Flow Kinematics

Morphologic features, wave forcing, and tidal elevation determine the flow characteristics of the rip current systems. Tidal fluctuations have been shown to modify the rip current flow characteristics, by increasing the rip currents flows to a relative maximum at low tidal elevations (Sonu, 1972;Aagaard *et al.*, 1997, Brander, 1999; Brander and Short, 2001). Mean velocity magnitudes (over 90 minutes) were computed for two sensors (PUV9, PUV6) located within two different rip current channels (Figure 6.4). The rip current velocities show a strong tidal modulation, with increasing speeds occurring with decreasing tidal elevation (Figure 6.16), concurrent with previous field observations (Sonu, 1972;Aagaard *et al.*, 1997, Brander, 1999; Brander and Short, 2001). Velocity magnitudes ($\sqrt{(u^2+v^2)}$)are computed as the sensors were relatively close to the feeder channels and the flow direction is not necessarily oriented offshore. Besides the temporal variability reflected in the nearshore flows by the tidal modulation, the rip current velocities are correlated with offshore sea-swell energy. Increases in wave height at high tide can also develop large return flows, an example of which is depicted in Figure 6.17.

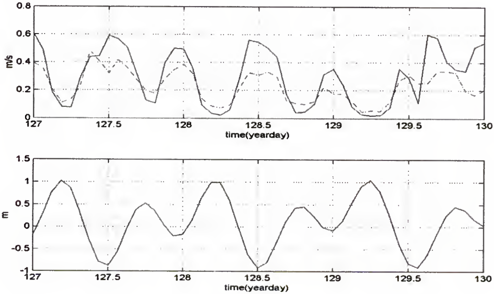

Figure 6.16 (top) Tidal modulation of rip currents speeds recorded within two different rip current channels for several days where the wave conditions were relatively constant; dashed line represents velocity magnitudes at PUV9, solid line at PUV6. (bottom) Concurrent tidal elevation measured at PUV6.

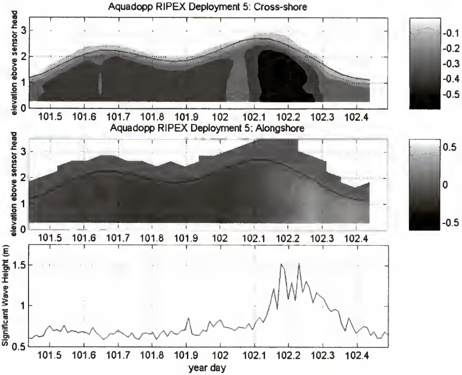

Figure 6.17 Measurements of vertical distribution of the cross-shore (top) and alongshore (middle) velocities as a function of tidal elevation within the rip current. (bottom) Significant wave heights measured at the sensor.

In general, flow is directed shoreward on the shore-connected shoals and seaward within the rip current channels. A histogram of occurrence of cross-shore and alongshore velocities are computed (Figure 6.18,6.19). The cross-shore flow is predominantly shoreward for instruments (PUV1,PUV2,PUV5) located on the shore-connected shoal and seaward for instruments (PUV6, PUV9, PUV10, PUV11) located within the rip channels throughout the experiment. There is a higher probability of seaward flow within the rip channel than shoreward flow over the shore-connected shoal (undertow). This suggests that there periods of time when the flow is seaward over the shore-connected shoal. Even though there is a return flow over the shore-connected shoal, flow is directed toward the rip channels, because of the alongshore velocities. The direction of alongshore velocities are relatively equal distributed for some instruments (PUV2,PUV6, PUV10) and directionally biased for other instruments, related to their location within the rip current celluar circulation (Figure 6.4). The morphologic evolution induces much of the directional variability in the alongshore currents (Figure 6.7).

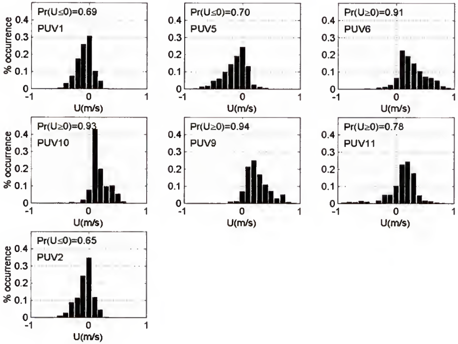

Figure 6.18 Histograms of 90 minute mean cross-shore velocities for yeardays 107-140. Positive U is offshore.

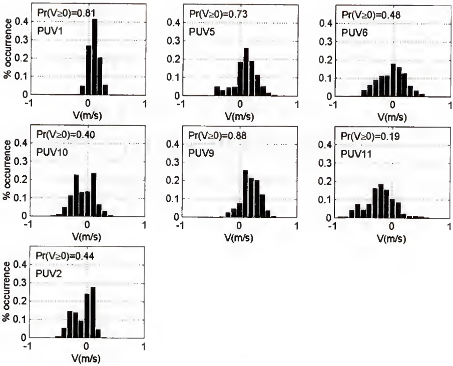

Figure 6.19 Histograms of 90 minute mean alongshore velocities for yeardays 107-140. Positive V is up coast.

The alongshore velocities varied in downcoast and upcoast orientation, which is related to the continuously evolving bathymetry. While approximately 75 m shoreward, PUV1 and PUV2 located within the alongshore array on the neighboring shore-connected shoal also consisted of onshore flows, though the magnitude is reduced. The alongshore velocities at these two sensor locations prefentially flowed toward the rip channel located at y=0 (RIP A), and were on the same order of magnitude in the cross-shore velocities (Figure 6.4). PUV10 was located within RIP A as well as close to the feeder channel associated with SHOAL A and the velocities were downcoast and offshore toward RIP A.

Three PUV sensors (PUV6,8,11) were all located across the channel in RIP A. These sensors measured significant offshore flows within the rip channels along with significant alongshore flows. PUV8 and PUV11 located on each side of the rip channel measured flows of the same order of magnitude directed toward the center of the channel. PUV9 located in RIP B had significant offshore flows similar in magnitude to PUV6 & PUV11 located in RIP A. PUV9 was located within the RIP B close to SHOAL C also had alongshore flows directed toward the center of RIP B.

Throughout the experiment, RIP A slowly migrated downcoast, which is reflected in rip current velocities at PUV8 that initially flowed upcoast turned and flowed downcoast. The local bathymetric differences can account for significant variations for the flow field within the rip channel. Thus, velocities are influenced by the local bathymetry, which was continuously being modified throughout the experiment. Haller and Dalrymple (2001) observed significant channel asymmetry of the cross-shore velocity components of the rip current, which they related to the variation in feeder channels. Even though the alongshore array was in approximately 1 meter depth at low tide, it was relatively close to the shoreline and is believed to be affected by the rip current feeder channels.

The vertical velocity profile (constructed from 8 electromagnetic current meters over the vertical) indicates that most of the flow on shore-connected shoal is shoreward and alongshore (Figure 6.20). There are periods, generally around high tides, when there is a seaward return flow. At high tides, waves generally break on the steep beachface inducing minimal alongshore variations in wave breaking creating a “quasi” two dimensional flow to exist. The presence of the rip channels still drain the surf zone.

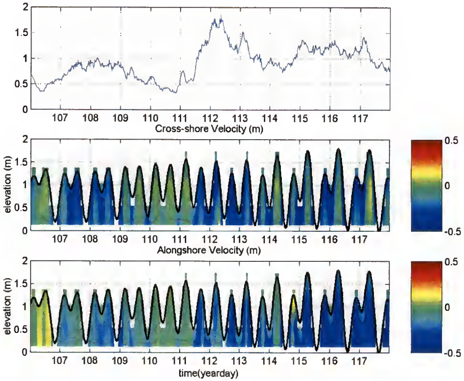

Figure 6.20 (top) H_{mo} provided for comparison (middle) hourly mean cross-shore profiles, (bottom) hourly alongshore profiles.

The velocities within rip channel increase with increasing sea-swell energy similar to observations by Shepard and Inman (1950). During the apex of storm for yearday 122, PUV9 located within the southern rip channel registered a maximum offshore flows of approximately 1 m/s, whereas PUV6 and PUV10 reached a maximum of approximately 1 m/s and 0.5 m/s, respectively. Interestingly for most of the experiment, the rip channels were visually apparent, due to the wave heights breaking on the shore-connected shoal and not within the rip channel (Figure 6.13). During the storm of yearday 122, wave heights exceeded of 3 meters with significant wave breaking occurring in the rip channel and the identification of rip channels was obscured by breaking waves. However, the measurements indicated that the return flow within the rip channels was significant.

Aagaard *et al.* (1997) and later by Brander and Short (2001) conceptualized that mass transport associated with waves over the longshore bar (shore-connected shoal) is entirely returned through the channel and achieved good correspondence for their field measurements. Wave mass-transport over the shore-connected shoal (Q_{in}) was computed by

$$Q_{in} = Q_{stokes} + Q_{roller} \tag{6.4}$$

$$Q_{stokes} = \frac{gH^2}{8C}\lambda_{rip}, Q_{roller} = \frac{0.9H^2}{T}\lambda_{rip} \tag{6.5}$$

where Q_{stokes} is the second order non-linear contribution and Q_{roller} is the mass transport due to the broken wave bore. The discharge over the shore-connected shoal is compared to the discharge out (Q_{out}) of the rip channel, defined as rip current velocity within the rip channel multiplied by the cross-sectional area. The Q_{out} is approximately half of the estimated Q_{in} (Figure 6.21). The additional flow contributions are associated with the nearshore pressure gradients. In the eulerian frame of reference, the shoreward mass transport occurs between the trough and crest region. The measurements are in an eulerian frame of reference predominantly below the trough-crest region and are not a measurement of Q_{stokes} and Q_{roller}. Additional flow shoreward and laterally occurs on the shore-connected shoal, presumably due to pressure gradients (Figure 6.18-6.20). Q_{in} is modified for the inclusion of $Q_{measured}$. This modification increases the total discharge over the shore-connected shoal to the approximately the same order of magnitude as Q_{out}, yet there still is significant amount of scatter amongst the data (Figure 6.22). Haller *et al.* (2002) determined that the integrated volume flux over an entire rip current cell was approximately zero for measurements below the trough without the inclusion of wave mass-transport, which is not the case here.

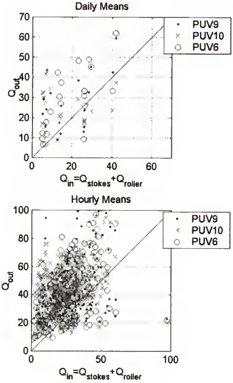

Figure 6.21 (top) daily and hourly (bottom) estimates of shore-connected shoal and rip channel discharge.

The beach system of Aagaard *et al.* (1997) is represented by a longshore bar-trough beach with a rip channel incised through the longshore bar. Thus, one might assume that when waves break on the bar that the mass flux is piled up within the longshore trough and is returned through the rip channel. However, Svendsen and Haas (2000) indicate that for thier

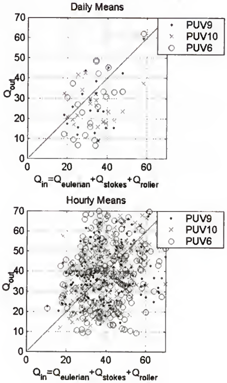

Figure 6.22 (top) daily and hourly (bottom) estimates of shore-connected shoal and rip channel discharge.

rip current spacing, a maximum of 35% wave flux is returned through the rip channel. It is less clear why the model works for the beach system of Brander and Short (2001), which is characterized as a low-tide terrace with incised rip channels, similar to the observations here. In this is more complex system, the mass flux is hypothesized to be most efficiently returned by flowing laterally directly into the channels, which is characterized by the measurements (Figure 6.18-6.20). PUV1 and PUV2 are located near the centerline of the shore-connected shoal, and indicate a significant amount of alongshore flow. The flow is larger at PUV1, due to continuity, since the water depth is shallower. The enhanced rip current flow associated with the mass transport of the roller is hypothesized to increase at mid to low tide, because of the saturation of wave breaking on the outer shoal, while at high tide the waves do not break here and is predominantly a function of Stokes drift.

Haller *et al.* (2002), in a laboratory setting, computed the volume flux per unit width over the bar and through the rip channel and found a linear relationship. Dronen *et al.* (2002), also in a laboratory setting, and Haller *et al.* (2002) found a linear relationship between dimensionless rip current velocity (Froude number) and normalized wave height (H_o/h_{shoal}), Eq 1. Note Haller *et al.* (2002) used the local water depth within the rip channel and Dronen *et al.* (2002) utilized the water depth over the shoal. Evaluating these parameters for 90 minute mean speeds ($\sqrt{(u2 + v2)}$) for sensors (PUV4,6,9,10) within the rip channel, illustrates an approximate linear relationship for $H_o/h_{shoal} < 1$ (Figure 6.23). For $H_o/h_{shoal} > 1$, the dimensionless return flow approaches a relative maximum. For $H_o/h_{shoal} > 1$, the waves on the shore-connected shoal become saturated (breaking wave heights are approximately constant) and the local mass transport does not increase. PUV4 was originally located within the rip channel, but as the rip channels slowly migrated downcoast, it became part of the shoal/feeder current system. This would cause the velocity to achieve a maximum before sensors located deeper within the rip channels.

PUV9 and PUV10 are located in relatively the same depth, though in different rip channels, and have a similar upper limit. While PUV6 was located slightly further offshore than PUV11, and it was centered more within the rip channel, it has a higher upper dimensionless return flow limit. The results for Dronen *et al.* (2002), indicate that their data begin to approach an upper limit with a dimensionless return flow velocity of 0.6 in the proximity of H_o/h_{shoal}. This result is slightly higher than our results, because the local water depth (h) was taken over the shoal and not within the rip channel. The dataset of Haller *et al.* (2002) does not appear to reach an upper limit, even though measurements occur at H_o/h_{shoal} of approximately 3, which may be associated with using monochromatic waves.

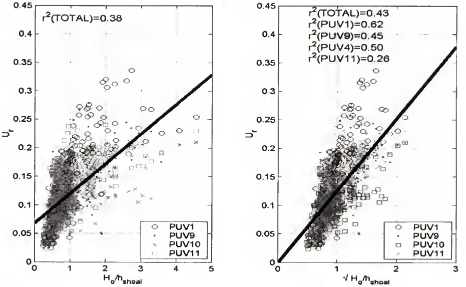

Figure 6.23 Dimensionless return flow, Ur, as function of H_o/h_{shoal} (left) and (H_o/h_{shoal}) (right) for 90 minute mean rip current flows measured at PUV1,9,10,11 for yeardays 107-140. Solid line represents least-squares linear fit for all sensors, total and individual sensor r^2 are presented.

Seabreeze Influence

Time series of significant wave height, wind speed, wind direction, nearshore current velocities, tidal elevations during two local sea breeze events for yearday 134-135 are shown in Figure 6.24. The background significant wave height is 0.5 meters and increased by approximately 0.5 m coinciding with the onset of sea breeze. The sea breeze for yearday 134 is correlated with increase in H_{mo} at PUV6. While a sea breeze event also occurs during yearday 135, the increase in wave height begins before the event. The onset of sea breeze for yearday 134-135 indicate that the rip current cross-shore velocity increases by approximately 20 cm/s during high tide and is of the same order of magnitude as the preceding low tide. The longshore velocity increased by 15 cm/s during the sea breeze event.

Summary

Detailed observations of morphology and hydrodynamics are documented on a complex beach located in Sand City, Monterey Bay, CA. During the course of the experiment, the morphology within the same morphodynamic state experienced significant erosional and accretional periods. There is an inverse relationship between erosional and accretional trends for the rip channels and shore-connected shoals, similar to observations of Brander (1999). The sediment distribution is representative of the morphologic features and the hydrodynamic setting.

Temporal variations in mean rip current velocities are related to tidal elevation, offshore sea-swell conditions, and diurnal sea breeze events. The rip current flows increase with decreasing tidal elevation, with increasing sea-swell energy, and with increasing energy during local sea breeze conditions. Rip current flows have similar relationships as found in laboratory measurements, yet the upper limit was not achieved in the laboratory.

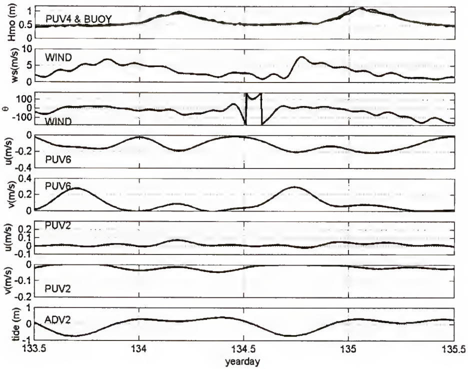

Figure 6.24 Offshore wave height at ADV2 showing increases in wave height associated sea breeze events. Cross-shore and alongshore velocity components for sensors within the rip channel and on the shore-connected shoal. Tidal elevation provided as reference.

CHAPTER 7
RIP CURRENT PULSATIONS

Introduction

Rip currents are strong shore-normal (jet-like) flows that originate within the surf zone and are directed seaward through the breakers, and have been known to reach velocities up to 2 m/s (Short, 1985). Field measurements of rip currents for the most part are based on visual observations, which introduce a high level of subjectivity to the data analysis and subsequent conclusions. Shepard *et al.* [1941] and Shepard and Inman [1950] provided some of the initial qualitative insight on rip current behavior on La Jolla Beach, California for which they found that the intensity and the distance that rip currents extended seaward increased with increasing wave height, and that the rip currents pulsed on the same time scale as the approaching wave groups.

Sonu [1972] extended the work by Shepard and Inman [1950] by obtaining some detailed quantitative measurements. Though his measurements were short in duration, rip currents also appeared to pulse on wave group scales and the magnitudes intensified during low tide conditions. Sonu [1972] placed one instrument within the rip channel and one on the shoal for a low and high tide cycle. He found that the infragravity velocities (rip current pulsations) were 90° out of phase with the infragravity elevation and suggested this relationship was representative of a infragravity standing wave. There have been only a few field measurements of rip currents owing to the extreme difficulty in deploying instruments within the rip current channels, which tend to migrate alongshore. More recent field studies investigating rip currents (Aagaard *et al.*, 1997; Smith and Largier, 1995; Brander 1999; Brander and Short, 2000; Brander, 2001) all noticed rip current pulsations on infragravity time scales in the measured rip current velocities. However, these latter experiments only focused on rip current measurements (within the rip channel); offshore wave measurements were not available to determine relationships between rip current behavior and the approaching wave groups. In addition, the surveying techniques did not provide the high resolution nearshore bathymetry necessary for a complete understanding of the processes.

Rip current pulsations generally have been attributed to modulations by surf beat resulting from the groupiness of the incident waves. Oscillations associated with rip currents can also be induced by shear instabilities as observed in the laboratory (Haller and Dalrymple, 2001), similar to those of longshore current instabilities (Oltman-Shay *et al.*, 1989). These motions generally occur at higher wave numbers than those of infragravity motions and can be quite energetic. This behavior was observed in the RIPEX-SBE field measurements, but is not the focus of this chapter (see chapter 8; Reniers *et al.*, 2003b).

Since the initial observations of surf beat (Munk, 1949, Tucker, 1950), a significant amount of research has been focused on the understanding of these motions, also referred to as infragravity waves. In general, infragravity waves are related to the modulation of the short-waves, generally referred to as wave groups. Infragravity waves can be subdivided into two primary waves: 1) (in the cross-shore) leaky waves that reflect off the beach and radiate offshore, and 2) (in the alongshore) edge waves that are trapped to the shoreline owing to refraction. Infragravity energy increases with decreasing depth, while short-wave energy dissipates due to wave breaking with decreasing depth (Suhayda, 1974, Huntley, 1976, Huntley *et al.*, 1981, Holman, 1981, Wright *et al.*, 1982, Guza and Thornton, 1982, amongst others). The infragravity energy is generally not affected by wave breaking and its contribution is most significant close to the shoreline. (Wright *et al.*, 1982, Guza and Thornton, 1982). Though most of the infragravity energy is attributed to the free long waves, the bound long waves coupled to the incident wave groups also make a significant contribution to the total infragravity spectrum (Okihiro et al, 1992, Elgar *et al.*, 1992, Herbers *et al.*, 1994, Ruessink, 1998).

The exact mechanism for the formation of infragravity waves is still unclear despite the extensive field and laboratory measurements, and theoretical investigations. Longuet-Higgins and Stewart [1962, 1964] postulated that bound infragravity waves are forced by spatial variations of momentum flux associated with the short wave group. Neglecting any mean currents and bottom shear stress, the cross-shore momentum equation is a balance of the cross-shore radiation stress, S_{xx}, (wave momentum flux) gradient with changes in the hydrostatic pressure owing to slow variations of the sea surface elevation, $\eta(x,t)$,

$$\frac{\partial \eta}{\partial x} = \frac{-1}{\rho(gh - C_g^2)} \frac{\partial S_{xx}}{\partial x} \tag{7.1}$$

where ρ is density of sea water, g is gravitational acceleration, and h is water depth (Longuet-Higgins and Stewart, 1964). Assuming that the bottom is locally flat and that η

<< h except very near the beach, and approximating the radiation stress with shallow water wave theory, Eq. 7.2 can be integrated to give

$$\eta(x,t) = -(2\frac{C}{C_g} - \frac{1}{2})\frac{E(x,t)}{\rho(gh - C_g^2)} \qquad (7.2)$$

where E is the modulated short wave energy, C_g is the group velocity, and C is the phase velocity, and the constant of integration is zero to conserve mass. The variations in η result in a long wave forced (or bound) by the short wave groups that travels 180° out-of-phase (represented by the negative sign) with the short wave energy modulations. Within the surf zone, the bound long wave is released as a free wave as the short wave groups dissipate due to breaking, and is reflected seaward at the shoreline.

A second proposed mechanism is that the temporal variations of wave breaking associated with short-wave groups act like a wave-maker generating infragravity motions onshore and offshore (Symonds *et al.,* 1982). A third hypothesis suggested by Gallagher (1978) is resonant forcing of edge waves by the swell wave difference frequencies and their alongshore wave number, k_y, matching the dispersion relationship for edge waves given by (Eckart, 1951),

$$\omega_e = \sqrt{gk_y(2n+1)\tan\beta} \qquad (7.3)$$

where ω_e is the edge wave radial frequency, g is acceleration due to gravity, n is the modal number, and β is the slope of the assumed plane beach.

The focus of this chapter is to describe the relative importance of infragravity motions on a complex beach system, and in particular their influences on rip current hydrodynamics with emphasis on rip current pulsations. Two hypotheses are proposed for rip current pulsations. The first is that the rip current pulsations are simply due to the infragravity wave motion as mentioned by Sonu [1972]. The second hypothesis is that maxima of the envelope of the groupy waves, through mass transport and forced long waves, transport and pond significant amounts of water within the surf zone (Munk, 1949, Shepard and Inman, 1950, Symonds *et al.*, 1982). During the subsequent minima in the wave groups, the ponded water seeks to return outside the surf zone. Initially, this return may occur more or less uniformly across the shoal; however, any small low area (incision) in the bar will be more hydraulically efficient resulting in a stronger flow through the rip channel. Previous field experiments did not obtain measurements both on the shoal and within the rip channel, except for Sonu[1972] which were relatively short in duration, so to date these hypotheses could not be properly evaluated.

In the following, a description of the field site and instrument arrays is presented in *The RIPEX-SBE Experiment* (below). The infragravity spectral estimates for the cross-shore and alongshore array and frequency-wavenumber spectra are discussed in *Observations of Infragravity Energy* (below). *Rip Current Pulsations* (below) qualitatively analyzes the cross-shore structure of the infragravity motions and their relationship with rip current pulsations. This is followed by a *Discussion* and *Conclusions*.

It is noted that this chapter is part 1 of a two part effort, and focuses on the data analysis and interpretation of processes. Part 2 (Reniers *et al.*, 2003a) focuses on modeling of the process. The data analysis interpretation benefits from the higher resolution model results, and the model veracity is demonstrated by the data analysis. On the other hand, the data analyses complement the modeling efforts and have stimulated new avenues to pursue that could only be identified by the model.

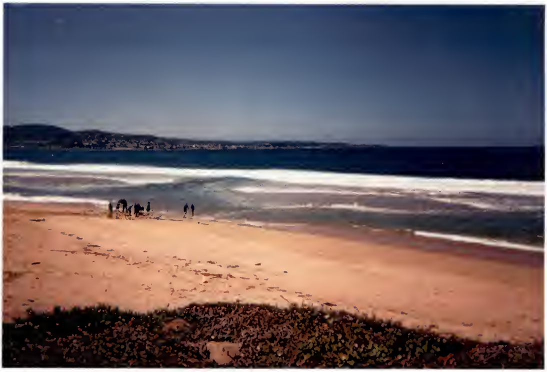

Figure 7.1 A snap shot picture of the RIPEX-SBE field location at the beginning of the experiment during low tide. Dark swaths represent the rip current channels and the light brown areas are the shore-connected shoals.

The RIPEX-SBE Experiment

A RIP current field EXperiment (RIPEX) was perfomed in conjunction with a Steep Beach Experiment (SBE) during the months of April and May 2001 in Sand City, CA located in Southern Monterey Bay. A snap shot picture of the experiment at

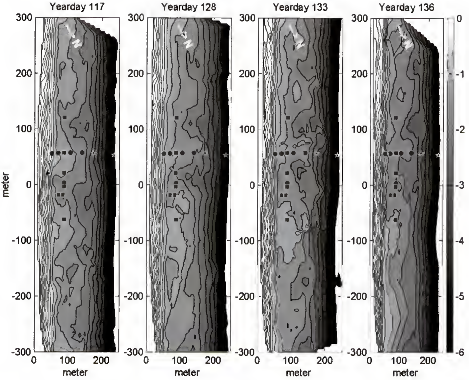

Figure 7.2 Bathymetric contour plots obtained from two methodologies 1) hydrographic survey system mounted aboard a personal watercraft (high-tide) and 2) water-tight back-pack mounted to a person (low-tide). The dots indicate pressure sensors, squares represent co-located pressure and bi-directional electromagnetic current meters, triangles represent ADCPs, and stars indicate acoustic doppler velocimeters.

the beginning of the experiments (Figure 7.1) illustrates the relatively planform layout of the rip current channels and shore-connected shoals at low tide. The foreshore of the beach was steep with a slope between 1:5 and 1:10 with beach cusps spaced at O(35 m). The profile flattened out to a low-tide terrace (1:100) incised with quasi-periodic O(150 m) rip channels, and then continued offshore with a 1:20 slope (Figure 7.2-7.3). This morphology is characterized as an intermediate beach system with transverse bars (shore connected shoal) and rip current channels (Wright and Short, 1983). Wave breaking occurred at the outer edge of the shoals during both high and low tide (except for low wave energy events when waves break directly on the beach).

The bathymetry was surveyed four times within the 20-day observation period using a real-time kinematic-differential global positioning system (KGPS) mounted on a personal watercraft (Chapter 4), at high-tide and using a KGPS backpack mounted on a person at low tide. Significant changes in the morphology occurred between surveys (compare the panels in Figure 7.2), suggesting that the surveys are synoptic in time but under sampled. The bed-level changes at the cross-shore array (upper panel of Figure 7.3) show strong erosion during the storm (yearday 122), though the profile shape stayed more or less the same. This is not the case for the bed-level at the alongshore instrument array (lower panel of Figure 7.3), where the changes were dramatic within rip/feeder-channels. The rip/feeder-channel located around $y = 125$ m actually disappears during the course of the experiment (panel b of Figure 7.2) and reappears at a later date (bathymetries at year days 133 and 136 in Figure 7.2). The rip-channel north of the shoal array.

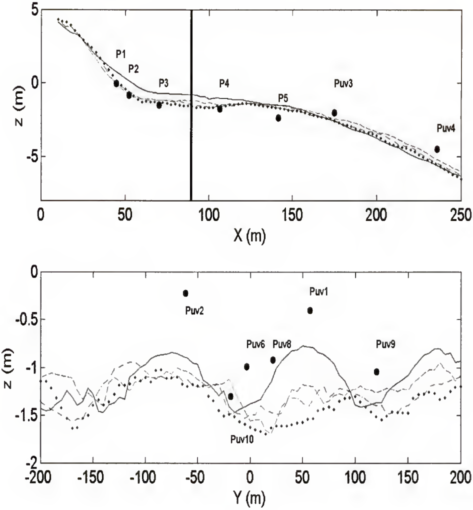

Figure 7.3 Cross-shore profile (top) and alongshore profile (bottom) corresponding to the instrument arrays from the measured bathymetry (Figure 7.2) for yeardays 117 (solid), 128 (dashed),133 (dashed-dotted), 136 (dotted). The vertical dashed line (top) is the location of the alongshore array. Instrument positions and elevations are represented by black dots.

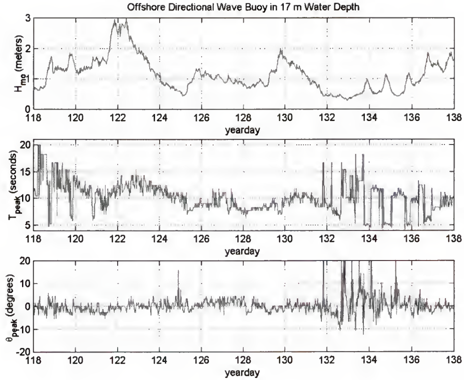

Figure 7.4 Directional wave buoy located in 17 m water depth, approximately 650 m offshore, (top) significant wave height (middle) peak wave period, and (bottom) peak wave direction.

propagated south during the period considered, resulting in the burial of PUV11 (lower panel of Figure 7.4), which was subsequently raised approximately 30 cm to continue measurements. The morphodynamics of the RIPEX/SBE experiment are discussed in Chapter 6.

The sea-swell and infragravity structure across the shore-connected shoal were measured with a cross-shore array of five pressure sensors. Velocities in the alongshore over the shore-connected shoal and rip channels were measured using an array of six two component electromagnetic current meters located approximately 50 meters offshore with respect to the mean shoreline (x=90 m in the local coordinate system). Additional instruments were deployed to extend the spatial coverage of the two primary arrays (see Figure 7.2). The current meters within the rip channels were oriented downward in order to obtain measurements during lower tidal elevations. Current meters on the shoal were oriented upward, resulting in their exposure at low tides. All instruments considered in this paper were synchronously sampled at 8 Hz throughout the duration of the experiment. The total suite of instruments provides an appropriate basis for capturing the temporal and spatial coverage of the swell, infragravity, and rip current dynamics.

The offshore wave climate, obtained using a directional Wave-Rider buoy located approximately 650 m offshore in 17 m depth, shows considerable variation in both wave height and wave period during the experiment (yearday 100-140) (Figure 7.4). The significant wave heights and peak periods ranged from 0.20-3 m and from 5 –20 s. Four storm events occurred around yeardays 122, 126, 130, and 138 during the experiment. The largest storm occurred on yearday 122 producing wave heights of up to 3 m. Diurnal sea breeze effects occurred between yeardays 134-137 creating high frequency motions on top on the typical swell wave climate. In view of the large temporal variability in wave height and period, the mean wave incidence angle shows surprisingly little variation with a predominant direction normal to shore. This lack in directional variability is associated with a relatively narrow aperture owing to the sheltering effects of the headlands of the bay, and strong refraction over Monterey Bay Canyon (Chapter 6), (Figure 7.4).

Observations of Infragravity Energy

Cross-shore and Alongshore Spectral Statistics

Since previous observations of rip current pulsations (Shepard and Inman, 1950; Sonu, 1972; Smith and Largier, 1995; Brander,1999) have documented occurrences on time scales of wave groups, the infragravity motions from outside the surf zone to close to the shoreline are analyzed using the cross-shore array measurements. Spectral estimates are generated from four 1024-s segments giving 8 degrees of freedom and a frequency resolution of 0.001 Hz. The total record (4096-s) was quadratically detrended to remove the tidal signature and each segment was demeaned before Fourier transformations were performed. Band-passed standard deviations are obtained by integrating the energy density spectrum within the infragravity band (0.004-0.04 Hz) and the sea-swell frequency band (0.04-0.35 Hz), given by

$$\sigma = \sqrt{\int_{f1}^{f2} E(f)df} \tag{7.4}$$

where E(f) is the spectral energy density as a function of frequency, f1 and f2 are the lower and upper limits within the frequency range, and $\sigma_\eta, \sigma_u, \sigma_v$ are the standard deviation for the sea surface elevation, cross-shore velocity, and the alongshore velocity within each of these two frequency bands, infragravity (lo) and the sea-swell (hi). H_{rms} is defined as $2\sqrt{2}\sigma_\eta$, and U_{rms} (V_{rms}) are defined as σ_u (σ_v) for the respective frequency ranges. The local sea-swell wave height is obtained by transforming the measured pressure spectra to surface elevation spectra using linear wave theory and integrated from 0.04 Hz to 0.35 Hz. For pressure sensors that were buried below the bed, the transformation defined by Raubenheimer *et al.* [1998] was utilized. Average sea-swell and infragravity wave periods are computed by

$$T_{m01} = \frac{\int_{f1}^{f2} E(f)df}{\int_{f1}^{f2} fE(f)df} \tag{7.5}$$

defined as the first moment wave period. This spatially integrated measure is used instead of peak frequency determined from the spectrum owing to the sensitivity of peak estimates to the frequency resolution.

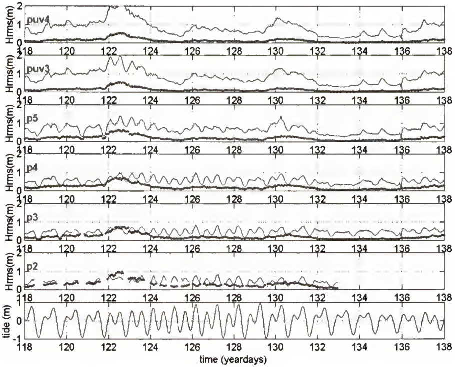

Figure 7.5 Time variation for the cross-shore array of $H_{rms,hi}$ and $H_{rms,lo}$ (bold line). Tidal elevation included for reference (bottom panel).

The time variation of wave height (H_{rms}) for both the sea-swell waves and infragravity waves across the beach profile are presented in Figure 7.5. The offshore sensor, PUV4, located in 6 m water depth, was generally well outside of the surf zone, except for the storm which occurred on yearday 122 (Figure 7.4). PUV3, located in 3 water depth, experiences wave breaking during storm events ($H_{rms,hi} > \sim 1.2$ m). P5 (2 m water depth), P4 (1.5 m water depth), P3 (1 m water depth), and P2 (1 m water depth) were all positioned on the shore-connected shoal. P5 located on the outer edge of the shoal exhibits times of wave breaking, whereas P4, P3, and P2 were generally inside the saturated surf zone induced by wave breaking, except during times of very low wave energy. $H_{rms,hi}$ on the shoal decreases with decreasing depth due to wave breaking and exhibits a strong tidal modulation similar to observations made by Thornton & Kim [1993]. The tidal modulation is more apparent for sensors shoreward of P5.

In contrast to $H_{rms,hi}$, $H_{rms,lo}$ increases with decreasing depth, and levels off to a relative maximum around P4, but still increases shoreward (Figure 7.5). The ratio of the $H_{rms,lo}$ at various cross-shore locations relative to PUV4 is two times greater within the surf zone than outside of wave breaking (Figure 7.6). The infragravity wave height does not vary with tidal elevation, which is similar to observations made at Duck, NC (Lippmann *et al.*, 1997). The low frequency wave amplitude varies predominantly as a function of the incoming storm energy; this is similar to previous observations (Holman, 1981, Guza and Thornton, 1982, Lippmann *et al.*, 1999, and others). In general, the infragravity energy increases shoreward from PUV3.

For more detailed explanations of the nodal structure and infragravity wave period, see Reniers *et al.*, 2003a. The wave period ($T_{mo1,lo}$) for infragravity waves at PUV4 is approximately 48 ±5 s where the periods are weakly modulated by tidal elevation, reaching a relative maximum at low tides. The computations of $T_{mo1,lo}$ are sensitive to energy density frequency distributions which vary tidally due to the nodal structure of the standing infragravity wave (Suhayda, 1974; Guza and Thornton, 1982; amongst others). Therefore sensors shoreward of PUV4 have slightly different values of $T_{mo1,lo}$ but all are approximately 50 ± 5s. Though there is a small variation in $T_{mo1,lo}$ tidally, it remains constant throughout the experiment. $T_{mo1,lo}$ for the alongshore array for U and V velocity components is also approximately 50s.

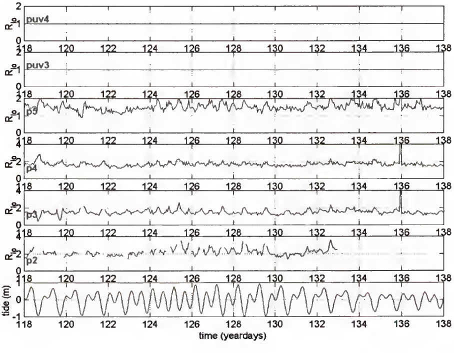

Figure 7.6 Time variation of cross-shore ratio of $H_{rms,lo}$ relative to PUV4. Tidal elevation included for reference (bottom panel).

The alongshore array traversed across the shore-connected shoals and rip channels (Figure 7.3) and consisted of co-located puv sensors; unfortunately, not all of the pressure sensors were operational throughout the deployment. Therefore, the analysis of the alongshore infragravity motions is primarily composed of U and V velocity components, corresponding to the cross-shore and longshore velocities, respectively. The $U_{rms,hi}$ is typically greater than $U_{rms,lo}$, except for certain conditions around low tide and during the storm events (Figure 7.7). Both $U_{rms,hi}$ and $U_{rms,lo}$ exhibit a small amount of tidal modulation, which is more apparent in the high-

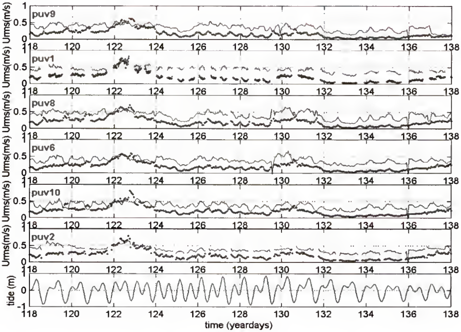

Figure 7.7 Time variation of alongshore array of $U_{rms,hi}$ and $U_{rms,lo}$ (bold line). Tidal elevation included for reference (bottom panel).

frequency band. The tidal modulation of $U_{rms,lo}$, given the non-tidal modulation observed in $H_{rms,lo}$, can be explained by the long wave relationship (ignoring bottom slope)

$$U_{rms,lo} = \eta_{rms,lo}\sqrt{\frac{g}{h}} \tag{7.6}$$

(Dean & Dalrymple, 1984). This relationship was evaluated using hourly statistics at PUV11, located within the rip channel, where both the electromagnetic current meter and pressure sensor

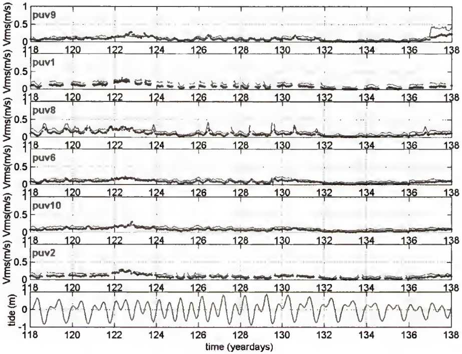

Figure 7.8 Time variation of the alongshore array for $V_{rms,hi}$, $V_{rms,lo}$ (bold line). Tidal elevation included for reference (bottom panel).

were operational throughout the experiment (Figure 7.9). The measurements support the linear theory relationship (Eq. 7.6) with an r^2 value of 0.93. The relationship is biased low, suggesting that there are no additional contributions of velocity motions. The long wave relationship explains infragravity velocities weak dependence on depth ($\sqrt{h^{-1}}$), which is discussed in further detail in the companion paper (Reniers *et al.*, 2003a). Both $U_{rms,hi}$ and $U_{rms,lo}$ are significantly larger than the corresponding alongshore counterparts (Figure 7.8). However, unlike the differences between $U_{rms,hi}$ and $U_{rms,lo}$, there is little difference between $V_{rms,hi}$ and $V_{rms,lo}$.

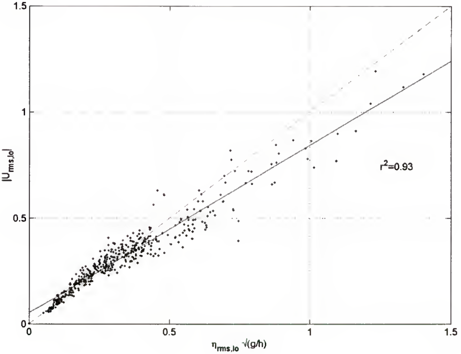

Figure 7.9 Comparison of long wave relationship (Eq. 7.6) computed at PUV11 for yeardays 118- 138. Linear regression results in a slope of 0.79, a y-intercept of 0.05, and r^2 of 0.93. Dashed line represents a prefect agreement for the long wave relationship.

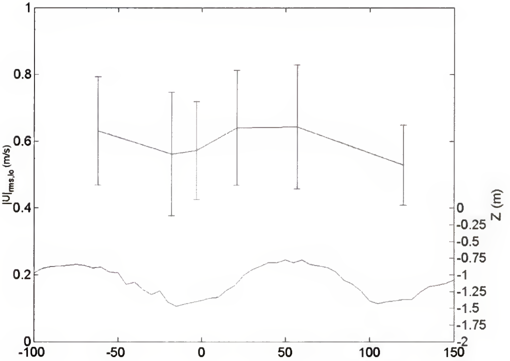

Figure 7.10 $|U_{rms,lo}|$ mean and standard deviations for yearday 122 for the alongshore array. The depth at the alongshore array is provided for reference.

Interestingly, the infragravity motions ($U_{rms,lo}$, $V_{rms,lo}$) in the rip channels are less than on the shoals, contrary to the general notion that the rip current pulsations are significantly larger within the rip channel. Small alongshore variation of the infragravity energy occurs even though there are relatively large alongshore differences in the bathymetric elevations. In order to remove any potential bias associated with current sensor-head orientation (misalignment with the shoreline), the speed $|U_{rms,lo}|$ is computed. The mean and standard deviation of $|U_{rms,lo}|$ are computed for velocity senors in the alongshore for yearday 122 (Figure 7.10). The smaller magnitude of the long wave velocities are less within the rip channels than on the shore-connected shoals is explained by the long wave relationship (Eq. 7.6). The following section analyzes the modal structure of the infragravity motion.

Edge Waves & Leaky Waves

Frequency-wave number spectra, $S(f,k_y)$, are computed from cross-shore and alongshore velocity measurements for the alongshore array using the iterative maximum likelihood estimator (IMLE) developed by Pawka [1983] and later evaluated by Oltman-Shay and Guza [1987]. Since infragravity motions of U and V in the alongshore are relatively uniform, we assume that the instrument measurements are statistically stationary (in the infragravity band) and homogeneous in space so that we can use the alongshore lag array to estimate the $S(f,k_y)$ spectra to discriminate between various modes of edge and leaky waves (Huntley, et al, 1981; Oltman-Shay and Guza, 1987). Owing to different instrument locations, each cross-spectral value was normalized such that the diagonals of the cross-spectral matrix are unity. Spectral estimates are generated from 4.55 hour records consisting of 32 segments giving 64 degrees of freedom and a frequency resolution of 0.002 Hz. Again, the total records were quadratically detrended to remove the tidal signature and each segment was demeaned before Fourier transformations were performed.

Ozkan-Haller *et al.* [2001] documented the existence of standing edge waves for a small pocket beach resulting from resonances related to the alongshore width of the beach for which the IMLE is invalid. Normalized alongshore infragravity and sea-swell spectra (Reniers *et al.* 2003a) were evaluated for the presence of standing edge waves to determine whether the IMLE analysis is appropriate. The normalized alongshore spectra indicate no wave-form structure (i.e. nodal points) so that the application of IMLE should provide reasonable results.

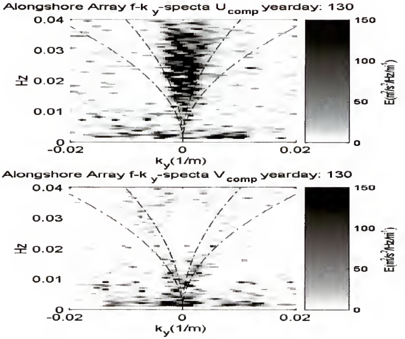

Figure 7.11 Frequency-wavenumber spectra for cross-shore velocities (upper panel) and alongshore velocities (lower panel) for the alongshore array computed for yearday 130; 64 DOF, df=0.002 Hz.

Even though the field measurement site is non-planar with quasi-alongshore periodic rip channels, the simple planar beach solution for edge waves is utilized to provide a conceptual understanding of the distribution of energy by frequency and wave number. An effective plane beach slope was determined for zero mode edge waves and for first mode edge waves (see Reniers *et al.*, 2003a) [Figure 7.11]. Low modes (modes 0-2) correspond to propagating edge waves, while high modes (modes >2) are undistinguishable from leaky waves within the surf zone.

The cross-shore velocity f-k_y-spectra (Figure 7.11) demonstrate that high mode edge waves and/or leaky waves are dominant, consistent with previous measurements on alongshore uniform beaches (Guza and Thornton, 1985). The nodal structure of the f-k_y-spectra suggests that the surf beat motion is primarily standing. The nodal structure varies slightly as a function of tide, due to the variation in the shoreline and shape of the profile. Note that there is a significant amount of energy at the very low frequency band (<0.004 Hz) in Figure 7.11; these motions are discussed in Chapter 8 and Reniers *et al.*, 2003b.

Analysis of f-k_y spectra throughout the experiment demonstrate that zero mode edge waves are dominant for the alongshore infragravity velocities (Figure 7.11). Interestingly, there is minimal energy along the mode1 edge wave dispersion curve. Renier et al., 2003 suggest that the instrument array was unfortunately positioned at cross-shore node for mode 1 edge waves. Further examination of edge wave nodal structure for a complex beach is explored by the Reniers et al., 2003b.

Results of f-ky spectra are consistent with observation of edge wave motions for open coastal beaches (Huntley *et al.*, 1981, Oltman-Shay and Guza, 1997), though the energy is not as broad-banded, and is most likely related to predominantly shore normal swell associated with this beach (Figure 7.5). Throughout the experiment low-mode energy propagated upcoast (+k_y) and downcoast (-k_y), consistent with previous observations at other open coast beaches, which show approximately similar amounts of upcoast and downcoast directed low-mode energy (e.g., Oltman-Shay *et al.*, 1989, Herbers *et al.*, 1995). On occasions, there is preferential downcoast directed low-mode energy which is observed in Figure 7.11.

Cross-Shore Structure of Wave Groups & Long Waves

The groupiness of the surface elevation (a measure of the infragravity wave bandwidth) is calculated from the short wave envelope, A(t). The wave envelope is obtained by low-pass filtering (cut-off frequency is 0.04 Hz) the Hilbert transform of the surface elevation at the sea-swell band (0.04- 0.35 Hz) [List, 1991]. The coefficient of variation, representative of the groupiness of the short-waves, is defined as

$$COV = \frac{\sigma_A}{\overline{A(t)}} \tag{7.7}$$

where is σ_A is the standard deviation of the envelope amplitude, and $\overline{A}(t)$ is the mean of the wave envelope. High values of COV indicates groupy waves with COV= 0.5 for two beating waves, while monochromatic waves represent the lower zero limit. High values of COV suggest that the mechanism for the generation of bound long waves (Longuet-Higgins and Stewart, 1962, 1964; List, 1991) or an infragravity wave-maker (Symonds et al, 1982) is present. A relatively high COV factor at around 0.4 was measured at PUV4 throughout the experiment and decreased with decreasing depth for subsequent inshore sensors (Figure 7.12). The decrease in COV is related to the destruction of the short-wave envelope due to wave breaking. The COV also modulates with tidal elevation due to depth limited breaking. Though there is a decrease in wave groupiness factor for most sensors on the shore-connected shoal located within the surf zone, there is still a presence of group-like structures, similar to observations by List [1991].

The wave group consists of the largest short waves traveling at the trough of the bound long wave, and since these short waves experience depth-limited breaking first, a shift in maximum of the wave envelope occurs in the vicinity of the unbroken short waves. This results in the short wave envelope propagating in-phase with the bound (free) long wave, resulting in a group-like structures within the surf zone (Abdelrahman and Thornton, 1988; List, 1991, Janssen *et al.*, 2000). An example of these processes occurs at P3 for yeardays 119-123 (Figure 7.12) where the COV decreases for PUV3, P5, and P4, but increases for P3 since wave breaking initiated further offshore allows this process to develop.

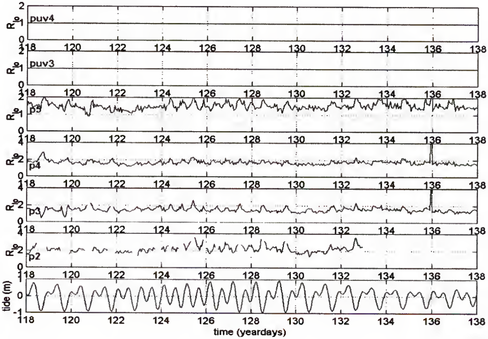

Figure 7.12 Time variation of COV for pressure sensors in the cross-shore array. Tidal

elevation included for reference (bottom panel).

The cross-shore propagation of wave groups and long waves is examined by calculating cross-correlation functions of the envelope of the short-wave energy and long wave elevation to provide a qualitative understanding of infragravity energy and the mechanisms related to the rip current pulsation behavior. This methodology is adopted from Abdelrahman and Thornton [1988] who investigated short wave groups and long waves in the field and Janssen *et al.* [2000] who investigated the process on a uniform slope in a laboratory setting.

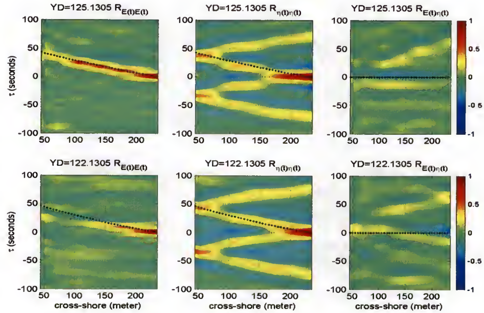

Figure 7.13 Cross-correlation between the measured offshore wave envelope to subsequent inshore wave energy measurements (left column), cross-correlation between offshore long wave elevation to subsequent inshore long wave elevation (middle column), and cross-correlation between the wave energy and long wave elevation for each subsequent inshore sensor (right column) for both a storm event on yearday 122 (lower row) and low wave energy event on yearday 125 (upper row). The dotted line represent the theoretical time lag for a dispersive wave at the group velocity.

The short wave group energy, E(t), is calculated from the short wave envelope, A(t),

$$E(t) = \frac{1}{2}\rho g A(t)^2 \tag{7.8}$$

The cross-shore propagation of the short wave group energy can be inferred from the cross-correlation between the short wave energy, E(x,t), evaluated at the furthest offshore pressure sensor (PUV4) with subsequent pressure sensors inshore, given by

$$R_{x_1 x_i}(x_i, \tau) = \frac{< E(x_1,t)E(x_i,t+\tau) >}{\sigma_{E(x_1,t)}\sigma_{E(x_i,t+\tau)}} \tag{7.9}$$

where subscript < > represents the ensemble average, τ is the associated time lag, subscript 1 refers to the offshore sensor PUV4 and subscripts i represent subsequent sensors in the cross-shore. The cross-correlation function has been normalized by the standard deviation for each signal. The value of the normalized cross-correlation function varies between -1 and +1.

Two wave events at high tide are examined in detail, a low wave energy event on yearday 125 (Figure 7.13, upper panels) and a large storm event on yearday 122 (Figure 7.13, lower panels). For the relatively small wave heights on yearday 125 (Figure 7.13, upper left panel), the shoreward propagating energy is identified by a ridge of high positive cross-correlation with increasing time lag moving shoreward, and then disappearing at about cross-shore distance 60 m where the waves break on the beach.

The theoretical time lag for a dispersive wave to propagate at the group velocity over a sloping bed between the two locations, is given by

$$\Delta t = \int_{\Delta x} \frac{dx}{C\frac{1}{2}\left(1 + \frac{2kh}{\sinh 2kh}\right)} \tag{7.10}$$

and coincides with the ridge of high positive cross-correlation. However, during the larger wave conditions on yearday 122 (Figure 7.13, lower left panel), the short wave energy is dissipated with the onset of depth limited breaking at the outer edge of the shoal at cross-shore distance 150 m, where a decrease in correlation occurs. At cross-shore distance 125m, the correlation becomes negative, and a negative correlation ridge exists to the shoreline (Figure 7.13, lower left panel) along the theoretical time lag (Eq. 7.10). There is a slight positive (correlation) ridge which travels to the shoreline before the negative ridge (Figure 7.13, lower left panel). As wave groups enter shallower water, the large waves in the center of the wave group begin to break first. This is a result of larger waves traveling on the trough of the bound wave (local wave set-down), which enhances the onset of wave breaking. This effectively causes a phase-shift within the short-wave energy to jump to the vicinity of unbroken waves, which are traveling on the crest of the bound long wave (local wave set-up). The unbroken waves traveling on the crest of the now shoreward propagating released bound waves (free wave), travel to the shore ahead of the original wave group (List, 1991; Janssen *et al.*, 2000, Reniers *et al.*, 2003a).

The propagation of the long waves, $_{lo}(t)$, is examined using similar cross-correlation analysis

$$R_{\eta_l\eta_l}(x_i,\tau)=\frac{<\eta_{lo}(x_1,t)\eta_{lo}(x_i,t+\tau)>}{\sigma_{\eta_{lo}(x_1,t)}\sigma_{\eta_{lo}(x_i,t+\tau)}} \tag{7.11}$$

where the long wave is defined by the band-pass filtered (0.004 - 0.04 Hz) surface elevation. The long waves are observed to propagate onshore (ridge of cross-correlation with increasing time lag going onshore), and reflect at the shoreline and travel seaward (ridge of cross-correlation with increasing time lag going offshore) [Figure 7.13, middle column]. Unlike the short wave energy, which is destroyed at breaking, the long wave structure remains visibly intact after short wave breaking for both small and large wave cases (Figure 7.13, middle column) and matches the theoretical time lag. Note that the correlation ridges associated with the negative time lags are related to the previous shoreward and seaward propagating long wave. This is consistent throughout the experiment, except during times of low wave energy and during low tides. For the most part, the destruction of the short wave group has little effect on the propagation of the long wave, indicating the bound long wave is released at breaking, and propagates as a free wave within the surf zone and is reflected offshore at the beach.

The forcing of the long waves by the short wave group energy is evaluated by cross-correlating their signals locally at each pressure sensor in the cross-shore,

$$R_{E\eta}(x_i,\tau)=\frac{<E(x_i,t)\eta_{lo}(x_i,t+\tau)>}{\sigma_{E(x_i,t)}\sigma_{\eta_{lo}(x_i,t+\tau)}} \tag{7.12}$$

A positive correlation of one (a negative correlation of one) indicates waves traveling in-phase (out of phase). A zero correlation indicates that the waves are not linearly correlated at that particular time lag or 90° out of phase.

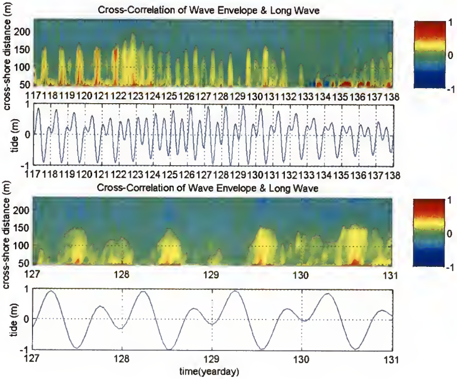

Figure 7.14 Timestack of hourly cross-correlation between the wave energy and long wave elevation at zero time lag in the cross-shore array. The upper two panels represent results from yeardays 117-138 and the lower two panels provide a zoomed in view for a shorter duration, yeardays 127-131. Note the white area represents a period when P2 malfunctioned. Tidal elevation included for reference (bottom panel).

During the small wave event (Figure 7.13, upper right panel), the cross-correlation is negative (180° out-of phase) at zero time lag across the profile until the wave energy is destroyed during breaking at the shoreline (~60 m), suggesting that the short wave groups are forcing a bound long wave. For the storm event, the negative correlation occurs offshore of where the waves break on the outer slope at about 175 m (Figure 7.13, lower right panel), though the maximum cross-correlation is slightly offset from zero time lag indicating a slight phase change associated with the bed slope (Janssen *et al.*, 2002). Within the surf zone, the slow variation in depth by the long waves modulates the depth-limited breaking of the short waves, resulting in a positive correlation (Abdelrahman and Thornton, 1988; Janssen at al., 2000).

The forcing of bound long waves by the wave group energy is examined for the entire data set by calculating hourly timestacks of cross-correlation between the short wave group energy and long wave motion at each cross-shore location at zero time lag, R_E (x_t, =0) (Figure 7.14). Again, negative correlation indicates forcing of bound long waves by short wave groups prior to breaking, and positive correlation indicates modulation of short wave energy by long waves after wave breaking. Typically, zero correlation (the transition from negative to positive correlation) represents the outer edge of the surf zone where the waves start to break. During high tide, the short waves break closer to shore and the wave envelope remains intact closer to the shoreline before being destroyed (Figure 7.14). At low tide, the waves break at the outer edge of the shore-connected shoals. Long wave forcing by wave groups is evident throughout the experiment, except on low wave days ($H_{rms,hi} < 1$). Note the white block is a period when the sensor P2 malfunctioned (Figure 7.14).

Rip Current Pulsations

Alongshore Structure of Current Velocities

Cross-correlations at = 0 for both the cross-shore and alongshore velocity components in the alongshore puv array are analyzed for low frequency motions to determine relationships between velocities on adjacent shore-connected shoals with those in the rip channels. Velocity components at PUV6 (Figure 7.3), at the approximate center of the alongshore array (y=-3 m), are correlated with other puv sensors in the alongshore array (x =85 m). The cross-correlation is high at zero time lag for long wave cross-shore velocities (Figure 7.15a, 7.16a). Note Figure 7.16 is a zoomed in view of Figure 7.15 to allow the reader a closer evaluation. This suggests that the long waves respond similarly across the shore-connected shoal and the rip channels and are unaffected by the presence of the complex bathymetry. Note that a few of the electromagnetic current meters were buried occasionally resulting is spurious data measurements. This occurred at two different periods: 1) yearday128-129 at y=-25m; and 2) yearday 134-138 y=125 m.

Since the alongshore array may not be parallel to the shoreline, the time lag for the maximum cross-correlation for the cross-shore velocities was computed. The absolute maximum time difference between sensors is approximately 5 seconds at low tide (Figure 7.15b, 7.16b) which suggests minimal array orientation bias with PUV9, located around y=120, appearing slightly closer to the shoreline. This also indicates that the complex bathymetry has minimal effects on the infragravity motion, even during low tides, and that the cross-shore infragravity motions are primarily responsible for the rip current pulsations at these frequencies. During lower tidal elevations, before the electromagnetic current meters were exposed, the temporal correlation value decreased, but still remained relatively high (Figure 7.15 a,b, 7.16 a,b). The time lag is discussed in further detail in the next section.

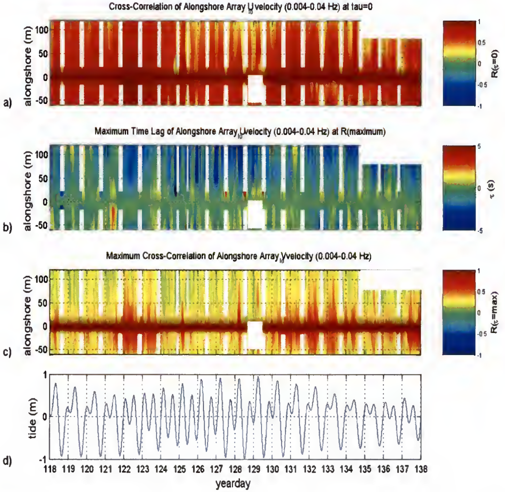

Figure 7.15 Cross-correlations at zero time lag between cross-shore velocities in the alongshore array (panel a) and alongshore velocities in the alongshore array (panel c). The time lag of the maximum correlation for the cross-shore velocities in the alongshore array (panel b). White blocks indicate times when the bi-directional electromagnetic current were exposed or the instrument was buried. Tidal elevation included for reference (panel d).

Cross-correlations within the alongshore array are examined to determine if any alongshore propagating waves exists (Figure 7.15 c, 7.16 c). Due to the fact that edge waves are present in the f-ky-spectra, the maximum correlation was computed for alongshore velocities, which depicts a smaller correlation except for times during the storm events when edge waves were a more dominant feature (Figure 7.11). The relative minimum correlation of alongshore velocities is related to the position of the alongshore array and the edge wave nodal structure (See Reniers *et al.*, 2003a).

During the operation of the PWC, we observed that wave breaking was generally less dramatic within the rip channels, and that the waves tended to break closer to shore (except for low tides or large storm events) owing to a combination of the rip channels being deeper than the neighboring shoals, wave refraction, and wave-current interactions. Similar observations were made by Haller *et al.* [1997] in a laboratory setting. Since there is minimal variation associated with the cross-correlation statistics in the alongshore, this suggests that the processes occurring within rip channels also release the bound long wave similar to wave breaking as measured on the shore-connected shoals.

Cross-Correlation of Infragravity Waves

Early in the experiment, there were 5 days where 4 of 7 pressure sensors in the alongshore array were operational, which span across the rip channel, located at y=-20, north of the cross-shore array. Unlike the electromagnetic current meters, the pressure sensors were below water throughout the tidal cycle, so the infragravity waves were cross-correlated to investigate any alongshore variations. At =0, there is a high correlation for long waves both on the shoal and within the rip channel (Figure 7.17a).

Similar to the alongshore correlations of velocity, the correlation decreases with lower tidal elevation. At extremely low tides, the correlation is zero, which corresponds to periods when the shore connected shoal is close to being exposed. The time lag for the maximum correlation is zero (Figure 7.17b), except for the lowest tidal elevations for which it is approximately 10 seconds. The temporal variation is

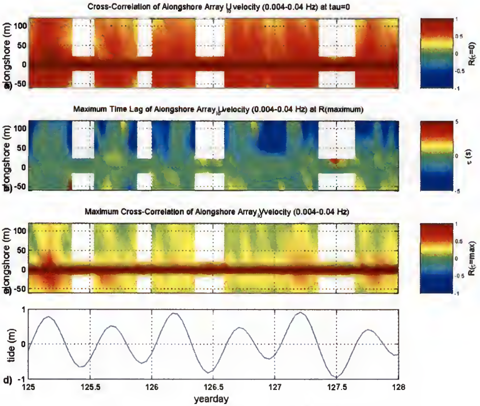

Figure 7.16 Zoomed in view of Figure 7.15, for yeardays 125-128. Cross-correlations at zero time lag between cross-shore velocities in the alongshore array (panel a) and alongshore velocities in the alongshore array (panel c). The time lag of the maximum correlation for the cross-shore velocities in the alongshore array (panel b). White blocks indicate times when the bi-directional electromagnetic current were exposed or the instrument was buried. Tidal elevation included for reference (panel d).

associated with the shore-connected shoal being close to being exposed while the rip channel has approximately 1 meter of water. The long wave propagation speed is retarded on the shore-connected shoal due to variation in the propagation speed associated with the shallower water depths. The theoretical time difference between a dispersive wave propagating at group velocity on a transect over the shoal and within the rip channel at low tide is approximately 9 seconds

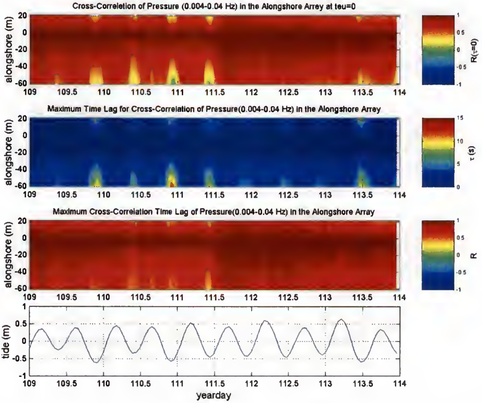

Figure 7.17 (panel a) Cross-correlations at zero time lag for pressure in the alongshore array. (panel b) The time lag of the maximum correlation for the cross-shore velocities in the alongshore array. Tidal elevation included for reference (panel c).

(utilizing Eq. 7.6 for these days), for which the wave within the rip current channel leads the wave on the shoal. This explains the time lag associated with the cross-correlation

(Figure 7.17, b).

Cross-Correlations Infragravity Motions with Rip Current Pulsations

Cross-correlations of the infragravity motions, wave group, long wave elevations, and rip current pulsations, are evaluated to determine the temporal characteristics associated with the rip current pulsations and infragravity forcing mechanisms. PUV11 is utilized as it was located within the rip channel, approximately 15 meters shoreward of the alongshore array, and because the co-located pressure sensor and electromagnetic current were operational throughout the experiment. The cross-correlation of the offshore wave group (PUV4) with the nearshore long wave (PUV11) are shown in (Figure 7.18a) along with the theoretical time lag for a dispersive wave to propagate at the group velocity (Eq. 7.10). The expected correlation value at the theoretical time lag is negative, since the bound long wave travels with the wave group (envelope) shoreward. The bound long wave may no longer be coupled to the wave group as it enters the surf zone and phase differences may occur (List, 1991). However, the measured cross-correlation at the theoretical time lag is zero.

The cross-correlation between infragravity elevation and infragravity velocity at PUV11 is zero at zero time lag (Figure 7.18b), with maximum correlations occurring at approximately 17 seconds. This relationship is indicative of a standing wave, due to the 90 degree phase difference between infragravity elevation and infragravity velocity. If the sensor was located at a spatial node or anti-node, zero correlation would be present for all time lags and one of the variables would be zero, which is not the case. The correlation is negative at ~-17 second time lag and positive at ~ 17 second time lag, which represents half of the infragravity wave period. If the infragravity elevation and infragravity cross-velocity were progressive waves, a maximum correlation would occur at zero time lag.

The cross-correlation of the offshore wave group (PUV 4) and the nearshore infragravity

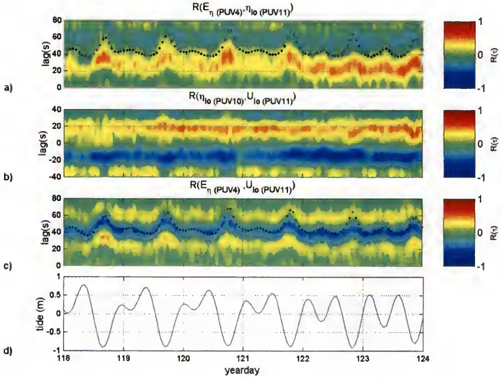

Figure 7.18 The cross-correlation for the offshore wave energy (PUV4) and the nearshore infragravity elevation (PUV11) [panel a]. The cross-correlation for nearshore infragravity elevation and nearshore infragravity velocity at PUV4 (panel b). The cross-correlation for the offshore wave energy (PUV4) and the nearshore infragravity cross-shore velocity (PUV11) [panel c]. The theoretical time lag for a dispersive wave propagating at the group velocity is shown as a dotted line. Tidal elevation included for reference (panel d).

velocity (rip current pulsation) [PUV11] is negatively correlated (Figure 7.18c) at the theoretical time lag. This is consistent with the infragravity bound long wave traveling with the wave group, but inconsistent with the result presented in Figure 7.18a. The results of this (Figure 7.18a) can not be properly interpreted without additional measuring positions, so a numerical model (DELFT3D) was employed to provide a better understanding. A discussion of the numerical model and results are outlined in a complementary paper (see Reniers *et al.*, 2003a).

The correlation remains relatively the same throughout the duration of the experiment, only varying with tidal elevation owing to difference in propagation speeds. The results indicate that the short-wave group and long wave evolution over the shoal is related to the cross-shore motions of the infragravity waves in the alongshore array. Simple stated, the rip current pulsations for this beach system are primarily forced by the standing long waves, which can be seen by the evolution of the wave groups and long waves. This will be discussed in more detail in the next section.

Discussion

Two hypotheses have been proposed for mechanisms forcing rip current pulsations. The first is that the rip current pulsations are simply due to the infragravity wave motions as observed by Sonu [1972]. The second hypothesis is that the surf zone has a maximum set-up during the breaking of high waves of a wave group that produces a hydraulic head, which discharges the water most efficiently through the rip channels during the subsequent low waves of the wave group (Munk, 1949; Shepard *et al.*, 1941). The results of analyses performed in the previous sections suggest that the rip current pulsations are related to the infragravity motion. This section will discuss the justification for adopting this hypothesis.

The cross-correlation between the infragravity elevation and infragravity velocity at PUV11 (Figure 7.18b) suggests that this motion is related to the standing wave structure of the bound and free long waves. If the rip current pulsations were driven by the hydraulic head, then the maximum of the infragravity velocity would occur during the minima of the wave groups during the release of the ponded water. The maximum nearshore infragravity velocity within the rip channel is highly (negatively) correlated at the theoretical maximum of the wave envelope (Figure 7.18c), but not at the minima.

The infragravity motion of velocity and elevation illustrate weak alongshore spatial variations with high correlations in the alongshore array (Figures 7.15-7.17). The time lag associated with the maximum correlation indicates there is a delay occurring on the shore connected shoal, which is explained by the propagation speed of the infragravity wave (gh) on the shore-connected shoal being slower than within the deeper rip channel.

The cross-correlation between the infragravity cross-shore velocity and infragravity elevation depicts zero-correlation at zero time lag with high negative and positive correlations occurring ± 17 seconds, which is consistent throughout the experiment (Figure 7.18 b). This suggests a standing wave pattern between elevation and velocity is present.

Average infragravity velocities within the alongshore array indicate that the velocities are smaller within the rip channel than on the shore-connected shoal. If the hydraulic head associated wave group mechanism was responsible for rip current pulsations, this should produce velocities which are greater within the rip channel than those on the shore connected shoal, which is not observed. If the wave group, hydraulic head hypothesis was the mechanism responsible for the rip current pulsations, we would expect to notice the rip pulsations present in f-k_y-spectra as broad-band energy (Figure 7.11) at the spatial length-scale of rip channel spacing (~125 m; k_y 0.008 m^{-1}). The f-k_y-spectra do not indicate such a relationship, except to indicate that the motions have a significant cross-shore dominance.

These results indicate that the rip current pulsations are related to infragravity motions and not the hydraulic head associated with the wave groups. Although the second hypothesis may coexist in the background, the primary mechanism is related to the infragravity waves. The morphology at this site is classified as an intermediate beach system with traverse bars (shore connected shoal) and rip current channels. Similar observations that rip current pulsations are controlled by standing infragravity waves were made by Sonu [1972] for Seagrove, Florida, located on the West Coast of Florida. We hypothesize that the rip current pulsations on other beach systems with bathymetrically controlled rip currents will have similar forcings, where surf beat is present.

Conclusion

The RIPEX-SBE experiments provided the necessary measurements to examine infragravity motions on a complex beach system and their effects on rip current hydrodynamics. $H_{rms,lo}$ increases shoreward and is correlated with the incoming sea-swell energy. $H_{rms,lo}$ did not vary with tidal elevation, whereas $U_{rms,lo}$ and $V_{rms,lo}$ are modulated slightly with tidal elevation and correlated with the incoming sea-swell energy. The undulations in the bathymetry produced weak alongshore variations in the infragravity velocities. The infragravity velocities within the rip channels are actually smaller than on the shore-connected shoal owing to continuity.

The infragravity energy was dominated by leaky and high mode edge waves with some energy located within the low mode edge waves. The small variation in wave direction associated with Monterey Bay, CA generates relatively narrow energy f-k_y-spectra (Figure 7.11) as compared with observations of infragravity waves on the open coast. In addition, highly energetic, very low frequency, motions were documented with higher wave numbers and lower frequencies than associated with infragravity waves (MacMahan *et al.*,2003b; Reniers *et al.*, 2003b).

The cross-shore structure of the infragravity motions illustrate that the forced long wave propagates shoreward 180° out-of-phase with the short wave envelope until the wave groups are destroyed by depth limited breaking. The long wave then continues shoreward as a free wave and subsequently is reflected at the shoreline as shown by the cross-correlation function between the long waves at various cross-shore locations. The results are consistent with the mechanism for long wave mechanisms proposed by Longuet-Higgins and Stewart (1962, 1964). Though this structure was observed across the shoal, the high correlation in the alongshore array, suggests that the bound long wave is also released within the rip channel. Time lags of the maximum correlation of the surface elevation with velocity suggest that infragravity waves propagate slower on the shore connected-shoal due to variation in the propagation speed during low tides.

Two hypothesis were proposed for the formation of rip current pulsation; 1) infragravity waves, and 2) variations in hydraulic head associated with wave groups. The measurements suggest the first hypothesis is valid, and do not support the second hypothesis. The second hypothesis is not supported by the following observations: 1) infragravity velocities are smaller within the rip channel than on the shore-connected shoal (Figure 7.10) and can be explained by linearized shallow water theory (Eq 7.6) [Figure 7.9]; 2) temporal alongshore uniformity in cross-shore velocities and elevation during mid to high tides (Figures 7.15-7.17); 3) the time lag of the maximum correlation in the alongshore array, during low tide, can be explained by variations of propagation speeds related to differences in bottom depths between the shore-connected shoal and rip current channels; 4) the maximum negative correlation occurs at the maximum of the wave envelope (Figure 7.17 c); and 5) the cross-shore structure of the infragravity waves indicates a strong relationship with rip current pulsations (Figure 7.18 b).

Therefore, the standing wave motion of the infragravity motion is the primary forcing for low frequency oscillations within the rip channel, termed rip current pulsations. The rip current pulsations are related to the characteristics of the surf beat (as discussed in previous studies), and increase with increasing storm energy and during lower tides. The conceptual model presented concurs with previous observations of rip current dynamics.

CHAPTER 8
VERY LOW FREQUENCY MOTIONS

Introduction

Velocity measurements within the surf zone for field experiments on planar and barred beaches illustrate that low-frequency (infragravity) motions are ubiquitous. Infragravity motions are the dominant energy source within the surf zone compared to the energy within the sea-swell band (Suhayda, 1974, Huntley, 1976, Huntley *et al.*, 1981, Holman, 1981, Wright *et al.*, 1982, Guza and Thornton, 1982, amongst others).

Energetic vorticity motions (non-gravity motions), typically occurring at frequencies less than infragravity motions where gravity is not the restoring force, also coexist in the surf zone. The distinction between gravity waves and vorticity motions is determined through frequency-wave number (f-k_y) spectral estimates computed from an array (generally 4 or more) of instruments. A single co-located pressure-velocity sensors may have potential bias due to standing wave motions (Lippmann et al., 1999). Gravity waves are located within the range of alongshore wavenumbers associated with downcoast (-k_y) and upcoast (+k_y) traveling mode 0 edge waves, while vorticity motions are located outside of this region (Figure 8.1). We define non-gravity motions for frequencies less than 0.004 Hz as very low frequency motions (VLFs), since infragravity waves in the literature have traditionally been referred to as low frequency motions. Furthermore, VLFs are considered to be predominantly composed of vorticity motions, due to the relatively small portion of the gravity motions within the VLF band.

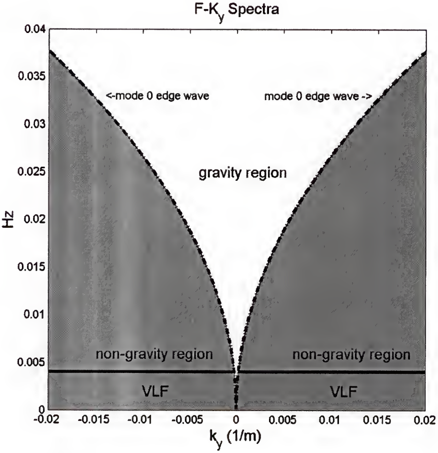

Figure 8.1 Simplified f-k_y-spectrum illustrating gravity and non-gravity region separated by mode 0 edge wave. The VLF (very low frequency) motions are further defined in the non-gravity region to frequencies less than 0.004 Hz.

Most studies of VLFs are shear instabilities of the longshore current (Oltman-Shay *et al.*, 1989), also referred to far-infragravity waves. In 1989, Oltman-Shay *et al.* discovered energetic motions in the longshore current located within the non-gravity regions in f-k_y space (Figure 8.1), ranging in frequencies from df-0.045 Hz. These motions were generally most energetic for frequencies less than 0.004 Hz. The longshore current instabilities have a near linear dispersion realtionship in f-k_y space related to the back shear of the at longshore current at the shoreline and longshore bar and propagate in the direction of the longshore current (Holman and Bowen, 1989, Oltman-Shay et al., 1989).

Since the initial discovery of longshore current instabilities by Oltman-Shay *et al.*, 1989, there has been significant efforts investigating this process via laboratory measurements (Reniers *et al.*, 1997), field measurements (Oltman-Shay *et al.*, 1989, Noyes *et al.*, 2002), and theoretical and modeling developments (Holman and Bowen, 1989; Allen *et al.*, 1996; Reniers *et al.*,1997; Slinn *et al.*,1998; Ozkan-Haller and Kirby, 1999; Dodd *et al.*, 2000). Though shear instabilities of longshore currents are the most commonly studied, a few studies have addressed VLFs in situations without strong longshore currents, or on complex beach systems. Dodd *et al.* (1992) investigated shear instabilities at Leadbetter Beach, California, (a planar beach) and the comparisons between measurements (NSTS) and theoretical predictions were not as conclusive as those at Duck, NC (a barred beach). In addition, longshore current instability theory fails to explain; 1) a low frequency cut-off for which shear instabilities should not be present (Dodd, 1994; Shrira *et al.*, 1997) and 2) how shear instabilities should be damped out by friction (Dodd *et al.*, 1992). In order to account for these discrepancies, Haller *et al.*(1999), using the methodology of Shrira *et al.* (1997), suggested that wave groups provide the necessary mechanics inducing perturbations to the system.

The initial observations of VLFs were documented during the Nearshore Sediment Transport Study by Tang and Dalrymple (1989), who related these observations to migrating rip currents associated with wave group forcing. This observation was later conceptualized and verified in the laboratory by Fowler and Dalrymple (1990). They measured VLFs composed of slowly migrating rip currents formed by intersecting wave groups. This mechanism is a modified version of Dalrymple's (1975) generation of stationary rip currents formed by two intersecting wave trains (monochromatic wave trains) at equal and opposing angles. The conceptual model by Fowler and Dalrymple(1991) confirms previous observations by Kim and Huntley (1986), who utilizing the cross-correlation function, determined temporal lags of ~26 seconds between cross-shore and alongshore velocity measurements at a co-located instrument. Kim and Huntley (1986) suggested that these delays were a result of intersecting wave groups caused by reflection or diffraction off a local headland.

Field investigations of rip currents (on complex beaches) by Sonu, 1972; Aagaard *et al.* (1997), Smith and Largier (1995), Brander (1999), Brander (2000), Brander and Short (2001) all noticed rip current velocity pulsations at infragravity frequencies. Chapter 7 and Reniers *et al.* (2003) demonstrated that rip current pulsations (within 0.004-0.04 Hz frequency band) are attributed to the cross-shore infragravity motions.

In addition to the energetic rip current pulsations, energetic motions in the very low frequency have also been observed within rip current systems (Smith and Largrier, 1995; Brander and Short, 2001; Haller and Dalrymple, 2001). Smith and Largier (1995) acoustically measured rip currents motions outside the breaker zone and found that they fluctuated aperiodically with temporal scales greater than 15 minutes and appeared

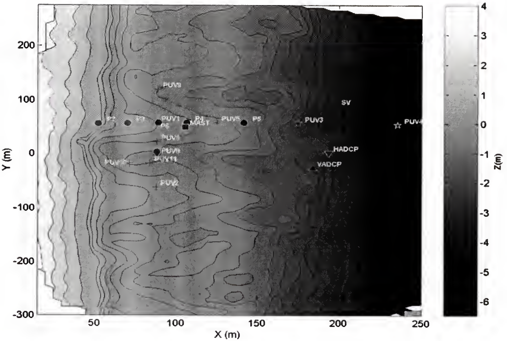

Figure 8.2 Bathymetry contour plots obtained from two methodologies 1) hydrographic survey system mounted aboard a personal watercraft (high-tide) and 2) water-tight back-pack mounted to a person (low-tide). The dots indicate pressure sensors, squares represent co-located pressure and bi-directional electromagnetic current meters, triangles represent ADCPs, and stars indicate acoustic doppler velocimeters.

unstable. Smith and Largier (1995) suggested that the rip current begins meandering in the early stages and reconnects back to the surf zone, but at later stages the meander pinches off and propagates offshore. We concur with the statement by Haller and Dalrymple (2001) that the rip current pulsations observed by Aagaard *et al.* (1997) are related to VLFs and not to that of surf beat. Brander and Short (2001) reexamined their original observations by Brander (1997) and found VLFs in their measurements. Thus, previous field experiments have either overlooked the amount of energy as [illegible] within these motions by not sampling sufficiently long enough to resolve them or attributed these signals to infragravity motions. A recent experiment by Miles *et al.* (2002) documented that suspension events were modulated by longshore current shear instabilities. Hence, VLFs may be important to sediment transport.

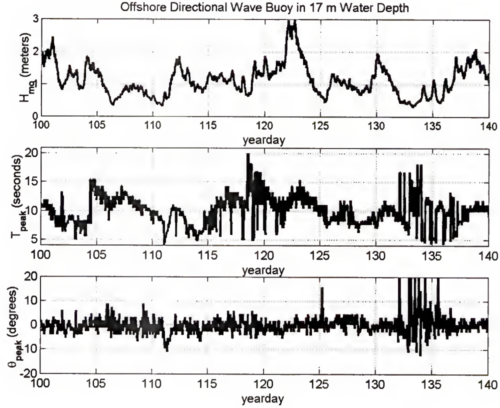

Figure 8.3 Wave climate measured by directional wave buoy located in 17 m water depth, approximately 650 m offshore, (top) H_{mo}, (middle) peak wave period, and (bottom) peak wave direction.

In a laboratory experiment, Haller and Dalrymple (2001) found that topographically controlled rip currents forced by monochromatic waves were fairly unstable (VLF). They developed an analytical model based on the instability growth of narrow jet-like motion based on these laboratory observations, which compared well.

Chen *et al.* (1999) obtained good agreement with the laboratory measurements of rip currents by Haller *et al.* (2002) using the fully nonlinear Boussinesq formulation. Yu and Slinn (2002) numerically evaluated wave-current interactions of rip current flows, indicating that the rip current instabilities (VLF) originate within the feeder channels and migrate offshore.

This chapter describes the characteristics of VLFs observed on a complex beach (next section) with dominant rip currents present in section titled Very Low Frequency Motions. Qualitative observations and statistical analysis of VLFs are explored. A simple conceptual model explaining the flow is outlined in the following section, followed by a discussion of potential VLF mechanisms and conclusions.

Field Site

Observations were obtained on a complex beach with quasi-periodically spaced rip current channels in Sand City, Southern Monterey Bay, California, during the RIP current field EXperiment (RIPEX)- Steep Beach Experiment (SBE) during the months of April and May 2001. The foreshore of the beach was relatively steep with a slope of about 1:10 with beach cusps O(35 m), which then flattened out to a low-tide terrace (1:100) with quasi-periodic O(150 m) incised channels (rip channels) and then continues offshore with a 1:20 slope (Figure 8.2). Two primary arrays were deployed; 1) an alongshore array consisting of 6 bi-directional electromagnetic current meters traversed the shore-connected shoals and 2) a cross-shore array consisting of primary pressure sensors with intermittent bi-directional electromagnetic current meters, which sampled synchronously at 8 Hz, and an upward looking ADCP located offshore of one of the rip channels sampled at 0.1 Hz. The offshore wave climate was recorded by a directional wave rider buoy located approximately 650 m offshore in 17 m depth. Considerable variation in both wave height and wave period occurred during the experiment (yearday 100-140) [Figure 8.3]. Bathymetric surveys were obtained using differential kinematic global positioning system (KGPS), mounted on a sonar equipped personal watercraft at high tide and mounted in an instrumented backpack placed on a person for walking the shore connected shoals at low tide. Beachface surveys were measured at low tide with the DGPS mounted on an all-terrain vehicle. For additional descriptions of the experiment, see Chapter 6.

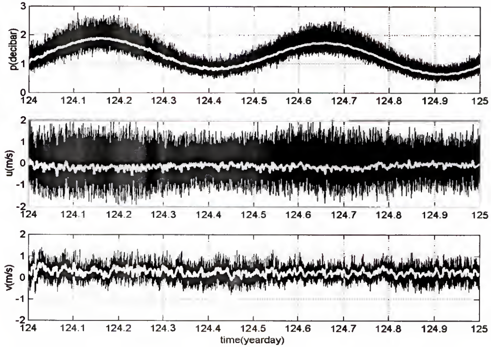

Figure 8.4 Raw time-series of pressure (top), cross-shore velocity (middle) and alongshore velocity (bottom) for PUV16 for yearday 124. The black line is the raw signal and the white line in the low-pass filtered signal (frequency cutoff of 0.004 Hz) representing the VLFs.

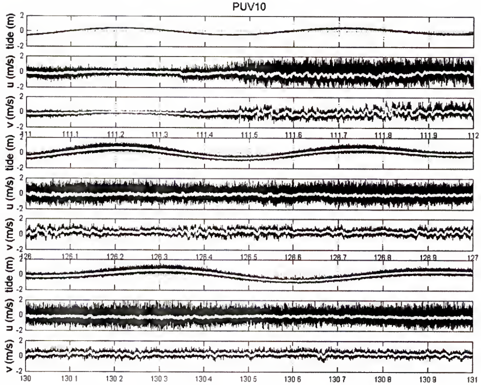

Figure 8.5 Time series at PUV10 for yearday 111 (top three), yearday 126 (middle three), and yearday 130 (bottom three). The blue line is the raw signal for pressure (top sub-figure for each yearday), cross-shore velocity (middle sub-figure for each yearday), and alongshore velocity (bottom sub-figure for each yearday) and the white is the low-pass signal (fc=0.004 Hz) for each measurement.

Very Low Frequency Motions

Similar to the experience encountered by Oltman-Shay *et al.* [1989], during the maintenance and inspection of the electromagnetic current meters, requiring daily removal of kelp, we often experienced significant pulsations. However, we initially attributed the rip currents pulsations to surf beat (Chapter 7, Reniers *et al.*, 2003). It was not until examining the time-series of the current meter data did we identify energetic low frequency oscillations in the current measurement, fluctuating on the order of 15 minutes.

Examples of VLFs can be seen in the low-passed (frequency cut-off of 0.004 Hz) time series for pressure, cross-shore velocity, and alongshore velocity measurements on yearday 124 (Figure 8.4). The upper limit of the VLFs will be discussed in more detail below. The pressure signal has minimal VLF signal, whereas the cross-shore and longshore velocities have a significant VLF signal (Figure 8.4). The VLF signal is persistent throughout the record.

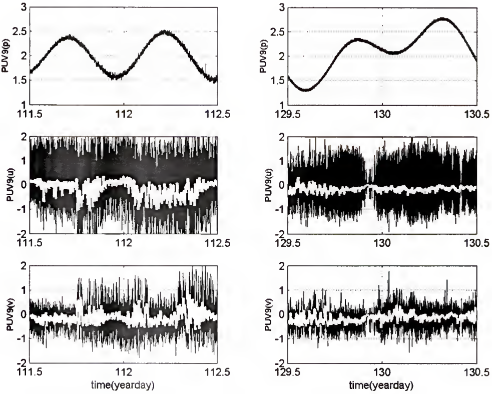

Figure 8.6 Time series of pressure (top), cross-shore velocity (middle), and alongshore velocity (bottom) of PUV9 for two similar storms occurring on yeardays 111-112 (left column) and 129-130 (right column).

A multitude of VLF behaviors were observed throughout the experiment. Time series of sea surface elevations, cross-shore, and alongshore measurements for sensor

(PUV 10) located within the rip channel for three different days (yearday 111, 126, 130) are displayed in Figure 8.5. For yearday 111, the measurements illustrate a segment when there is a dramatic increase in sea-swell energy and the VLFs spin up (Figure 8.5 a,b,c). During yearday 126, the VLFs increase in amplitude focused about rising and falling tidal stages (Figure 8.5 d,e,f), while yearday 130 demonstrates a period when the VLFs remain relatively constant throughout the day (Figure 8.5 g,h,i). For all three days, the alongshore VLF component qualitatively appears larger than the associated cross-shore component.

Next we qualitatively evaluate the how VLF relate to the underlying bathymetry. The rip current channels varied throughout the experiment, with rip channels being well defined early in the experiment (<yearday 122) and not well defined after the storm event of yearday 122. Two similar storm events (yearday 111-112 and yearday 129-130) with relatively the same wave height and wave period were chosen to determine if the underlying rip channel bathymetry has an influence on the magnitude of the VLFs. The amplitude of the VLF fluctuations of yearday 111-112 are qualitatively larger than on yearday 129-130 (Figure 8.6), suggesting bottom morphology influences the VLFs as the result of potentially stronger shear current within the rip channels. Note that the decrease for cross-shore and alongshore velocities for yearday 129-130 is related to a chunk of kelp getting entangled on the electromagnetic current meter. There is a difference in VLF response with tidal elevation for these two events. The VLFs are suppressed around low tides for yearday 111-112, while the VLFs are suppressed at high tide for yearday 129-130. This suggests that tidal elevation also has an important role. The electromagnetic current meters were

upward oriented until yearday 117, at which point the sensor heads were flipped to a downward orientation to allow for measurements during low tides. However, yearday 130 is the only day where extremely low tides and significant storm energy were both present. Thus, further evaluation of the reduction of VLFs during very low tidal elevations could not be performed throughly. Haller and Dalrymple (2001) observed a reduction in rip current shear instability intensity with lower water elevations.

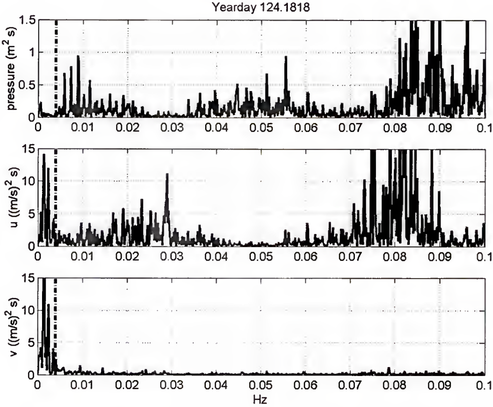

Figure 8.7 Spectral estimates of pressure (top), cross-shore velocity (middle), and alongshore velocity (bottom). The region to the left of the vertical line represents VLFs.

Fourier estimates are generated from 2.28 hour records resulting in 2 degrees of freedom and a frequency resolution of 0.0001 Hz. The total record was quadratically detrended to remove the tidal signature. This result demonstrates a significant amount of energy within the VLF frequency band for both the cross-shore and alongshore velocity components, while the energy within the sea surface displacement is almost non-existent (Figure 8.7). Energetic spectral bands are the VLF (<0.004 Hz) for the cross-shore and alongshore velocities, infragravity (0.004-0.04 Hz) and sea-swell band (0.04-0.35 Hz) for pressure and the cross-shore velocities. Band-passed variances are obtained by integrating the energy density spectrum, E(f), within the VLF band (<0.004) given by

$$\sigma = \sqrt{\int_{df}^{0.004Hz} E(f)df} \tag{8.1}$$

and $\sigma_{\eta,}\sigma_{u,}\sigma_{v}$ are the variances for the sea surface elevation, cross-shore velocity, and the alongshore velocity. Average VLF wave periods are computed by

$$T_{m01} = \frac{\int_{df}^{0.004\,Hz} E(f)df}{\int_{df}^{0.004\,Hz} fE(f)df} \tag{8.2}$$

defined as the first moment wave period (average wave period). The spectral moment is used instead of peak frequency owing to the sensitivity of the measure to the frequency resolution (df). The average VLF period is approximately 900 seconds for both cross-shore and alongshore VLF motions (Figure 8.8-8.9). Interestingly, the average VLF period is larger for the alongshore motions than for the cross-shore motions. Though the distribution of VLF periods vary slightly between sensors, most VLF periods fall within the 500-1000 second temporal range.

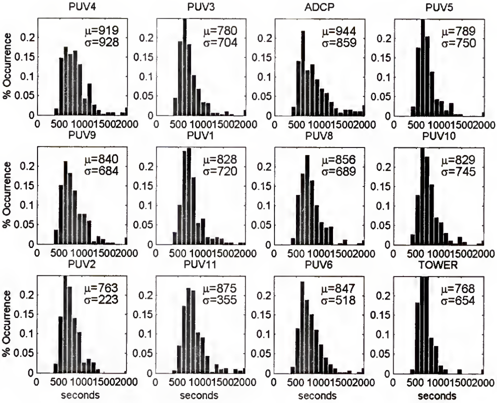

Figure 8.8 Histogram of $T_{mo,vlf}$ for the cross-shore velocities for sensors located inside and outside of the surf zone.

$U_{rms,vlf,}$ is computed from ($\sqrt{}(u_{rms,vlf}^2+v_{rms,vlf}^2)$) to eliminate any potential bias associated with current meter orientation and spatial location within the rip current system. $U_{rms,vlf}$ for PUV6 has daily variability, but the overall velocity trend increases with increasing sea-swell energy (Figure 8.10). Qualitatively, some of the daily variability can be associated with tidal modulation, which results in an inverse relationship, VLF velocities increasing during decreasing tidal elevations. This relationship is visibly evident for yeardays 126-130 (Figure 8.10), which is a period of relatively constant sea-swell wave energy. However, additional variability is also present, resulting in a poor overall VLF-tidal correlation (r=0.15).

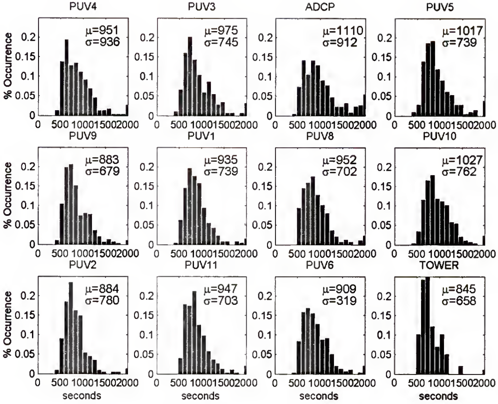

Figure 8.9 Histogram of $T_{mo,vlf}$ for the alongshore velocities for sensors located inside and outside of the surf zone.

Daily means and standard deviations are computed for yearday 111 to determine any spatial variability. VLF velocity ($U_{rms,vlf}$) has minimal alongshore variability and is not affected by the alongshore bathymetric variability of the shore-connected shoals and rip channels (Figure 8.11). The VLF fluctuations are not focused within the rip channels, differing from observations by Haller and Dalrymple (2001). This suggests the VLF motions may not be a result of rip current instabilities, but caused by a different mechanism. The cross-shore variability of mean and standard deviation indicate minimal differences (Figure 8.11) within the surf zone, but outside the surf zone, the magnitude of the velocities quickly decreases (Figure 8.11). Thus, the VLFs are energetic (~0.2 m/s) within the surf zone with minimal alongshore variability and decreases (~0.05 m/s) outside the surf zone.

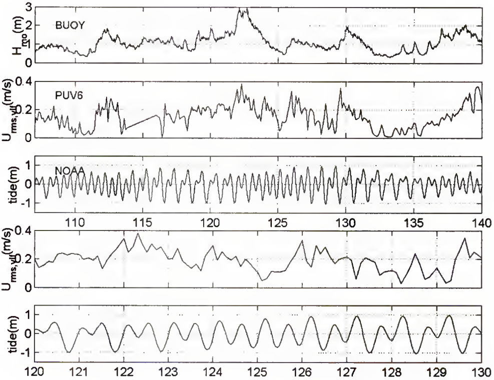

Figure 8.10 Variance of $U_{\text{vlf,rms}}$ for PUV6 located within the rip channel. (top) Significant wave height measured at the wave buoy for reference. (third, bottom) Tidal elevation measured at the NOAA station for reference. (bottom two plots) yeardays 120-130, (top three plots) yeardays 107-140.

The linear long wave relationship is (ignoring bottom slope)

$$|U|_{\text{rms,vlf}} = \eta_{\text{rms,vlf}}\sqrt{\frac{g}{h}} \tag{8.3}$$

where g is gravitational acceleration and h is the local water, is utilized to determine if the VLFs are forced by very low frequency sea-surface disturbances. Linear regression (Figure 8.12) indicates the VLFs are not forced by displacements in sea surface elevation (gravity is not the restoring force), as the VLF velocities are greater than the surface elevation potential forcing and are not statistically correlated (r^2=0.3).

Lippmann *et al.* (1999) used the ratio of the energy variances between velocity to pressure, R,

$$R = \frac{< u_{vlf}^{\ 2} > + < v_{vlf}^{\ 2} >}{< p_{vlf}^{\ 2} >} \bigg/ \frac{g}{h} \tag{8.4}$$

where <> is the variance within the frequency band, to discriminate when only gravity waves are present (R=1 with equal partitioning between kinetic and potential energy) and R>1 when shear instabilities are present. This methodology was developed for a dissipative beach with no wave reflections, whereas the RIPEX beach has significant wave reflections (Chapter 7, 2003a; Reniers et al, 2003a; Thornton *et al.*, 2003a). A beach with wave reflections results in cross-shore nodal structures and the R-method will either over or under estimate equal partitioning between kinetic and potential energy. This will occur, even if no shear instabilities are present and cannot accurately provide meaningful results for reflected beaches. An example of a standing wave pattern for RIPEX with strong nodal structure is shown in Figure 8.7. Where there is a corresponding increase in pressure variance within the infragravity and sea-swell band, there is a decrease in cross-shore velocity variance (and vice-a-versa). Therefore, this method can not be utilized to evaluate shear instability presence within the infragravity band from a single co-located puv sensor on a reflective beach.

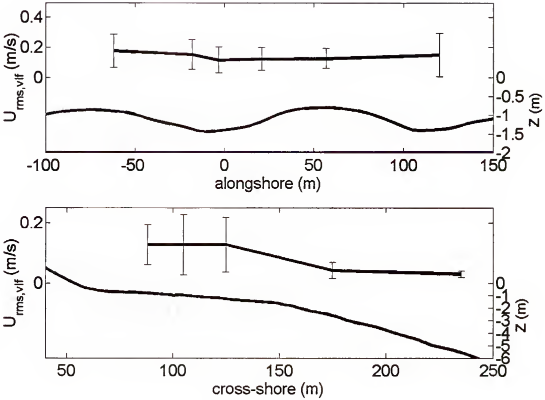

Figure 8.11 The computed VLF velocity magnitude for sensors in the alongshore profile (top panel) and the cross-shore panel (bottom panel).

Normalized spectra (NS) for various sensors were analyzed to evaluate the presence of standing waves within VLF frequency range. The normalized spectrum is computed by

$$NS_{high-tide(low-tide)}(f) = \frac{1}{N}\sum_{i=1}^{N}\frac{E_i(f)}{\int E_i(f)df} \qquad (8.5)$$

where i is the individual spectral estimates sub-divided into high and low tides. The normalized spectra provides nodal location in frequency space (Figures 8.13-8.15). The normalized alongshore velocity spectra (Figure 8.13) show a relative increase in energy at low tides for sensors outside the surf zone and a very increase in energy for sensors within the surf zone. Note there is no normalized low tide spectral estimate for PUV1, PUV2, PUV5, which are located on the shore-connected shoal and the sensors were exposed at low tide. The energy steadily increases from high frequency to low frequency with no nodal structure present in the alongshore velocities. However, the normalized cross-shore velocity spectra (Figure 8.14) display both nodal and antinodal structure, indicating the presence of standing waves. Nodal locations within the infragravity band are absent at PUV4 and become more apparent at PUV3 (located closer to shore). The nodal structure varies with tidal elevation and its juxtaposition associated with standing wave for the various water depths. The energy increases within the infragravity band and decreases at about 0.004 Hz, where an increase occurs again within the VLF band. There is also a slight increase in energy during low tide. The normalized pressure spectra (Figure 8.15) also indicates the presence of nodal structure which varies tidally and is more apparent with sensors closer to shoreline. The overall energy increases within the infragravity band and starts to decrease at frequencies slightly less than 0.004 Hz then rises slightly and levels off within the VLF band.

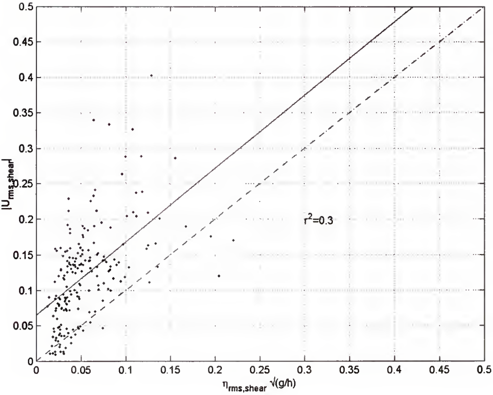

Figure 8.12 Comparison of long wave relationship (Eq. 8-3) computed at PUV11 for yeardays 118- 138. Linear regression results in r^2 of 0.3. Dashed line represents an agreement for the long wave relationship.

The dashed vertical line is the theoretical first nodal location numerically computed for a complex profile utilizing the method outlined by Guza and Thornton (1985) for standing infragravity wave for a shore-connected shoal profile, relative to the mean water level. The theoretical first nodal point corresponds well with a nodal point based on the measurements and corresponds to the lowest frequency node. Therefore, the range defined within the VLF frequency band does not contain any nodal areas and the relationship (Eq.8-4) defined by Lippmann *et al.* (1999) can be applied within the VLF band. The R values are quite large (>>1) supporting the idea that the observed VLFs are not gravity waves and are related to shear instabilities, where gravity is not the restoring force (Figure 8.16). Noyes *et al.* (2002) determined that the R method over-estimated the shear contributions for longshore currents on average by 15%. Even accounting for this over-estimation, the R values are still large.

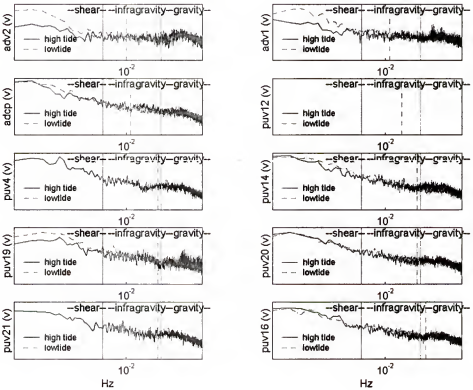

Figure 8.13 Normalized spectra for the alongshore velocity component for high (-----) and low tide (-.-.-) throughout the experiment. The vertical magenta line is the vlf-infragravity frequency cut-off (0.004 Hz) and the vertical cyan line is the infragravity-sea-swell frequency cut-off (0.04 Hz). The vertical dashed line indicates the nodal position for the cross-shore location for this complex beach system during mean tide.

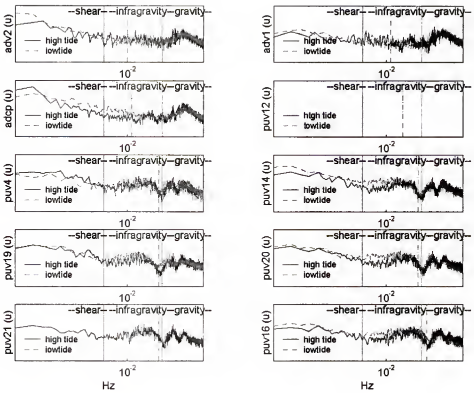

Figure 8.14 Normalized spectra for the cross-shore velocity component for high (-----) and low tide (-.-.-) throughout the experiment. The vertical magenta line is the vlf-infragravity frequency cut-off (0.004 Hz) and the vertical cyan line is the infragravity-sea-swell frequency cut-off (0.04 Hz). The vertical dashed line indicates the nodal position for the cross-shore location for this complex beach system during mean tide.

An increase in rip velocity should result in an increase in shear, as the rip channel width is constrained, then an increase and if the VLF motions are related to the instabilities of the rip currents, then an increase rip current velocity should increase instabilities. Noyes *et al.* (2002) observed that the magnitude of the longshore instabilities increases with increasing longshore current flows. It has been shown that rip current velocities increase with increasing wave energy and decreasing tidal elevation (Chapter 6, and others) and the VLF rms correlate with sea-swell energy and tidal elevation. The U_{rms}

for sensors within the surf zone were plotted as a function of mean (90 minutes) rip current velocity for PUV9 (Figure 8.17). This relationship has a significant amount of scatter, suggesting the motions are not completely a result of the rip current shear (Figure 8.17). This poor correlation (r^2=0.18) is surprising, since the R-values were much larger than 1. The VLF rms of sensors within the surf zone were also plotted as a function of the offshore wave height at the buoy (Figure 8.17). Since there appears qualitatively to be an upper limit associated with the VLF rms for both mean currents and wave heights, correlations were determined for the square-root of these two metrics, resulting in a slight increase in correlation. The relationships for VLF rms and $\sqrt{H_0}$ have a better correlation (r^2=.49) than the correlation of the $\sqrt{U}$ (r^2=0.22) and suggests that VLFs are influenced by external wave forcing. These results are surprising, since generally there is a correlation between wave heights and rip current strengths (Brander, Dronen, Haller, Chapter 6).

Cross-correlation analysis was preformed to determine alongshore spatial relationships of VLFs. The VLF cross-shore velocity within the rip channel was correlated with adjacent sensors in the alongshore array (PUV1,2,6,8,9,11) at zero time lag (Figure 8.18), similar analyses were performed on the VLF alongshore velocity (Figure 8.18). For the VLF cross-shore velocities in the alongshore array, the correlation varies spatially with positive correlation between the rip channels and negative correlation on the shore-connected shoals. The correlations suggests a spatial relationship associated with the underlying bathymetry and rip current flow characteristics (this is discussed in more detail below). The correlation of VLFs in the alongshore velocity is high during storm events when the VLFs are the most energetic (Figures 8.10). The time lag associated with the maximum correlation for the cross-shore velocities is zero for positive correlation and the time lag varies for the negative correlation between positive and negative periods of approximately 800 seconds. The time lag of the maximum positive alongshore correlations is zero.

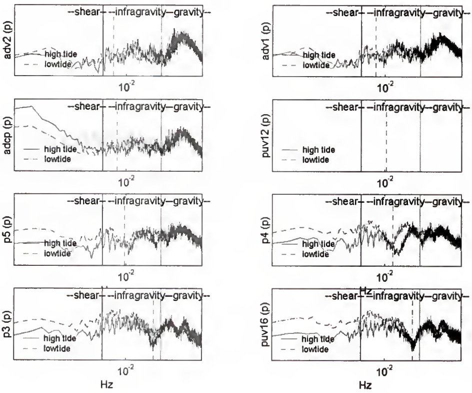

Figure 8.15 Normalized spectra for the pressure component for high (-----) and low tide (-.-.-) throughout the experiment. The vertical magenta line is the vlf-infragravity frequency cut-off (0.004 Hz) and the vertical cyan line is the infragravity-sea-swell frequency cut-off (0.004 Hz). The vertical dashed line indicates the nodal position for the pressure for this complex beach system during mean tide.

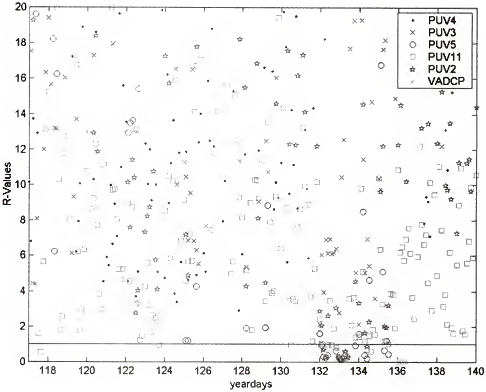

Figure 8.16. Computed R-values (equation 8-4) for operational co-located PUV sensors. R-values greater than 1 represent non-gravity waves.

Frequency-wave number spectra are calculated using the iterative maximum likelihood estimator (IMLE) (Pawka, 1983) evaluated by Oltman-Shay and Guza (1987) for detection of edge waves and later by Oltman-Shay *et al.* (1989) for the detection of longshore current shear instabilities. The IMLE has been tested and verified for use on a complex beach system in Chapter 7 and Reniers *et al.* (2003) through comparisons of model and field measurements. This methodology has been utilized in Chapter 7 for determination of the presence of edge waves for this data set. There is a division between the energy with the VLF (<0.004 Hz) and the infragravity energy (0.004-0.04 Hz) for the

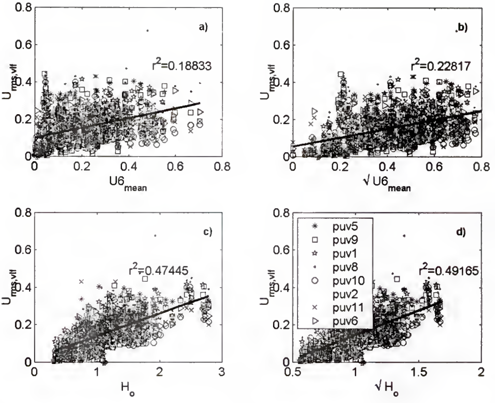

Figure 8.17 $U_{rms,vlf}$ plotted as function of 90 minute mean velocities at $U_{rms,vlf}$ versus $U6_{mean}$ (a), $\sqrt{U6_{mean}}$ (b), H_o (c), $\sqrt{H_o}$ (d) .

alongshore and cross-shore velocity components for the alongshore array (Figure 8.19). This is unlike the characteristics of shear instabilities of longshore currents, where a linear dispersion relationship is present (Oltman-Shay *et al.*, 1989). For the cross-shore frequency-wave number spectra (Figure 8.19, see for example), the energy within the VLF frequency band is generally concentrated around k_y equal ± 0.008, approximately equal to rip channel spacing, while the alongshore frequency-wave number spectra (Figure 8.19), energy is generally focused around k_y =0. It is

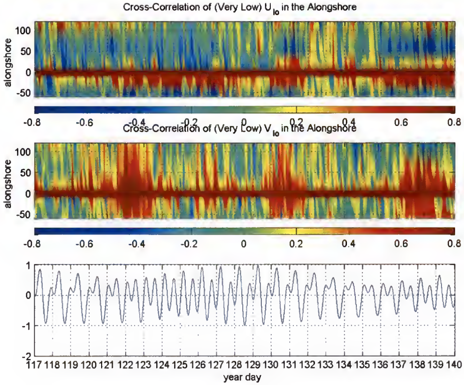

Figure 8.18 Cross-correlations of VLF cross-shore velocities (top) and alongshore velocities (middle) in the alongshore array at zero time lag. (bottom) Tidal elevation given for reference.

surprising that there are two different spatial scales associated with the VLFs, whereas longshore currents generally have similar spatial scales for both cross-shore and alongshore f-k_y-spectra (Oltman-Shay et al., 1989). F-k_y-spectra were computed for yeardays 107-138, and the spectral energy was integrated over the VLF frequency bands, which is plotted as a wave number spectra timestack (Figure 8.20). The energy within the VLF cross-shore velocities is generally focused around rip channel spacings and higher harmonics of the rip channel spacing. The energy within VLF alongshore velocity is focused about k_y=0, suggesting a wave length that is infinitely long.

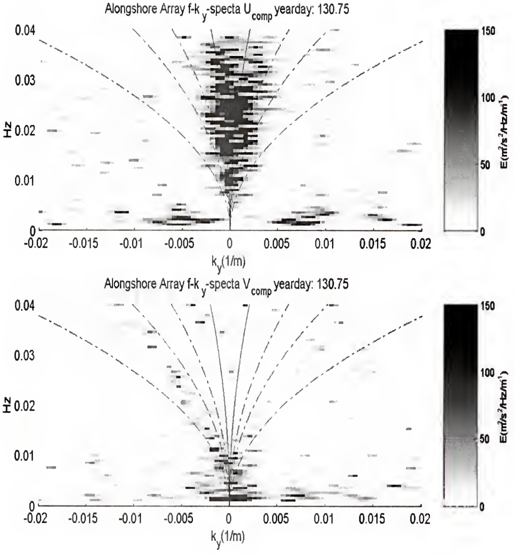

Figure 8.19 F-ky-Spectra computed using IMLE method for cross-shore (top) and alongshore (bottom) velocities for the alongshore array for yearday 130.75.

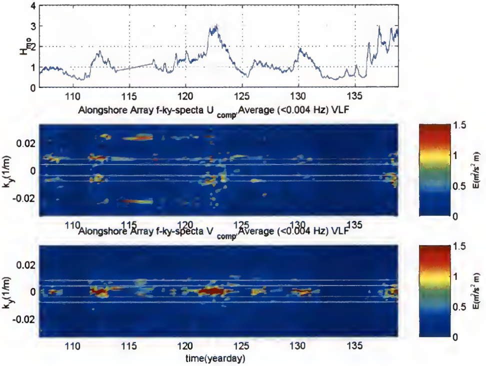

Figure 8.20 Significant wave height measured at PUV4 (top) provided for reference. Integrated energy within the VLF frequency band for cross-shore (middle) and alongshore (bottom) velocities in the alongshore array.

Rip Current Conceptual Model

A simple conceptual model of rip current cell circulations was developed to aid in interpreting the VLF behavior observed in the f-k_y-spectral observations. In the model, a three-dimensional Gaussian stream function is utilized, defined by

$$\Psi(x,y)=\sum_{n=0}-1^{n}A_{1}e^{-\lambda_{1}\left(\left[x-x_{c}\right]^{2}+\left[y-y_{c}\right]^{2}\right)} \tag{8.6}$$

where A_1 is the amplitude of the Gaussian curves, $_1$ represent the radial distance, and

x_c, y_c represent the center of the cell. Velocities are defined as stream function derivatives,

$$u = -\frac{\partial \Psi}{\partial y}, v = \frac{\partial \Psi}{\partial x} \quad (8.7)$$

Each rip current speed cell is converted into velocity vectors so that the velocities are oriented in the proper direction to represent a rip current (Figure 8.21). Multiple rip current cells are located in space representing approximate locations of potential rip current cells in the RIPEX bathymetry (Chapter 6), as well as the appropriate length scales. The overlapping of neighboring rip currents cells is additive, such that the section of cells located in close proximity to other cells are faster than cells than sections which are further apart than other cells (superposition). Rip current cells are separated in the vicinity of onshore transport and close together for offshore transport, producing faster offshore flows representative of rip currents. The center of each rip current cell is sinusoidally oscillated (<0.004 Hz) with random amplitude, which causes the entire rip current cell to meander in the cross-shore and alongshore directions.

Simulations are approximately two hours with a sampling interval of 5 seconds, similar to the f-k_y-spectral inputs of the velocity measurements. F-k_y-spectral estimates are computed using 2D FFT resulting in 40 DOF and spectral resolution (df) of 0.0004 Hz. Three scenarios were numerically performed: 1) the rip current cells only oscillate in the cross-shore (mean cross-shore amplitude of 15m), 2) the rip current cells only oscillate in the alongshore (alongshore amplitude of 15m), and 3) the rip currents cells oscillate in both directions (cross-shore and alongshore amplitude of 15 m and 2m).

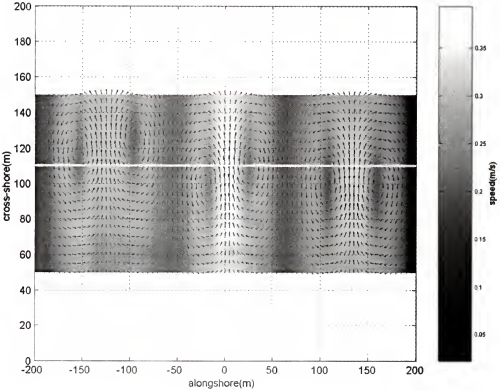

Figure 8.21 An example of conceptual model of rip current velocity cells. Solid line is the location for computations of the two-dimensional FFT.

The results indicate that when the rip current cells only oscillate in the cross-shore, k_y of the cross-shore velocities is equivalent to the rip current spacings, while k_y of the alongshore velocities is spread around zero (Figure 8.22-top). This is similar to the measurements obtained from the alongshore array of the field experiment (Figure 8.19-8.20). For strictly alongshore oscillations (Figure 8.22 -middle), k_y is focused around rip current spacing for both cross-shore and alongshore velocities. The last case was for a slight amount of alongshore oscillation (8 m) dominated by cross-shore oscillation (30 m) and tends to smear out the f-k_y-spectra (Figure 8.22- bottom), which are most comparable to the field measurements (Figure 8.19-8.20). We also performed a scenario with equal cross-shore and alongshore movements, which produced results similar to the case with just alongshore oscillations (Figure 8.22 -middle). This that suggests the rip current cells during the experiment mostly oscillated in the cross-shore with small alongshore oscillation.

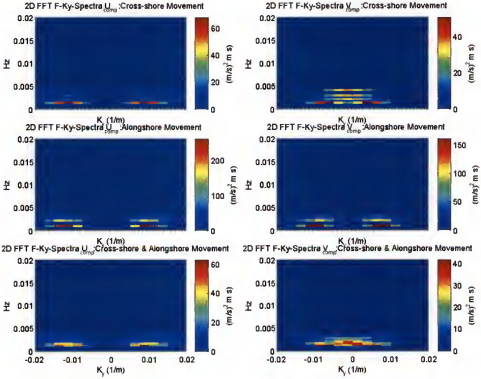

Figure 8.22 F-ky-spectral estimates using 2D FFT for conceptual model of rip current cell oscillation; (top row) cross-shore rip current cell with 15 m amplitude, (middle row) alongshore rip current cell with 15 m amplitude, (bottom row), cross-shore and alongshore oscillation of rip currents with 15 m and 4 m, respectively.

Spectral energy in the VLF band increases with cross-shore amplitudes (Figure 8.23). It is hypothesized that when the two rip current cells in the field approach one another the effect is cross-shore displacement. This mechanism was not included in this simple model. This simple conceptual model provides an understanding in the rip current cell behavior, by providing comparable results as to the measurements of the f-k_y-spectra.

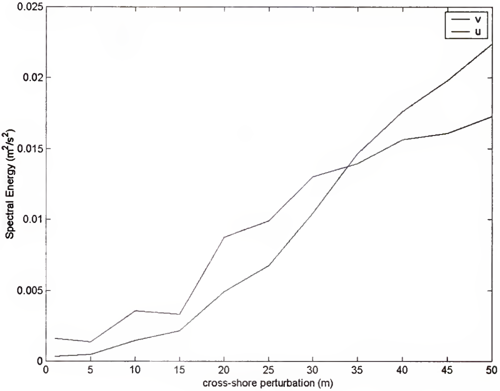

Figure 8.23 Spectral energy estimates for cross-shore rip current cell oscillations with various amplitudes.

Discussion

The results and analysis presented suggest various characteristics of rip current motions within the very low frequency range. Some of the laboratory observations by Haller and Dalrymple (2001) resemble the field observations. The fluctuations of the alongshore velocity component is slightly longer than the cross-shore velocity component. However, in the laboratory, the VLFs are concentrated within the rip channel neck and decrease in intensity around the neighboring regions, while in the field, the VLFs are of similar magnitude, regardless of sensor location within the surf zone. This may be a result of the relative close proximity of rip current cells in the field (rip current spacing ~ 125 m), which were not completely independent, whereas the rip current systems in the laboratory (rip spacing current ~9.20 m) were relatively independent. Haller and Dalrymple (2002) determined that using an undistorted Froude number with a length scale ratio of 1/50 would result in a rip current system in nature having 450 m rip spacing, 90 m rip width, breaking wave heights 1.3-3.8 m, wave periods of 5.7-7.1 s, and mean rip current velocities of 1.0-2.1 m/s. This is much different then the field conditions during the RIPEX field experiment. During RIPEX, the rip current system corresponded to a rip current spacing of 125 m, 60 m rip current width, wave heights at P5 of 0.3-2 m, 4-10 s wave period, and 0-1 m/s mean rip current velocities. There is a significant difference between the field and laboratory scaled rip current flow speeds, which may be a result of the differences in geometry, rip channel alongshore spacing, width of channel, width of bar, and depth of channel. This results in significant differences in rip current shear, computed as the mean velocity within the rip channel divided by the width of the rip channel. The shear for the laboratory is 0.11 m/s/m for 20 cm/s rip flow and the 1.82 m rip channel width, while in the field for RIPEX the shear is 0.008 m/s/m for a 0.5 m/s rip flow and a 60 m rip channel width. This difference suggests that the mechanism observed in the laboratory has significantly more shear, and thus, the mechanisms responsible for the instabilities may be different as well as their spatial occurrences.

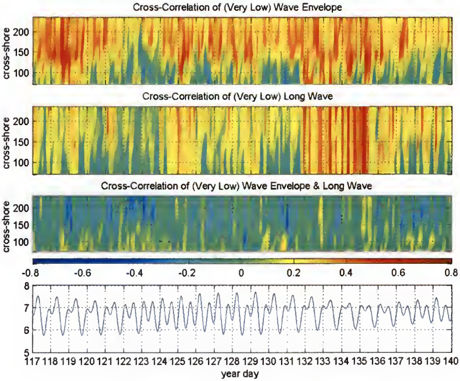

Figure 8.24 (top) Cross-correlation of group modulations (groups of wave groups) for inshore sensors in the cross-shore array with respect to the offshore sensor (PUV4) at zero time lag. (upper middle) Cross-correlation of very low frequency pressures for inshore sensors with PUV4 at zero time lag. (lower middle) Cross-correlation of group modulations and very low frequency pressure at each sensor in the cross-shore array at zero time lag. (bottom) Tidal elevation provided for reference.

The characteristics of the morphology is also different. The laboratory experiment is represented by a longshore bar with a well defined trough with straight rip channels cutting through the bar, which may confine the flow more than the complex morphology of a shore-connected shoal with smaller feeder channels and incised rip channels that increase in width as a function of cross-shore distance. The wave forcing is also considerable different, as the laboratory experiment used monochromatic waves and field conditions consisted of wave groups, making it difficult to determine the mechanism(s) responsible for the VLFs.

At least five mechanisms have been suggested that may force the onset of rip current VLFs, 1) instability of the jet-like flow (Haller and Dalrymple, 2001; Yu and Slinn, 2002), 2) the variation of infragravity motions propagating over an complex bottom, 3) variable wave driven torque (Oh and Dean, 1996; Haller et al., 2002), 4) temporal variations of wave groups (groups of wave groups), 5) crossing of wave groups (Fowler and Dalrymple, 1990). The observed VLFs may be forced by a combination of these mechanisms. The first idea has already been discussed and will not be mentioned in further detail.

The second mechanism suggests that alongshore infragravity variability associated with a complex bathymetry is responsible for rip current VLFs. It was determined that rip current pulsations are simply a result of standing infragravity motions (Chapter 7; Reniers *et al.*, 2002). The cross-correlations of velocity measurements in the alongshore suggested minimal temporal variations at mid-to-high tides. During low tide, the correlations still remained high, but a temporal lag developed for the infragravity waves on the shoal, which was related to a reduction in propagation speeds, ($\sqrt{(gh)}$) due to the shallower water depths. This variation in propagation speed will induce a shear between the infragravity velocities of the rip channels and the shore-connected shoals, ultimately creating the instability of migrating rip current cells. This mechanism is consistent with the observations of rip current (shear) VLFs, such that the VLFs are smaller during higher tidal elevations when the time lags are minimal (Figure 8.8). The VLF energy also increases with increasing sea-swell wave energy for which the infragravity energy increases producing a larger shear (Figure 8.8). Also, when comparing VLFs energy for two storms with differing alongshore variability, the well defined rip channels produced larger VLFs (Figure 8.5).

Mechanism 3 proposes that the wave heights associated with the groups induce a temporally variable vorticity driven torque opposing the flow, due to alongshore variability of wave heights and water depths (Oh and Dean, 1996) or gradients in Syy (Haller *et al.*, 2002). This mechanism relies on the proposition that the wave height increase within the rip channel owing to wave-current interaction, and are not refracted toward the shoals, which would decrease the wave amplitude. The increase in wave height within the rip creates a negative feedback, which produces a counter torque potentially making the system unstable and oscillating the rip current cells in the cross-shore. These observations have been observed and computed in the laboratory for monochromatic waves by Oh and Dean (1996) and Haller *et al.* (2002). The maximum offshore flow infragravity pulsation occurs at the maximum of the wave groups, further increasing the wave heights during the period of time which has the most influence. The opposing force does create a counter flow, only reducing the steady flow. The temporal variability of wave driven torque may induce the rip current cells to migrate on and offshore triggering the instability. This mechanism is only valid for conditions when wave breaking within the rip channel is minimal. This mechanism fails to explain conditions when wave breaking occurs in the rip channels, which is generally during storm events when the VLFs are most energetic.

There is a significant temporal mismatch between forcing in the infragravity (or sea-swell band) and the VLF response only appear in the very low frequency band. The above trigger mechanisms may not allow for VLFs to occur within the frequency band of interest.

In mechanism 4, the slow variation of wave groups inject energy into the surf zone, which is slowly dissipated by bottom friction (Ryrie, 1981; Reniers *et al.*, 2003). Wave groups vary on long time scales (>250 seconds), defined as groups of wave groups, and are analyzed to determine their potential influence on rip current VLFs. We define these variations as group modulations to avoid confusion with short-wave groups. Interestingly, group modulations and low frequency pressure modulations (>250 seconds) respond in a similar manner to that of short-wave groups and low frequency pressure(Figure 8.24). The group modulation outside the surf zone is negatively correlated with the group modulation within the surf zone, and is similar for the VLF long wave. The zero correlation value represents the width of the surf zone and varies with the incoming sea-swell energy. It also appears that the VLF long wave is correlated with group modulation, being inversely correlated outside the surf zone and positively correlated within the surf zone. Evaluating the cross-shore structure for potential reflections of a VLF wave indicates that energy propagates into the surf zone and none of it is reflected offshore, similar to analysis evaluating cross-shore infragravity wave structure (Janssen et al, 2002, Chapter 7). Thus, this group modulation in the surf zone may be responsible for the rip current VLFs. Cross-correlations were computed for PUV4 and PUV10 between group modulation offshore and VLF pressure, cross-shore, and alongshore velocity (Figure 8.24). The correlation is relatively high for pressure, with some correlation in cross-shore velocity, and no correlation with alongshore velocity. The results are not conclusive and whether the group modulation is a triggering mechanism or just coincidental, requiring further investigation with a more detailed field array.

The last mechanism proposes that directionally spread short-waves force a flow response within the surf zone. This idea is based on the work by Fowler and Dalrymple (1990) for the generation of migrating rip currents. Since the rip currents appear coupled to morphologic features, the rip currents only migrate slightly due to the non-linear interaction of the directionally spread short-wave forcing within the surf zone. This produces alongshore movement with long wave lengths and very long time-scales, similar to the observations here. Reniers *et al.*, 2003 examined the morphodynamic behavior of complex beaches and found a relationship of the alongshore morphologic scale (spacing of rip channels) with the directional spreading of the short waves. The forced flows were important in the development of rip current channels, and were still persistent after the formation. This process is difficult to assess due to the complexity of the bathymetry and the potential interactions induced by the bathymetric features. For example, Reniers *et al.*, 2003 an energy peak in the observed f-ky edge wave spectra at the rip current spacing scale , which appears to be a coupling of the edge waves to the morphology.

I have suggested many potential mechanisms, for which we can not accurately state which of these mechanism(s) contribute to the observed very low frequency motions. More detailed measurements in a two dimensional spatial array is required to evaluate more completely the above mechanisms or by numerical experiments (Reniers et al., 2003).

Conclusion

Energetic motions within the very low frequency (<0.004 Hz) were observed throughout the RIPEX experiment. The VLFs were present everywhere on the beach system, composed of shore-connected shoals with incised rip channels. VLF velocities were approximately 25 cm/s within in the surf zone and decreases to approximately 5 cm/s outside of the surf zone. The VLF energy is concentrated within the very low frequency band frequency band (<0.004 Hz) differing from observations of shear instabilities of the longshore current(Oltman-Shay *et al.*, 1989), residing in higher frequencies. Previous field measurements of rip currents seemed to have documented this signal, but a conclusive interpretation was not available (Aagaard *et al.*, 1997, Brander and Short 2001). Haller and Dalrymple (2001) illustrated through detailed measurements in a laboratory and an analytical model that the jet-like flow of the rip current is unstable. Field measurements of VLFs have some similar characteristics to the laboratory measurements (Haller and Dalrymple, 2001), but the system differs in morphological set-up, rip channel spacing, wave forcing, and hydrodynamic scales, which induce differences in characteristics of the VLFs.

VLF energy increases with increasing sea-swell energy and is slightly correlated with tidal modulation. The variation in tidal elevation creates variability in wave forcing, sea-swell energy within the surf zone, infragravity energy, and rip current flows. Computed R-values (Figure 8.16) are significantly larger than1 suggesting that the VLFs are not driven by gravity waves and that they should be associated with the shear of the rip currents. Yet there is not a strong correlation between variances of the VLFs and flow hydrodynamics (Figure 8.15) . A better relationship exists between VLF variance and Ho/Dc (Figure 8.17) indicating that wave forcing may be responsible for triggering the rip current cell instability.

The alongshore velocities are correlated in the alongshore when the VLFs are most energetic, while the cross-shore velocities are not correlated (Figure 8.18). F-k_y-spectra indicate that the VLFs of the cross-shore velocities are coupled to the spacing of the rip current channels, while alongshore velocities are concentrated around k_y=0 (Figure 8.19-8.20). A simple model suggesting that the entire rip current system oscillates producing results similar to the measurements (Figure 8.21), confirming the relatively uniform variance within the surf zone (Figure 8.8-8.10). It is suggested that rip currents tend to oscillate more in the cross-shore than the alongshore.

CHAPTER 9
DISCUSSION, CONCLUSIONS, AND FUTURE WORK

Many new developments are a result of this dissertation focusing around rip currents filling in some scientific (and measurement) voids currently missing in the literature. Furthermore, additional questions have originated from this research.

Under the original hypothesis that rip currents are ubiquitous and ephemeral, a portable system was designed and developed to obtain measurements associated with rip currents. A personal watercraft was instrumented with hydrographic surveying gear and an Acoustic Doppler Current Profiler to obtain nearshore bathymetry and currents (Chapters 3-4). The system has become a valuable oceanographic instrument by providing the necessary information for understanding nearshore morphodynamics for long-term monitoring on various beaches. Not long after the development of the hydrographic PWC, many schools and institutions have built their own version of the PWC system. The addition of the ADCP has resulted in minimal success, though new developments in ADCP technology will allow for future evaluation of the PWC as portable platform for measuring nearshore currents.

The motivation of this rip current research is determining the onset of rip currents for forecasting the occurrences of rip currents, which result in significant amount of lifeguard rescues and/or loss of life. The initial hypothesis was that rip currents were ephemeral. Long-term analysis of video images as Duck, NC indicate that rip current channels are relatively quasi-persistent suggesting rip currents are always present, but with various flow speeds (Chapter 5).

The strength of the rip current is associated with the local wave forcing, wind forcing, and tidal elevation. Various flow conditions were documented at RIPEX, a simple conservation of mass argument with additional contributions of flows associated with local pressure gradients were applied to the data (Chapter 6). This resulted in a significant amount of scatter and more effort is required to understand this problem better.

If rip current channels are always present, when are the rip currents most active? Most documentation of rip currents indicated that the maximum velocity measured within the rip channel is generally faster than the an Olympic 50 m swimmer. I had many opportunities to test my swimming ability during the daily maintenance of instruments during RIPEX. I often found that I could swim back to shore even when directly in the rip current channel. The mean currents were slower than anticipated, while the maximum currents were faster than excepted. Yet, there were other times when the rip current swiftly moved me offshore causing me to swim back to shore over the shore-connected shoals. The variability of the rip current strength was related to the groupiness of the incoming sea-swell waves (Chapter 7). The rip current pulsations are related to the standing infragravity waves as originally suggested by Sonu (1972).

In addition to documenting rip current pulsations, we uncovered energetic fluctuations for motions less the 0.004 Hz, referred to as VLFs (Chapter 8). The VLFs are interesting features that require additional research to understand these motions and their linkage to the underlying morphology.

My views and "gut feelings" of rip current have changed throughout this investigation. My recommendation to nearshore coastal communities, lifeguards, and beach-goers is that education should be the primary goal. Knowing how to safely exit a rip current is much more successful, than knowing when the rip current will occur.

Future work should focus on additional measurements on a complex beach, in particular, a longshore bar-trough system. Video images coupled with nearshore bathymetric field campaign will allow for long-term documentation of morphodynamics. Techniques of using video technology to compute flow speeds is also a requirement. The investigation of VLFs on a planar beach with minimal longshore currents is needed to formulate some hypotheses proposed for their formation. Most of this proposed future work will be commenced during my post-doctoral position in the next few months.

A brief summary of each chapter follows.

In Chapter 3, the configuration of a conventional echosounder surveying system mounted onto a PWC is described. This system provides a useful platform for measuring nearshore beach profiles. This system yielded a large amount of nearshore bathymetric data with a relatively high repeatability in both the horizontal and vertical. The system set up and sampling scheme allow beach profile data to be measured without the necessity of a pitch and roll sensor. The system is also able to collect data across the entire surf-zone, including the region inside the breakers, and can be deployed from many beaches along the coast in energetic seas; these operations are beyond the capabilities of conventional surveying systems.

Chapter 4 describes evolution of the PWC platform to a relatively common and effective tool for coastal scientists and engineers for measuring nearshore bathymetry. With the addition of an ADCP, nearshore currents can also be obtained. The field test of a PWC with an ADCP demonstrated that there was a significant amount of vertical variation in the velocity profile, requiring depth averaging. Temporal and spatial averaged data collected by a moving platform in a random wave field have severe limitations. Without averaging, the error was approximately 20 cm/s and 10 cm/s for a 1 second average. These errors are all within the specification of the instrument. New ADCP models will have a faster sampling rate and zero-blanking which will dramatically reduce the velocity error. The vessel speed varied with the wave motion such that a sampling error was introduced which is on the order of 10 cm/s. Arete Associates have shown success with their field tests. However, additional field tests are required within the surf zone to determine the limitations of the ADCP on the PWC. In addition to the ADCP limitation, the sampling associated with measuring cross-shore velocity profiles still needs to be addressed.

In Chapter 5, video images are examined as provide as a means for examining the formation, spacing, and persistence of rip channels. The concurrent wave conditions and surf zone width have largely been shown not to be responsible for the formation of the active rip currents. The bar-rip channel configuration is a persistent feature that often remains in place for months, and has been observed to migrate in the alongshore and cross-shore directions. Only extremely large storms with substantial longshore currents have a major impact on the reconfiguration of the bar morphology.

Periodic bathymetric measurements and video images are required to assess accurately the bar morphology during times when the video imagery techniques fails and to further establish relationships between the two methodologies. Our future rip current research is focused on these types of measurements.

In Chapter 6, detailed observations of morphology and hydrodynamics are documented on a complex beach located in Sand City, Monterey Bay, CA. During the course of the experiment, the morphology within the same morphodynamic state experienced significant erosional and accretional periods. There is an inverse relationship between erosional and accretional trends for the rip channels and shore-connected shoals, similar to observations of Brander (1999). The sediment distribution is representative of the morphologic features and the hydrodynamic setting.

Temporal variations in mean rip current velocities are related to tidal elevation, offshore sea-swell conditions, and diurnal sea breeze events. The rip current flows increase with decreasing tidal elevation, with increasing sea-swell energy, and with increasing energy during local sea breeze conditions.

In Chapter 7, the RIPEX-SBE experiments provided the necessary measurements to examine infragravity motions on a complex beach system and their effects on rip current hydrodynamics. The low frequency energy, $H_{rms,lo}$ increases shoreward and is correlated with the incoming sea-swell energy. $H_{rms,lo}$ did not vary with tidal elevation, whereas $U_{rms,lo}$ and $V_{rms,lo}$ are modulated slightly with tidal elevation and correlated with the incoming sea-swell energy. The undulations in the bathymetry produced weak alongshore variations in the infragravity velocities. The infragravity velocities within the rip channels are actually smaller than on the shore-connected shoal owing to continuity.

The infragravity energy was dominated by leaky and high mode edge waves with some energy located within the low mode edge waves. The small variation in wave direction associated with Monterey Bay, CA generates relatively narrow energy f-k_y-spectra as compared with observations of infragravity waves on the open coast. In addition, highly energetic, very low frequency, motions were documented with higher wave numbers and lower frequencies than associated with infragravity waves (MacMahan *et al.*,2003b; Reniers *et al.*, 2003b).

The cross-shore structure of the infragravity motions illustrate that the forced long wave propagates shoreward 180° out-of-phase with the short wave envelope until the wave groups are destroyed by depth limited breaking. The long wave then continues shoreward as a free wave and subsequently is reflected at the shoreline as shown by the cross-correlation function between the long waves at various cross-shore locations. The results are consistent with forced long wave mechanisms proposed by Longuet-Higgins and Stewart (1962, 1964). Though this structure was observed across the shoal, the high correlation in the alongshore array, suggests that the bound long wave is also released within the rip channel. Time lags of the maximum correlation of the surface elevation with velocity suggest that infragravity waves propagate slower on the shore connected-shoal due to variation in the propagation speed during low tides.

Two hypothesis were proposed for the formation of rip current pulsation; 1) infragravity waves, and 2) variations in hydraulic head associated with wave groups. The measurements suggest the first hypothesis is valid, and do not support the second hypothesis. The second hypothesis is not supported as demonstrated by the following observations: 1) infragravity velocities are smaller within the rip channel than on the shore-connected shoal (Figure 7.10) and can be explained by linearized shallow water theory (Eq 7.6) [Figure 7.9]; 2) temporal alongshore uniformity in cross-shore velocities and elevation during mid to high tides (Figures 7.15-7.17); 3) the time lag of the maximum correlation in the alongshore array, during low tide, can be explained by variations of propagation speeds related to depth differences between the shore-connected shoal and rip current channels; 4) the maximum negative correlation occurs at the maximum of the wave envelope (Figure 7.17 c); and 5) the cross-shore structure of the infragravity waves indicates a strong relationship with rip current pulsations (Figure 7.18 b).

Therefore, the standing wave motion of the infragravity motion is the primary forcing for low frequency oscillations within the rip channel, termed rip current pulsations. The rip current pulsations are related to the characteristics of the surf beat (as discussed in previous studies), and increase with increasing storm energy and during lower tides. The conceptual model presented concurs with previous observations of rip current dynamics.

In Chapter 8, energetic motions within the very low frequency, VLF, (<0.004 Hz) were observed throughout the RIPEX experiment. The VLFs were present everywhere on the beach system, composed of shore-connected shoals with incised rip channels. VLF velocities were approximately 25 cm/s within in the surf zone and decreased to approximately 5 cm/s outside of the surf zone. The VLF energy is concentrated within the very low frequency band frequency band (<0.004 Hz) differing from observations of shear instabilities of the longshore current(Oltman-Shay *et al.*, 1989), residing in higher frequencies. Previous field measurements of rip currents seemed to have documented this signal, but a conclusive interpretation is not available (Aagaard *et al.*, 1997, Brander and Short 2001). Haller and Dalrymple (2001) illustrated through detailed measurements in a laboratory and an analytical model that the jet-like flow of the rip current is unstable. Field measurements of VLFs have some similar characteristics to the laboratory measurements (Haller and Dalrymple, 2001), but the system differs in morphological set-up, rip channel spacing, wave forcing, and hydrodynamic scales, which induce differences in characteristics of the VLFs.

VLF energy increases with increasing sea-swell energy and is slightly correlated with tidal modulation. The variation in tidal elevation creates variability in wave forcing, sea-swell energy within the surf zone, infragravity energy, and rip current flows. Computed R-values, ratio between kinetic and potential energy, (Figure 8.16) are significantly larger than unity suggesting that the VLFs are not driven by gravity waves and that they should be associated with the shear of the rip currents. Yet there is not a strong correlation between variances of the VLFs and flow hydrodynamics (Figure 8.15) . A better relationship exists between VLF variance and Ho/Dc (Figure 8.17) indicating that wave forcing may be responsible for triggering the rip current cell instability.

The alongshore velocities are correlated in the alongshore when the VLFs are most energetic, while the cross-shore velocities are not correlated (Figure 8.18). F-k_y-

spectra indicate that the VLFs of the cross-shore velocities are coupled to the spacing of the rip current channels, while alongshore velocities are concentrated around $k_y=0$ (Figure 8.19-8.20). A simple model is proposed in which the entire rip current system oscillates producing results similar to the measurements (Figure 8.21), confirming the relatively uniform variance within the surf zone (Figure 8.8-8.10). It is suggested that rip currents tend to oscillate more in the cross-shore than the alongshore.

REFERENCES

Aagaard, T., B. Greenwood, and J. Nielsen, Mean currents and sediment transport in a rip channel, *Mar. Geol., 140,* 24-45, 1997.

Abdelrahman, S.M. and E.B. Thornton, Changes in the short wave amplitude and wave number due to the presence of infragravity waves, in *Proc. ASCE Coastal Hydrodynamics,* New York pp. 458-478, 1988.

Arthur, R. S., A note on the dynamics of rip currents, *J. Geophys. Res., 67,* 2777-2779.

Aubrey, D. G., Inman, D. L., and Winant, C. D., The statistical prediction of beach changes in Southern California, *J. Geophys. Res.,* 85, 3264-3276, 1980.

Bascom, W.N., and McAdam, D., Beach and surf conditions on the beaches of the Oregon and Washington Coasts between August 27 and September 27, 1945, *HE-116-229,* University of California, Berkeley, California, 1947.

Beach, R. A., Holman, R. A., and Stanley, J., Measuring nearshore bathymetry on high energy beaches, *American Geophysical Union Fall Meeting,* San Francisco, F286, 1994.

Bickley, W., The plane jet. *Phil. Mag. Ser., 7,* 727-731.

Birkemeier, W.A. and Mason, C., The CRAB: A unique nearshore surveying vehicle, *J. Surveying Engrg.,* ASCE 110(1), 1-7, 1984.

Bowen, A. J., Rip Currents, 1, Theoretical investigations, *J. Geophys. Res., 74,* 5467-5478, 1969.

Bowen, A. J. and R.A., Shear Instabilities of the Mean Longshore Current, 1: Theory. *J. Geophys. Res.,* 94, 18023-18030, 1989.

Bowen, A. J., and D. L. Inman, Rip Currents, 2, Laboratory and field observations, *J. Geophys. Res.*, 74, 5479-5490, 1969.

Brander, R.W., Field observations on the morphodynamic evolution of low wave energy rip current system. *Mar. Geol., 157*, 199-217, 1999.

Brander, R.W., and A.D. Short, Morphodynamics of a large-scale rip current system at Muriwai Beach, New Zealand. *Mar. Geol., 165*, 27-39, 2000.

Brander, R.W. Measurements of flow velocity and sediment transport in a rip current, *In Proc. Int. Conf. Coast. Engrg.* 2000.

Chen, Q., R.A.Dalrymple, J.T. Kirby, A.B. Kennedy, and M.C. Haller, Boussisnesq modeling of a rip current system, *J. Geophys. Res., 104,* 20617-20637.

Clausner, J.E., Birkemeier, W.A., and Clark, G.R., Field comparisons of four nearshore survey systems, *CERC-86-6*, US Army Corp of Engineers, Waterways Experiment Station, Vicksburg, Mississippi, 1986.

Cooke, D.O., The occurrence and geologic work of rip currents off southern California, *Mar. Geol.*, 9,173-186, 1970.

Cote, J. M., The measurement of nearshore bathymetry on intermediate and dissipative beaches, M.S. thesis, Oregon State University, 1999.

Dally, W. R., Johnson, M. A., and Osiecki, D. A., Initial development of an amphibious ROV for use in big surf, *Mar. Tech. Soc. J., 28(1) 3-10, 1994.*

Dally, W.R., An Overview of coastal surveying technology for documenting beach-inlet interaction, *J. Coastal Research.,* 18, 291-300, 1993.

Dalrymple, R.A., Prediction of strom/normal beach profiles, J. Waterway, port, coastal, and ocean engineering, Vol. 118, No2., 193-200

Dalrymple, R.A. A Mechanism for Rip Current Generation on an Open Coast. *J. Geophys. Res.,* 80, 3485-3487, 1975.

Dalrymple, R.A., Rip Currents and Their Genesis. *Summaries 16th International Conference on Coastal Engineering, Conference Paper* No 140, 1978.

Dalrymple, R.A., and C. J. Lozano, Wave-Current Interaction Models for Rip Currents. *J. Geophys. Res.,* 83, 6063-6071, 1978.

Dean, R. G. Heuristic Models of Sand Transport in the Surf Zone. *Proceedings of the 1st Australian Conference on Coastal Engineering,* pp 209-214, 1973.

Dodd, N., V. Iranzo, and A.J.H.M. Reniers, Shear instabilities of wave driven alongshore currents, *Rev. Geophysics, 38,* 437-436, 2000.

Dronen, N., H. Karunarathna, J. Fredsoe, B. M. Sumer, and R. Deigaard, An experimental study of rip channel flow, *Coastal Eng., 45(3-4),* 223-238, 2002.

Dugan, J.P., W.D. Morris, K.C. Vierra, C.C. Piotrowski, G.J. Farruggia and D.C. Campion, Jet ski based nearshore bathymetry and current survey system, *J. Coastal Res.*, 17 (3), 302-327, 2001.

Dugan, J.P., Vierra, K.C., Morris, W.D., Farruggia, and Campion, D.C., Unique vehicles used for bathymetry surveys in exposed coastal regions, *US Hydrographic Conference Soc. Natl. Mtg.,* Mobile, AL, 1999..

Eckart C., Surface waves on water of variable depth, Wave Rep. 100. Scripps Institution of Oceanography, La Jolla, CA, 1951.

Elgar, S., T.H.C. Herbers, M. Okihiro, J. Oltman-Shay, and R.T. Guza, Observations of infragravity waves, *J. Geophys. Res., 97,* 15573-15577, 1992.

Falques, A., A. Montoto, and D. Vila, A note on hydrodynamic instabilities and horizontal circulations in the surf zone, *J. Geophs. Res., 104,* 20605-20615, 1999

Fowler, R.E., and R. A.Dalrymple, Wave group forced nearshore circulation, in *Coastal Engineering 1990: Proceedings of the 22nd International Conference,* edited by B. L. Edge, pp. 729-742, Am. Soc. of Civ. Eng., New York, 1990.

Gibeaut, J. C., Gutierrez, R., and Kyser, J. A., Increasing the accuracy and resolution of coastal bathymetric surveys, *J. Coastal Res., 14(3), 1082-1098,* 1998.

Gourlay, M. R., Beach and dune erosion tests, Delft Hydraulics Laboratory Report No. M935/M936, Delft, 1968

Guza, R.T. and E.B. Thornton, Swash oscillations on a natural beach, *J. Geophys. Res., 87,* 483-491, 1982.

Guza, R.T. and E.B. Thornton, Observations of surf beat, *J. Geophys. Res., 90,* 3161-3172, 1985.

Haas, K.A. and I.A. Svendsen, Laboratory measurements of the vertical structure of rip currents, *J. Geophys. Res., 107,*

Haller, M.C., R.A. Dalrymple, and I.A. Svendsen, Experimental study of nearshore dynamics on a barred beach with rip channels, *J. Geophs. Res., 107,* 14: 1-21, 2002.

Haller, M.C., R.A. Dalrymple, and I.A. Svendsen, Rip channels and nearshore circulation, *In Proc., Coast. Dyn.* 594-603, 1997.

Haller, M.C. and D.A. Dalrymple, Rip current instabilities, *J. Fluid Mech., 433,* 161-192, 2001.

Haller, M.C., U. Putrevu, J. Oltman-Shay, and R. A. Dalrymple, Wave group forcing of low frequency surf zone motion, *Coastal Eng. J. , 41(2),* 121-136, 1999.

Hammack, J., N. Scheffner, and H. Segur, A note on the generation and narrowness of periodic rip currents. *J. Geophys. Res.* 96, 4909-4914, 1991.

Headquarters, USACE., Hydrographic surveying, Engineer Manual, Washington, D.C., 1994

Herbers, T.H.C., S. Elgar, and R.T. Guza, Infragravity-frequency (0.005-0.05 Hz) motions on the shelf. Part II: forced waves, *J. Phys. Oc., 24,* 917-927, 1994.

Herbers, T.H.C., S. Elgar, and R.T. Guza, Generation and propagation of infragravity waves, *J. Geophys. Res., 100,* 24863-24872, 1995.

Herbers, T.H.C., Elgar, S. and R.T. Guza, Directional spreading of waves in the nearshore, *J. Geophys. Res., 104,* 7683-7693, 1999.

Hino, M., Theory on formation of rip-current and cuspidal coast, in *Coastal Engineering 1974: Proceedings of the 14th International Conference,* pp. 901-919, Am. Soc. of Civ. Eng., 1974.

Holman, R.A. and A.J. Bowen, Edge waves on complex beach profiles, *J. Geophys. Res., 84,* 6339-6346, 1979.

Holman, R.A., Infragravity energy in the surf zone, *J. Geophys. Res., 86,* 457-468, 1981.

Huntley, D.A. and A.D. Short, On the spacing between observed rip currents. *Coast. Eng.,* 17, 211-225, 1992.

Huntley, D.A., R.T. Guza, and E.B. Thornton, Field observations of surf beats. 1. Progressive edge waves, *J. Geophys. Res., 86,* 6451-6466, 1981.

IHO, IHO standards for hydrographic surveys. International Hydrographic Organization, *Special Publication No. 44. 3rd edition.* International Hydrographic Bureau, Monaco, 1987.

Janssen , T.T., J.W. Kamphuis, A.R. Van Dongeren, and J.A. Battjes, Observations of long waves on a uniform slope, *In Proc., Int. Conf. Coast. Engrg.,* 2192-2205, 2000.

Kim, C.S. and D.A. Huntley, On time delays in the nearshore zone between onshore and longshore currents at incident wave frequencies. *J. Geophys. Res.* 91, 3967-3978, 1986.

Keulegan, G. H., Depths of Offshore Bars, *Beach Erosion Board, Corps of Engineers*, pp 10, 1945.

Lascody, R. L., East central Florida rip current program, National Weather Service *In-house Report,* pp 10, 1998.

Lillycrop, W. J., Parson, L. E., and Irish, J., Development and operation of the SHOALS airborne lidar hydrographic survey system. Laser Remote Sensing of Natural Waters: From Theory to Practice, *SPIE- Int. Soc. for Optical Engrg.,2964, 26-37, 1996.*

Lippmann, T.C., T.H.C. Herbers, and E.B. Thornton, Gravity and shear wave contributions to nearshore infragravity motions, *J. Phys. Oc., 29,* 231-239, 1999.

List, J.H., Wave groupiness variations in the nearshore, *J. Coastal Eng.,* 15: 475-496, 1991.

Liu, P. L.-F. and C. C. Mei, Water motion on a beach in the presence of a breakwater, I and II, *J. Geophys. Res., 81,* 3079-3094, 1976.

Longuet-Higgins, M.S. and R.W. Stewart, Radiation stress and mass transport in surface gravity waves with application to "surf beat", *J. Fluid Mech., 29,* 481-504, 1962.

Longuet-Higgins, M.S. and R.W. Stewart, Radiation stress in water waves: a physical discussion, with applications, *Deap Sea Res. 11,* 529-562, 1964.

Luschine, J. B. (1991) A study of rip current drownings and weather related factors. *National Weather Digest* pp.13-19.

McKenzie, P. Rip-current systems, *J. Geol., 66,* 103-113, 1958.

Mei, C. C. and D. Angelides, Longshore circulation around a conical island, *Coast. Eng., 1,* 31-42, 1977.

Miles J.R., P.E. Russell, B.G. Ruessink, and D.A. Huntley, Field observations of the effect of shear waves on sediment suspension and transport. *Continental Shelf Res. 22*, 657-681, 2002.

Munk, W.H., Surf Beats. *Eos. Trans. Amer. Geophys. Union., 30*, 849-854, 1949.

Murray, A. B. and G. Reydellet, A rip current model based on hypothesized wave/current interaction, *J. Coastal Res., 17(3),* 517-530, 2001.

Noda. E. K., Wave-induced nearshore circulation, *J. Geophy. Res., 79,* 4097-4106, 1974.

Noyes J.T.A., R.T. Guza, S. Elgar, and T.H.C. Herbers, Comparison of methods for estimating nearshore shear wave variance. *J. Atmospheric & Oceanic Tech., 19,* 136-143, 2002.

Oh, T. M. and R. G. Dean, Three-Dimensional Hydrodynamics on a Barred Beach, *Proceedings of the 25th International Conference on Coastal Engineering,* Am. Soc. Civ. Eng., pp. 3680-3693, 1996.

Okihiro, M., R.T. Guza, and R.J. Seymour, Bound infragravity waves, *J. Geophys. Res., 97,* 1453-11469, 1992.

Oltman-Shay, J. and R.T. Guza, Infragravity edge wave observation on two California Beaches, *J. Phys. Oceanogr., 17,* 644-663, 1987.

Oltman-Shay, J., P.A. Howd, and W.A. Birkemeier, Shear instabilities of mean longshore current. 2. Field observations, *J. Geophys. Res., 94,* 18031-18042, 1989.

Ozkan-Haller, H.T. and J.T. Kirby, Nonlinear evolution of shear instabilities of the longshore current: A comparison of observations and computations, *J. Geophys. Res., 104,* 25953-25984, 1999.

Ozkan-Haller, H.T., Vidal, C., Losada,I. J., Medina, R., and M.A. Losada, Standing edge waves on a pocket beach, *J. Geophys. Res., 106,*16,981-16,966, 2001.

Pawka, S.S., Island shadows in wave directional spectra, *J. Geophys. Res., 88,* 2579-2591, 1983.

Ranasinghe, R., G. Symonds,, K. Black, and R. Holman Processes governing rip spacing persistence, and strength in swell dominated, microtidal environment, *Proc. 27 Int., Conf., on Coastal Engrg., ASCE*, 493-499, 2002.

Raubenheimer, B., S. Elgar, and R.T. Guza, Estimating wave heights from pressure measured in the sand bed, *J. Wtrway., Port, Coast., an d Oc. Engrg., 124 (3),* 151-154, 1998.

Reniers, A. J. H. M., A. .R. van Dongeren, J. A. Battjes, and E. B. Thornton, Linear modeling of infragravity waves during Delilah. *J. Geophys. Res.* 2002

Reniers, A.J.H.M., MacMahan, J., Stanton, T.P., and E.B. Thornton, Infragravity motions on a complex beach, Part 1: Modeling. submitted to *J. Geophys. Res.* 2003a.

Reniers, A.J.H.M., MacMahan, J., Stanton, T.P., and E.B. Thornton, Dynamics of very low frequency motions. in preparation for *J. Geophys. Res.* 2003b.

Ruessink, B.G., The temporal and spatial variability oof infragravity energy in a barred nearshore zone, *Continental Shelf Res., 18,* 585-605, 1998.

Ruessink, B.G., Bound and free infragravity waves in the nearshore zone under breaking and non-breaking conditions, *J. Geophys. Res., 103,* 12,795-12,805, 1998.

Sallenger, A. H., Howard, P. C., Fletcher, C. H. III, and Howd, P. A., A system for measuring bottom profile, waves, and currents in the high-energy nearshore environment, *Mar. Geol.,* 51, 63-76, 1983.

Sasaki, T. Simulation on shoreline and nearshore current. *Proceedings of Civil Engineering In the Oceans, ASCE,* pp 179-196, 1975.

Seymour, R.J., and Bothman, D.P., A hydrostatic profiler for nearshore surveying, *Coast. Eng.,* 8. 1-14, 1984.

Shepard, F.P., Undertow, rip tide, or "rip current", Science, 84, 1936.

Shepard, F.P., K.O. Emery, and E.C. La Fond, Rip currents: a process of geological importance, *J. Geol., 49,* 337-369, 1941.

Shepard, F.P., and D.L. Inman, Nearshore water circulation related to bottom topography and refraction, *Trans. Am. Geophys. Union, 31,* 196-212, 1950.

Short A.D., Rip current type, spacing and persistence, Narrabeen Beach, Australia, *Mar. Geol., 65,* 47-71, 1985.

Smith, J.A. and J.L. Largier, Observations of nearshore circulation: rip currents, *J. Geophys. Res., 100,* 10967-10975, 1995.

Sonu, C.J., Field observations of nearshore circulation and meandering currents, *J. Geophys. Res., 77,* 3232-3247.

Suhayda, J.N., Standing waves on beaches, *J. Geophys. Res., 79,* 3065-3071, 1974.

Svendsen, I. A., Wave heights and set-up in a surf zone, *Coast. Eng. , 8,* 303-329, 1984.

Svendsen, I. A., K. A. Haas, and Q. Zhao, Analysis of rip current systems, in *Coastal Engineering 2000, Proceedings of 27th International Conference*, edited B. L. Edge, pp. 1127-1140, Am. Soc. Civ. Eng., New York, 2000.

Symonds G., D.A. Huntley, and A. J. Bowen, Two-dimensional surf beat: long wave generation by time varying breakpoint, *J. Geophys. Res., 87,* 492-498, 1982.

Tam, C. K. W., Dynamics of rip currents, *J. Geophys. Res., 78,* 1937-1943, 1973.

Tang, E.C.S. and R.A. Dalrymple, Rip currents and wave groups, in *Nearshore Sediment Transport,* edited by R.J. Seymour, pp. 205-230, Plenum, New York, 1989.

Thornton, E.B., and C. S. Kim, Longshore current and wave height modulation at tidal frequency inside the surf zone, *J. Geophys. Res., 98,* 9499-9508, 1993.

Tucker, M.J., Surfbeats: sea waves of 1 to 5 minutes' period, in *Proc. Royal Soc. London Ser. A 202,* pp. 565-573, 1950.

USLA, United States Lifeguard Association, www.usla.org

Vagle, S., D.M. Farmer, and G.B. Deane, Bubble transport in rip currents, *J. Geophy. Res., 106,*11677-11689, 2001.

Wind, H.G. and C. B. Vreugdenhil, Rip-current Generation Near Structures. *Journal of Fluid Mechanics* 171:459-476, 1986.

Work, P.A., Hansen, M., and Rogers, W. E., Bathymetric surveying with GPS and heave, pitch, and roll compensation." *J. Surveying Engrg.,* ASCE 124(2), 73-90, 1998.

Wright, L.D., R.T. Guza, and A.D. Short, Dynamics of high-energy dissipative surf zone, *Mar. Geol., 45,* 41-62, 1982.

Wright, L.D. and A.D. Short, Morphodynamic variability of surf zones and beaches:a synthesis, *Mar. Geol., 56,* 93-118, 1984.

Zyserman, J., J. Fredsoe, and R. Deigaard, Prediction of the dimensions of a rip current system on a coast with bars. *Proceedings of the International Coastal Conference, 1990.*, 959-972, 1990.

BIOGRAPHICAL SKETCH

James (Jamie) MacMahan was born in Bridgeton, New Jersey on February 29, 1972. He spent much of his childhood growing up in Cumberland County, New Jersey. He attended Cumberland Regional High School in Upper Deerfield, New Jersey. Upon graduation in 1990, he attended in Stockton State College originally intending to pursue marine biology, until he realized he did not like biology, but enjoyed physical oceanography. He was lucky in life to find a subject that interested him early on. He became interested in estuarine oceanography and pursued his Master's degree at the University of South Carolina with Dr. Bjorn Kjerfve. He pursued nearshore processes at the University of South Carolina with Dr. Gail Kineke and Dr. Tim Kana and learned to tinker with electronics from Dr. John Dickerson. His interests narrowed, and he focused his efforts on surf zone hydrodynamics, in particular, rip currents. Upon completion of this body of work, Jamie is about to embark on post-doctoral position collaborating with Dr. Ed Thornton, who is Dr. Robert Dean's first doctoral student. It is Jamie's ultimate goal to develop a successful research program at an academic institution.

I certify that I have read this study and that in my opinion it conforms to acceptable standards of scholarly presentation and is fully adequate, in scope and quality, as a dissertation for the degree of Doctor of Philosophy.

Robert G. Dean

Robert G. Dean, Chair
Graduate Research Professor of
Civil and Coastal Engineering

I certify that I have read this study and that in my opinion it conforms to acceptable standards of scholarly presentation and is fully adequate, in scope and quality, as a dissertation for the degree of Doctor of Philosophy.

Robert J. Thieke, Co-Chair
Assistant Professor of
Civil and Coastal Engineering

I certify that I have read this study and that in my opinion it conforms to acceptable standards of scholarly presentation and is fully adequate, in scope and quality, as a dissertation for the degree of Doctor of Philosophy.

Edward B. Thornton

Edward B. Thornton
Distinguished Professor of
Oceanography, Naval
Postgraduate School

I certify that I have read this study and that in my opinion it conforms to acceptable standards of scholarly presentation and is fully adequate, in scope and quality, as a dissertation for the degree of Doctor of Philosophy.

Michel K. Ochi
Professor Emeritus of Civil and
Coastal Engineering

I certify that I have read this study and that in my opinion it conforms to acceptable standards of scholarly presentation and is fully adequate, in scope and quality, as a dissertation for the degree of Doctor of Philosophy.

Joann Mossa
Associate Professor of
Geography

This dissertation was submitted to the Graduate Faculty of the College of Engineering and to the Graduate School and was accepted as partial fulfillment of the requirements for the degree of Doctor of Philosophy.

May 2003

Pramod Khargonekar
Dean, College of Engineering

Winfred M. Phillips
Dean, Graduate School